

**‘Computer Analysis for Registration and Change Detection of Retinal  
Images’**

A dissertation presented by

Adham Abdulkhair Elmuntser

To School of Computing, Science & Engineering at University of Salford

Submitted in Partial Fulfillment of the Requirements for the Degree of

**Doctor of Philosophy**

in Computer Science and Engineering

Supervised by Prof. Apostolos Antonacopoulos

April 2021

Committee in charge:

## Contents

List of Tables .....	7
List of Figures.....	8
Abstract.....	12
ACKNOWLEDGMENTS .....	13
Chapter 1 – Introduction.....	14
Overview.....	14
1.1 Background.....	14
1.2 Motivation of Research.....	16
1.3 Aims and Objectives .....	16
1.4 Retinal Image Characteristics and Challenges.....	18
1.5 Problem statement.....	20
1.6 System Prototype .....	21
1.7 Contributions .....	25
1.8 Thesis overview .....	25
Chapter 2 – Medical Background.....	28
Overview.....	28
2.1 Medical Image Computing for registration and segmentation .....	28
2.2 The Retina and the anatomy of human eye.....	29
2.2.1 The Retina .....	29
2.2.2 The Optic disc .....	29
2.2.3 The Vessel Network.....	29
2.2.4 Retinal Conditions.....	30
2.2.4.1 Diabetic Retinopathy .....	30
2.2.5 Diagnosing Techniques .....	30
2.2.6 Retinal Abnormalities and Artefacts .....	30
2.3 Retinal Images .....	31
2.4 The necessity of an automatic system that supports ophthalmologists in their diagnosis .....	31

2.5 Conclusion .....	35
Chapter 3 – Colour Distance Measurement.....	37
Overview.....	37
3.1 Introduction.....	37
3.2 Colour Science Principles .....	37
3.2.1 Colour Attributes.....	38
3.2.2 Colour Spaces.....	39
3.2.3 Opponent Colour .....	40
3.2.4 L*A*B* Colour Space .....	40
3.2.5 HSV Colour Space .....	41
3.2.6 Colour Difference Metric .....	42
3.2.7 Euclidean Distance .....	42
3.2.8 Maximum Colour Difference .....	42
3.3 Colour Image Difference .....	43
3.4 The Related Works of the Calculation of the Colour Difference between two Colour Images.....	43
3.4.1 The Related Works based on Techniques of Digital Signal Processing .....	44
3.4.2 The Related Works based on Average Calculation.....	45
3.4.2.1 The Matković ‘s Algorithm (1997) .....	45
3.4.2.2 The Zhan, Zuo, & Li (2016)’s Algorithm .....	46
3.4.3 The Related Works based on Histogram Calculation .....	46
3.4.3.1 The Approach of Hong and Luo (2006) .....	47
3.4.3.2 The Approach of Lee and Plataniotis (2014).....	48
3.4.3.3 The Histogram Comparison algorithm .....	48
Chi-Square (Chisqr).....	49
Alternative Chi-Square .....	49
(ChisqrAlt).....	49
3.4.3.4 The Evaluation of Histogram Comparison metrics within different colour spaces for retinal images.....	49
3.4.4 The Related Works based on Specific formula.....	53

3.3.4.1 The Measurement of the Accuracy of an Image Processing Operation (Bubak, et al., 2004) .....	54
3.3.4.2 The Template Matching algorithm .....	54
3.5 The issues required to develop a new method for calculating a colour distance .....	55
3.6 The Developed Similarity Measurement Algorithm.....	55
3.7 Discussion .....	56
3.8 Conclusion .....	59
Chapter 4 – Colour Mapping .....	61
Overview .....	61
4.1 Introduction.....	61
4.2 Histogram specification algorithm.....	62
4.2.1 The algorithm .....	63
4.2.2 The Results and Discussion.....	64
4.3 The Developed Colour Mapping Algorithm.....	67
4.3.1 The algorithm .....	67
4.3.2 The Results of the Developed Algorithm compared with the Histogram specification algorithm .....	74
4.3.3 The Colour-Distance-and-Edge-Matching-Rate-Based Evaluation.....	79
4.3.3.1 Part1: The Colour Distance Calculation for Evaluation.....	79
4.3.3.2 Part2: Edges Matching Rate Calculation for Evaluation.....	79
4.3.3.3 The Evaluation Results of Histogram Specification algorithm .....	81
4.3.3.4 The Evaluation Results of the Developed Colour Mapping Algorithm .....	83
4.3.4 The Results and Discussion.....	84
Chapter 5 – Preprocesses .....	85
Overview .....	85
5.1 Image Resizing .....	85
5.2 Retina Cropping .....	85
5.3 Background extension.....	87
5.4 Green Channel Separation .....	89
5.5 Deriving Retina Mask.....	90

5.6 Weber Space Transforming .....	91
5.6.1 Evaluation of using Weber Space Transform in the developed algorithm .....	92
5.7 Bright Lesions reduction.....	99
5.8 Retina Border Extending .....	100
5.9 Sharpening of bifurcation and its edges (using Modified Unsharp Masking technique) .....	105
5.10 Conclusion .....	106
Chapter 6 - Control Points Detection .....	107
Overview.....	107
6.1 Feature-Extraction for Registration Control Points .....	107
6.1.1 Previous Approaches for Feature Extraction .....	107
6.2 Retina-Bifurcation-based Detection of Control Points.....	108
6.2.1 Optic Disc Centre .....	108
6.2.2 Cross Points between optic disc and vessels.....	109
6.2.3 Cross Points between Bifurcations.....	110
6.2.4 Previous Approaches in Vessel Segmentation .....	111
6.2.5 The Developed Algorithm for Retinal Bifurcation Detection.....	112
6.2.5.1 Skeletonization .....	113
6.2.5.2 Image thinning for Skeletonization .....	114
6.2.5.3 Reducing of gaps among bifurcations .....	115
6.2.5.4 The Verification of the Skeletonization Thinning.....	116
6.2.5.5 Image thinning for Improved Skeletonization.....	116
6.2.5.6 Cutting of Small Branches.....	116
6.2.5.7 Removing the patterns with small dimensions .....	119
6.2.5.8 Creating of Watershed marker for vessel segmentation.....	120
6.2.5.9 Segmentation by Watershed .....	121
6.2.5.10 The overall algorithm of the developed method for retinal Bifurcation Detection.....	121
6.3 Future Works .....	124
6.4 Conclusion .....	124
Chapter 7 – Registration and Changes Detection.....	125

Overview.....	125
7.1 Previous Approaches in Image Registration.....	125
7.1.1 Image registration classifications .....	125
7.1.2 Retinal image registration and its classifications .....	129
7.1.2.1 Vessel-based Classifications .....	130
7.1.2.1.1 Vessel-based Methods .....	130
7.1.2.1.2 Non-vessel-based methods .....	131
7.1.2.2 Automation-based classifications .....	133
7.2 Image Registration .....	134
7.2.1 Registration Theory .....	134
7.2.2 The Registration Problem.....	135
7.3 The Developed Algorithm .....	135
7.4 The Evaluation and Results .....	145
7.4.1 FIRE: Fundus Image Registration Dataset.....	145
7.4.2 Evaluation.....	145
7.4.2.1 Using SURF features as Control Points .....	147
7.4.2.2 The evaluation of the developed Bifurcations-based Registration Algorithm .....	149
7.5 The Developed Algorithm for Change Detection.....	151
7.6 The Future Works .....	155
7.7 Conclusion .....	155
Chapter 8: Thesis Conclusion.....	157
Overview.....	157
8.1 Summary of the Thesis .....	157
8.2 Research Progress History .....	158
8.3 Technical Problems of the Research.....	160
8.4 Contributions .....	162
8.5 Summary of the results .....	163
8.6 Additional Developing Features .....	166
8.7 Future Work.....	167

8.8 Overall Conclusion .....	168
References .....	169

## List of Tables

<i>TABLE 3.4.3.3 – 1: THE FORMULAS OF THE HISTOGRAM COMPARISON METRICS.</i> .....	49
<i>TABLE 3.4.3.4 - 1: THE COMPARISON AMONG THE RESULTS OF THE METRICS USED IN HISTOGRAM COMPARISON ALGORITHM IN BGR COLOUR SPACE.</i> .....	52
<i>TABLE 3.4.3.4 - 2: THE COMPARISON AMONG THE RESULTS OF THE METRICS USED IN HISTOGRAM COMPARISON ALGORITHM IN LAB COLOUR SPACE.</i> .....	52
<i>TABLE 3.4.3.4 - 3: THE COMPARISON AMONG THE RESULTS OF THE METRICS USED IN HISTOGRAM COMPARISON ALGORITHM IN HSV COLOUR SPACE.</i> .....	52
<i>TABLE 4.2.2 - 1: THE OUTPUTS OF HISTOGRAM SPECIFICATION ALGORITHM, THE RESULTED IMAGES, THROUGH SIXTY-FOUR EXPERIMENTS.</i> .....	66
<i>TABLE 4.3.2 - 1: AN EXAMPLE OF THE RESULTED IMAGE AND ITS HISTOGRAMS BY THE DEVELOPED ALGORITHM COMPARED WITH THE HISTOGRAM SPECIFICATION ALGORITHM.</i> .....	74
<i>TABLE 4.3.2 - 2: THE RESULTED IMAGES OF THE DEVELOPED ALGORITHM COMPARED WITH THE HISTOGRAM SPECIFICATION ALGORITHM.</i> .....	78
<i>TABLE 4.3.3.3 – 1: THE TESTS RESULTS OF COLOUR DISTANCE CALCULATION FOR THE HISTOGRAM SPECIFICATION METHOD BY USING CHISQRALT METHOD OF HISTOGRAM COMPARISON WITHIN LAB COLOUR SPACE</i> .....	82
<i>TABLE 4.3.3.3 – 2: THE PROCESSING TIME IN SECOND FOR THE TESTS RESULTS OF COLOUR DISTANCE CALCULATION FOR THE HISTOGRAM SPECIFICATION METHOD BY USING CHISQRALT METHOD OF HISTOGRAM COMPARISON WITHIN LAB COLOUR SPACE</i> .....	82
<i>TABLE 4.3.3.3 – 3: THE TESTS RESULTS OF EDGES COMPARISON, EDGES MATCHING PERCENTAGES (%), FOR THE HISTOGRAM SPECIFICATION METHOD WITHIN GREEN COLOUR SPACE.</i> .....	82
<i>TABLE 4.3.3.4 – 1: THE TESTS RESULTS OF COLOUR DISTANCE CALCULATION FOR THE DEVELOPED METHOD BY USING CHISQRALT METHOD OF HISTOGRAM COMPARISON WITHIN LAB COLOUR SPACE</i> 83	
<i>TABLE 4.3.3.4 – 2: THE ELAPSED TIME IN SECOND FOR THE TESTS RESULTS OF COLOUR DISTANCE CALCULATION FOR THE DEVELOPED METHOD BY USING CHISQRALT METHOD OF HISTOGRAM COMPARISON WITHIN LAB COLOUR SPACE</i> .....	83
<i>TABLE 4.3.3.4 – 3: THE TESTS RESULTS OF EDGES COMPARISON, EDGES MATCHING PERCENTAGES (%), FOR THE DEVELOPED METHOD WITHIN GREEN COLOUR SPACE.</i> .....	83
<i>TABLE 7.4.2-1: THE INITIAL EVALUATION.</i> .....	149

## List of Figures

FIGURE 1.4 - 1: TWO EXAMPLES OF NON-UNIFORM ILLUMINATION IN A RETINAL IMAGE AND WRONG OPTIC DISC SEGMENTATION.....	19
FIGURE 1.4 - 2: THE DIFFERENT STRUCTURES OF OPTIC DISC.....	20
FIGURE 1.4 - 3: THE GOOD AND POOR QUALITY IN A RETINAL IMAGE.....	20
FIGURE 2.3 - 1: AN EXAMPLE OF A RETINAL IMAGE (FROM FIRE DATASET, CODE: S59_1) IN A NORMAL CONDITION (HERNANDEZ-MATAS, ET AL., JUL. 2017).....	31
FIGURE 3.4.3.4 - 1: THE SELECTED EIGHT RETINAL IMAGES FROM MESSIDOR DATASET.....	50
FIGURE 3.4.3.4- 2: THE AVERAGES OF THE COLOUR DISTANCES AND PROCESSING TIMES IN THE TWO TESTS BY THE PROPER METRICS OF HISTOGRAM COMPARISON ALGORITHM WITHIN SPECIFIC COLOUR SPACE.....	53
FIGURE 4.2 - 1: HISTOGRAM SPECIFICATION ALGORITHM.....	63
FIGURE 4.3.1 - 1: THE REFERENCE IMAGE AND ITS HISTOGRAM.....	68
FIGURE 4.3.1 - 2: THE REFERENCE MASK.....	68
FIGURE 4.3.1 - 3: THE SOURCE IMAGE AND ITS HISTOGRAM.....	69
FIGURE 4.3.1 - 4: FIGURE DERIVING OF SOURCE MASK.....	69
FIGURE 4.3.1 - 5: THE TRANSFORMED IMAGE AND ITS HISTOGRAM.....	69
FIGURE 4.3.1 - 6: THE HISTOGRAM OF EACH CHANNEL, BLUE, GREEN, AND RED CHANNEL FOR THE REFERENCE IMAGE.....	71
FIGURE 4.3.1 - 7: THE GREEN HISTOGRAM OF THE REFERENCE IMAGE, SHOWING THE FIRST AND THE LAST BIN NUMBER IN EACH CURVE OR CHANGE IN THE HISTOGRAM.....	71
FIGURE 4.3.1 - 8: DERIVING OF COMMON MASK.....	73
FIGURE 4.3.1 - 9: THE OUTPUT OF THE MERGING OF THE MODIFIED THREE CHANNELS.....	73
FIGURE 4.3.1 - 10: THE FINAL OUTPUT OF THE PROPOSED ALGORITHM FOR THE COLOUR MAPPING.....	74
FIGURE 4.3.3.2.1 - 1: EDGES OF IMAGE1, REFERENCE IMAGE.....	80
FIGURE 4.3.3.2.1 - 2: EDGES OF IMAGE2, SOURCE IMAGE.....	81
FIGURE 5.2 - 1: ROI CROPPING.....	86
FIGURE 5.3 - 1: BACKGROUND EXTENSION.....	88
FIGURE 5.4 - 1: GREEN CHANNEL.....	89
FIGURE 5.4 - 2: THE COMPARISON BETWEEN GREEN AND GRAY SCALE THROUGH APPLYING EDGES DETECTION ON THE SAME IMAGE.....	89
FIGURE 5.5 - 1: RETINA MASK.....	90
FIGURE 5.6 - 1: TRANSFORMING TO WEBER SPACE.....	91
FIGURE 5.6.1 - 1: AN EXAMPLE OF THE ENHANCED IMAGE BY THE DEVELOPED ALGORITHM.....	92
FIGURE 5.6.1 - 2: A DRIVE GROUND TRUTH (IN WHITE COLOUR).....	92
FIGURE 5.6.1 - 3: A GROUND TRUTH (IN RED) + THE EXTRACTED BIFURCATIONS (IN GREEN) BY THE DEVELOPED ALGORITHM IN THIN FORM (THE OVERLAP IS IN ORANGE COLOUR).....	93



FIGURE 5.6.1 - 4: A GROUND TRUTH (IN RED) + THE EXTRACTED BIFURCATIONS (IN GREEN) BY THE DEVELOPED ALGORITHM IN THICK FORM (THE OVERLAP IS IN ORANGE COLOUR).....	94
FIGURE 5.6.1 - 5: THE TWO COMPARISONS BETWEEN VESSELS GROUND TRUTH AND THE EXTRACTED VESSELS (IN THIN FORM) BY THE DEVELOPED ALGORITHM WITH AND WITHOUT USING WEBER SPACE TRANSFORM. ....	95
FIGURE 5.6.1 - 6: THE TWO COMPARISONS BETWEEN VESSELS GROUND TRUTH AND THE EXTRACTED VESSELS (IN THICK FORM) BY THE DEVELOPED ALGORITHM WITH AND WITHOUT USING WEBER SPACE TRANSFORM. ....	96
FIGURE 5.6.1 - 7: THE COMPARISON BETWEEN THE NUMBER OF THE DETECTED CONTROL POINTS (CROSS POINTS BETWEEN VESSELS) WITH AND WITHOUT USING WEBER SPACE TRANSFORM, IN THE THIN VESSELS FORM, BY THE DEVELOPED ALGORITHM. ....	97
FIGURE 5.6.1 - 8: AN EXAMPLE OF 390 DETECTED CONTROL POINTS FROM FIRE DATASET IMAGE CODE: S03_2 (BY THE CURRENT DEVELOPED ALGORITHM WITHOUT USING WEBER SPACE).....	97
FIGURE 5.6.1 - 9: AN EXAMPLE OF 349 DETECTED CONTROL POINTS FROM FIRE IMAGE CODE: S03_2 (BY PREVIOUS DEVELOPED ALGORITHM WITH USING WEBER SPACE).....	98
FIGURE 5.7 - 1: IMAGE SEGMENTATION BY K-MEANS CLUSTERING.....	99
FIGURE 5.7 - 2: THE EFFECT OF APPLYING K-MEANS CLUSTERING ON THE GREEN CHANNEL OF A RETINAL IMAGE.....	99
FIGURE 5.7 - 3: THE RESULTS OF RETINA BORDER EXTENDING .....	100
FIGURE 5.8 - 1: BORDERS EXTENDING.....	100
FIGURE 5.8 - 2: THE ALGORITHM OF RETINA BORDER EXTENDING .....	101
FIGURE 5.8 - 3: EXAMPLES OF THE BORDERS EXTENDING RESULTS BY USING DIFFERENT KERNEL SIZES: 3 X 3, 5 X 5, 7 X 7, AND 9 X 9. ....	104
FIGURE 5.9-1: SHARPENING OF BIFURCATION AND ITS EDGE.....	105
FIGURE 6.2.2 - 1: THE INTERSECTION BETWEEN OPTIC DISC AND THE VESSELS NETWORK. ....	109
FIGURE 6.2.2 - 2: THE CROSS POINTS BETWEEN OPTIC DISC AND THE VESSELS NETWORK. ....	109
FIGURE 6.2.2 - 3: THE DETECTED CROSS POINTS, INTERSECTION, BETWEEN OPTIC DISC AND THE VESSELS NETWORK. ....	110
FIGURE 6.2.3 - 1: EXAMPLE 1: THE DETECTED CROSS POINTS, INTERSECTION, BETWEEN THE RETINAL VESSELS. ....	110
FIGURE 6.2.3 - 2: EXAMPLE 2: THE DETECTED CROSS POINTS, INTERSECTION, BETWEEN THE RETINAL VESSELS. ....	111
FIGURE 6.2.5.1 - 1: THE ALGORITHM OF SKELETONIZATION .....	113
FIGURE 6.2.5.1 - 2: THE OUTPUT OF SKELTONIZATION BEFORE ITS UPDATING WITH SOME CORRECTIONS. ....	114
FIGURE 6.2.5.2 - 1: THINNING OF SKELETONIZATION .....	115
FIGURE 6.2.5.3 - 1: PATTERN DETECTION OF BIFURCATION SKELETON AND REDUCING OF GAPS AMONG BIFURCATIONS .....	115

FIGURE 6.2.5.6 - 1: THE REMOVAL OF SMALL BRANCHES FROM VESSELS .....	116
FIGURE 6.2.5.6 - 2: THE RESULT OF FIRST EXECUTION OF SMALL BRANCHES CUTTING .....	118
FIGURE 8.2.6 - 3: THE RESULT OF SECOND EXECUTION OF SMALL BRANCHES CUTTING .....	118
FIGURE 6.2.5.7 - 1: PATTERN DETECTION OF BIFURCATIONS SKELETON AFTER ENHANCEMENT [5 DETECTED PATTERNS].....	119
FIGURE 6.2.5.7 - 2: THE REMOVED PATTERNS FROM VESSELS SKELETON AFTER ENHANCEMENT [381 REMOVED PATTERNS].....	119
FIGURE 6.2.5.7 - 3: THE BIFURCATION SKELETON, IN GREEN COLOUR, WITHIN A RETINAL IMAGE, AFTER REMOVING OF ALL THE PATTERNS WITH SMALL DIMENSIONS.....	120
FIGURE 6.2.5.8 - 1: THE INCORPORATION PROCESS OF CREATING A WATERSHED MARKER FOR BIFURCATION DETECTION.....	120
FIGURE 6.2.5.9 - 1: THE RESULT OF SEGMENTATION .....	121
FIGURE 7.1.1 - 1: MEDICAL REGISTRATION CLASSIFICATION (MAINTZ & VIERGEVER, 1996).....	128
FIGURE 7.1.2 - 1: AN EXAMPLE OF THE REGISTRATION OF TWO RETINAL IMAGES BY THE DEVELOPED ALGORITHM.....	129
FIGURE 7.1.2.1.2 - 1: AN EXAMPLE OF 390 DETECTED CONTROL POINTS FROM FIRE DATASET IMAGE CODE: S03_2 (BY THE CURRENT DEVELOPED ALGORITHM).....	133
FIGURE 7.1.2.2 - 1: THE CONTROL MARKS .....	133
FIGURE 7.2.1 - 1: IMAGE REGISTRATION.....	134
FIGURE 7.3 - 1: THE EXAMPLE-1 OF THE RETINA AREA DETECTION FOR A DARK RETINAL IMAGE (IMAGE FIRE DATASET CODE: S37_1).....	136
FIGURE 7.3 - 2: THE EXAMPLE-2 OF THE RETINA AREA DETECTION FOR A DARK RETINAL IMAGE (IMAGE FIRE DATASET CODE: S42_2).....	136
FIGURE 7.3 - 3: AN EXAMPLE OF CONTROL POINTS DETECTION FOR FIRE DATASET IMAGE PAIR: S71..	137
FIGURE 7.3 - 4: THE PRE-PROCESSED IMAGE, FIRE CODE: S03_1, USED FOR SIMILARITY MEASUREMENT. .....	138
FIGURE 7.3 - 5: AN EXAMPLE OF SMALL OVERLAP DURING COMPARING THE FIRE IMAGE PAIR: S71 IN THE FIRST GROUND TRUTH POINT.....	141
FIGURE 7.3 - 6: AN EXAMPLE OF SMALL OVERLAP DURING COMPARING THE FIRE IMAGE PAIR: S71 IN THE FIRST GROUND TRUTH POINT.....	142
FIGURE 7.3 - 7: AN EXAMPLE OF A DETECTED MATCHED POINT BEFORE THE PROCESS OF THE BEST MATCH DETECTION (OR CORRECTION PROCESS), THROUGH FIRE IMAGE PAIR: S71 IN THE SECOND GROUND TRUTH POINT, THE CALCULATED SIMILARITY VALUE IS 0.999 (OR 99.9%). .....	143
FIGURE 7.3 - 8: THE DETECTION OF THE BEST MATCH, THROUGH FIRE IMAGE PAIR: S71 IN THE SECOND GROUND TRUTH POINT, SIMILARITY VALUE (OF THE RESULT OF THE DEVELOPED ALGORITHM) IS 0.999677, WHEREAS SIMILARITY VALUE (OF THE GROUND TRUTH) 0.999458.....	144
FIGURE 7.3 - 9: THE REGISTRATION RESULT BY THE DEVELOPED BIFURCATIONS-BASED ALGORITHM. .	144

FIGURE 7.4.2 - 1: REFERENCE IMAGE (FIRE IMAGE PAIR: S71) (A KEYPOINT IS COLORED BY RED, AND SURROUNDED BY GREEN RECTANGLE WHICH IS REPRESENTED THE TESTING AREA IN MATCHING PROCESS).....	146
FIGURE 7.4.2 - 3: THE X-COORDINATE OF THE MOST-RIGHT PIXEL IN THE RED DOT (X=41).....	147
FIGURE 7.4.2-1: FIRST TEN IMAGES IN FIRE DATASET IN S-CATEGORY.....	148
(THE IMAGES WHICH ARE USED IN THE INITIAL EVALUATION) .....	148
FIGURE 7.4.2.2 - 1: THE EVALUATION RESULTS BETWEEN THE CURRENT DEVELOPED SYSTEM AND FOUR EXISTED METHODS SHOWN IN FIRE DATASET .....	150
FIGURE 7.5- 1: CHANGE DETECTION CORRECTION BY REMOVING THE NO-CHANGE PIXELS .....	152
FIGURE 7.5- 2: THE DETECTED CHANGES.....	152
FIGURE 7.5- 3: THE MASK OF THE DETECTED CHANGES (THE BINARY IMAGE) .....	152
FIGURE 7.5-4: THE CHANGES IN OVERLAP AREA IN BOTH IMAGES .....	153
FIGURE 7.5-5: THE HIGHLIGHTING OF CHANGES IN BOTH IMAGES.....	153
FIGURE 7.5-6: AN EXAMPLE OF THE 3D-HIGHLIGHTING OF CHANGES IN THE SECOND IMAGE OF A TEST PAIR.....	154
FIGURE 8.3 - 1: THE DETECTED CONTROL POINTS, HIGHLIGHTED BY RED CIRCLES, DETECTED BY THE DEVELOPED BIFURCATIONS-BASED ALGORITHM.....	160
FIGURE 8.3 - 2: AN EXAMPLE OF A PAIR OF RETINAL IMAGES WITH THE CONTROL POINTS, HIGHLIGHTED BY GREEN CIRCLES, WHICH ARE THE FEATURES DETECTED BY SURF ALGORITHM.....	161
FIGURE 8.3 - 3: IMAGE REGISTRATION.....	161
FIGURE 8.5 - 1: THE OUTPUTS OF THE DEVELOPED SYSTEM. ....	163
FIGURE 8.5 -2: THE REGISTRATION RESULT ALGORITHM.....	164
FIGURE 8.5 -3: THE POSSIBLE MATCHES AMONG THE CONTROL POINTS. ....	164
FIGURE 8.5 - 4: THE OUTCOMES OF THE PROPOSED ALGORITHM FOR IMAGE COLOUR MAPPING.....	165
FIGURE 8.6 - 1: THE SOFTWARE FEATURE OF DISPLAYING OF UNLIMITED NUMBER OF IMAGES WITH A NAVIGATION FACILITY USING SCROLL BAR.....	166
FIGURE 8.6 - 2: THE SOFTWARE FEATURE OF SHOWING PIXEL VALUES OF A SELECTED AREA IN AN IMAGE .....	167
FIGURE 8.6 - 3: THE SOFTWARE FEATURE OF CHOOSING TWO IMAGE AND DISPLAYING THEM IN ONE WINDOW IN MAXIMIZED SIZE.....	167

## **Abstract**

The current system of retinal screening is manual; It requires repetitive examination of a large number of retinal images by professional optometrists who try to identify the presence of abnormalities. As a result of the manual and repetitive nature of such examination, there is a possibility for error in diagnosis, in particular in the case when the progression of disease is slight. As the sight is an extremely important sense, any tools which can improve the probability of detecting disease could be considered beneficial. Moreover, the early detection of ophthalmic anomalies can prevent the impairment or loss of vision.

The study reported in this Thesis investigates computer vision and image processing techniques to analyse retinal images automatically, in particular for diabetic retinopathy disease which causes blindness. This analysis aims to automate registration to detect differences between a pair of images taken at different times. These differences could be the result of disease progression or, occasionally, simply the presence of artefacts. The resulting methods from this study, will be therefore used to build a software tool to aid the diagnosis process undertaken by ophthalmologists.

The research also presents a number of algorithms for the enhancement and visualisation of information present within the retinal images, which under normal situations would be invisible to the viewer; For instance, in the case of slight disease progression or in the case of similar levels of contrast between images, making it difficult for the human eye to see or to distinguish any variations.

This study also presents a number of developed methods for computer analysis of retinal images. These methods include a colour distance measurement algorithm, detection of bifurcations and their cross points in retina, image registration, and change detection. The overall analysis in this study can be classified to four stages: image enhancement, landmarks detection, registration, and change detection. The study has showed that the methods developed can achieve automatic, efficient, accurate, and robust implementation.

## ACKNOWLEDGMENTS

At the beginning, to **my parents** a special thanks and appreciation for their support along my life even if they are far away from me.

And my best regards and thanks to my ex-supervisor **Professor Tim Ritchings** for all he has given to me, ranging from respect, direction to assistance.

I am very thankful to my supervisor, **Professor Apostolos Antonacopoulos**, who has made efforts to support me continuously to reach this level in my research

I thank and appreciate all the time given to me by **Dr. Mahmoud Moustafa**, an ophthalmic specialist, to answer my questions related eye disease and features of medical images of human eye.

Furthermore, I give my best thanks to **Dr. Ivan Wood**, an ophthalmic expert, who has provided me with specialist advice and interesting information about ophthalmology.

Also, I would like to thank all **the staff in the University of Salford** who they have worked to ensure that the educational environment in the University will be as best as possible.

Meanwhile, I must express my gratitude to **my wife** for her support and encouragement.

## **Chapter 1 – Introduction**

### **Overview**

This chapter starts by introducing the background to the general problem and this research as well as the reasons for pursuing it, which are considered as the motivations for this work. The aims and objectives of this study are outlined and the characteristics and problems that impede the achievement of the objectives of this research are discussed. Subsequently, the research plan lists the work stages in the research. Finally, this chapter presents the developed system prototype proposal for the registration process and changes detection between two retinal images.

### **1.1 Background**

Retinal diseases are highly detrimental conditions affecting the human eye, which may lead to weakening or loss of the sense of sight. There are several retinal pathological cases, for instance, Diabetic Retinopathy, Glaucoma and Age Related Macular Degeneration are conditions which affect the human retina. The presence of these diseases, if allowed to progress, causes irreparable damage to the structure of the retina. However, if these conditions are detected early, vision can be saved. It is necessary, therefore, to detect and treat retinal diseases as early as possible.

The essential structure of the retina is composed of the optic disc, the fovea, and the vascular network. The optic disc, sometimes also referred to as the optic nerve head, is usually the brightest partition in a retinal image. It has approximately a circular shape. It is the place from where all the vessels emerge and to where the brain connects. The fovea is a small depression in the retina on where the centre of the vision field is focused. This region has the highest visual acuity. The vascular network consists of branches of blood vessels, arteries, or veins, in the tree shape.

In ophthalmology, the retinal or fundus image is considered as the fundamental facility in the diagnosis of illness. Ophthalmologists would be aided in their work significantly if they had access to an efficient tool which would aid them to automatically discover differences between certain retinal images of a patient (in order to diagnose potential diseases), instead of relying on optometrists to routinely compare an extremely large number of images. It is obvious that the role of optometrists cannot be ignored. However, in this crucial situation, there is a high possibility of diagnostic fault, particularly in slight evolution of disease.

Therefore, an automatic screening system is required for scanning the significant number of images and identifying the regions of dissimilarity. Such dissimilarities are caused by natural effects, or by pathological progressions.

This research is investigating the development of a computer vision application to detect such dissimilarities to support the efforts of ophthalmologists and optometrists in their daily work. Consequently, the detection and diagnosis process will be enhanced.

Despite the tens of research approaches and applications in this field, it is difficult to identify a reliable approach for all pathological conditions. Such difficulty by reasons of some obstacles such as natural effects, sensitivity of screening devices or cameras, the resolution and size of photographs, and the colour range used in a camera. In addition to a variety of diseases and their abnormal progressions.

In recent years, there has been substantial number of instruments and software systems developed over the world relating to the medical sector, for instance, the applications of patient data entry and expert systems for analysis and diagnosis. Nowadays, there are increasing developments particularly in the imaging technology characterized by high image resolution and high quality of the screening machines; Consequently, they have spread worldwide, in particular in the medical sector where it provides visual facilities for showing the patient data acquired from different screening systems, especially such data being difficult to perceive with the eyes.

Therefore, such technology allows the eye-care experts to have the ability to examine, in detail, particular places which were considered as unreachable regions in the human body. Furthermore, by analyzing such pathological data, it can deduce useful information concerning the healthy condition of a patient and even suggest some guidelines for treatment and healing.

The computer analysis of retinal images, for this research, involves operations that aim to compare multiple ocular fundus images which have been taken at regular intervals. For instance, a diabetic patient should have a new retinal image taken every 3 to 6 months. This is a routine screening practice and is currently done manually by means of visual inspection.

This research is a study of image processing with regard to the retina, being a vital part in the human eye. It involves a study of existing algorithms relating to the image processing techniques that can be applied on retinal images, for example, image enhancement, image segmentation, circle detection, registration and feature extraction. Consequently, a reliable

new system is aimed to be created as a part of this academic investigation, the essential function of such system is to automatically match two retinal images to detect the differences. By highlighting such changes, this outcome can be considered as a beneficial assistance to boost the detection of ophthalmological illness.

## **1.2 Motivation of Research**

The motivation of this research results directly from the medical requirements. It is required to automate and speed up the process of retina examination to detect any changes, especially in the early disease stages when these changes are very slight and hard to detect by human eye. Such early detection may lead (with appropriate treatment) to the reduction of the effects of retinal diseases which may lead to blindness.

Another motivation is the lack of professional ophthalmologists in poor and some developing countries. Also, the reduction of potential errors in diagnosis and lack of ophthalmological follow-up, are considered as additional incentives for carrying out this research. A patient may lose his/her sight due to either the clinical diagnosis being wrong or an initial diagnosis not being made and the patient not followed up.

Furthermore, there is an urgent requirement to develop new techniques that aid eye-specialists in their diagnoses. There are three reasons for this requirement. They are: the very substantial number of patients infected with eye diseases that can lead to blindness, the various conditions of eye diseases, and the significant costs, in particular for those who have lost their eyesight.

Finally, there are still problems that cause mis-registration, in medical images, as shown in many instances of published research work. Such research and problems are considered as additional motivation to develop new algorithms for the solution of the mis-registration.

## **1.3 Aims and Objectives**

This research aims to develop new approaches for automated registration to detect the locations of changes between a pair of retinal images acquired within a period of time; This period is recommended to be around a six-month lapse. More specifically, it aims to develop a reliable method to register time-separated retinal images, taking into consideration that all the developed processes, within this method, should be robust enough to handle changes in



contrast, lighting, and changes in location. In other words, this study aims to develop an automated, efficient, accurate and robust method for retinal images registration and change location detection in them. In order to successfully pursue the above aims, the following objectives should be achieved:

✓ **A critical evaluation of the state-of-the-art**

By looking for published articles related to ophthalmology and digital image processing, especially diabetic retinopathy and retinal fundus images; and writing up a literature review. Consequently, such investigation will lead to the selection of the most appropriate algorithms for this study.

✓ **New image enhancement methods for retinal images**

By such algorithm, it can be examined as many as possible of the various retinal images (taken under different conditions). This algorithm will improve the lighting and contrast within retinal images, in an attempt to highlight the information that is semi-hidden or difficult to see by human eye, within the image. Such algorithm must involve a process to correctly balance the colours of two images, and to reduce the gradient in background colors. Technically, the Image Enhancement process must include Image Sharpening Colour Normalization, and Image Smoothing.

✓ **Algorithm for Control point detection**

The control points are used to align the possible matching between the two images. On the other hand, through these points, the possible registrations between two images, can be predicted.

✓ **Colour distance measurement algorithm**

By this algorithm, colour difference or similarity between two tested images can be measured.

✓ **Image registration algorithm for retinal images**

It provides correct alignment between two images.

✓ **Difference detection algorithm for retinal images**

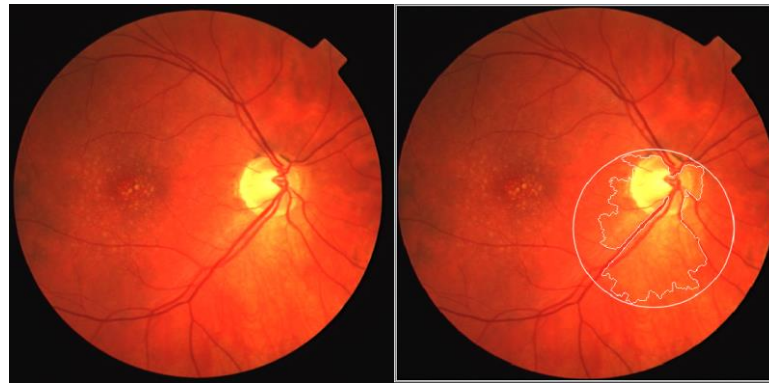
This algorithm should have the ability to automatically find the location of changes between two registered images.

All the developed processes within such algorithms should be robust enough to handle differences occurred in retinal images. For instance, disease progression, the presence of artefacts, aging, or lighting difference could cause some changes in retinal images.

#### **1.4 Retinal Image Characteristics and Challenges**

The retinal image characteristics represent the most significant challenges to the development of an effective registration algorithm. One of the obstacles for such development is the variation between retinal images. This variation is due to a number of different characteristics of retinal images. These characteristics include:

1. Colour Intensity properties of images. There are a variety of colour values among retinal images. This could be due to cameras or lighting.
2. The curved surface of the retina.
3. The unalignment: Over the time, a retinal image for a patient may be changed. This change could be a position change in some points in the retina. This leads to unalignment issue between the recent image and the old ones.
4. The non-uniform illumination and poor contrast in colour retinal images. These are the result of external illumination effects such as glaring and fade-out. For instance, this is the major obstacle to achieving optic disc segmentation. Figure 1.4-1 shows two examples of wrong segmentation of optic disc due to such non-uniformity; the result of such segmentation is clarified by white surrounding border.



a) Example-1



b) Example-2

*FIGURE 1.4 - 1: TWO EXAMPLES OF NON-UNIFORM ILLUMINATION IN A RETINAL IMAGE AND WRONG OPTIC DISC SEGMENTATION.*

5. Various blood vessel structures, and the thinness of vessels.
6. The different structures of optic disc, which are due to the position and shape of the optic disc, and the presence of the blood vessels in the retina, for example there are some optic discs divided by vessels in many parts in some retinal images, as shown in figure 1.4-2.

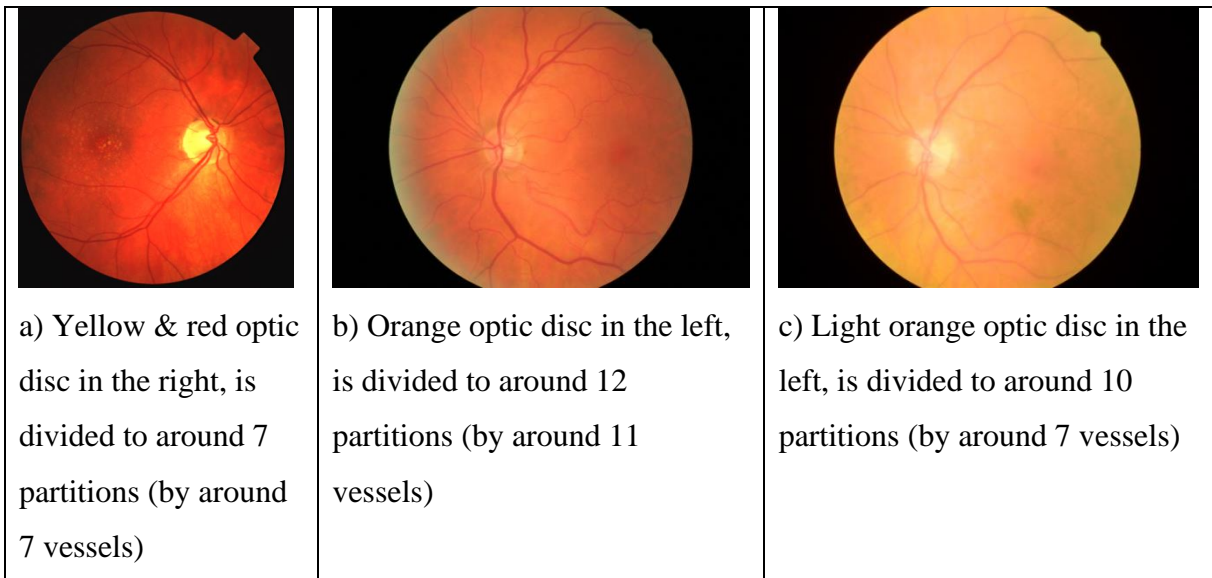


FIGURE 1.4 - 2: THE DIFFERENT STRUCTURES OF OPTIC DISC.

- The low-quality of some retinal images. Figure 1.4-3 shows the same retinal image in a good and a poor quality. For instance, the poor quality could be as a result of some external effects such as lighting or there is a problem in a camera.

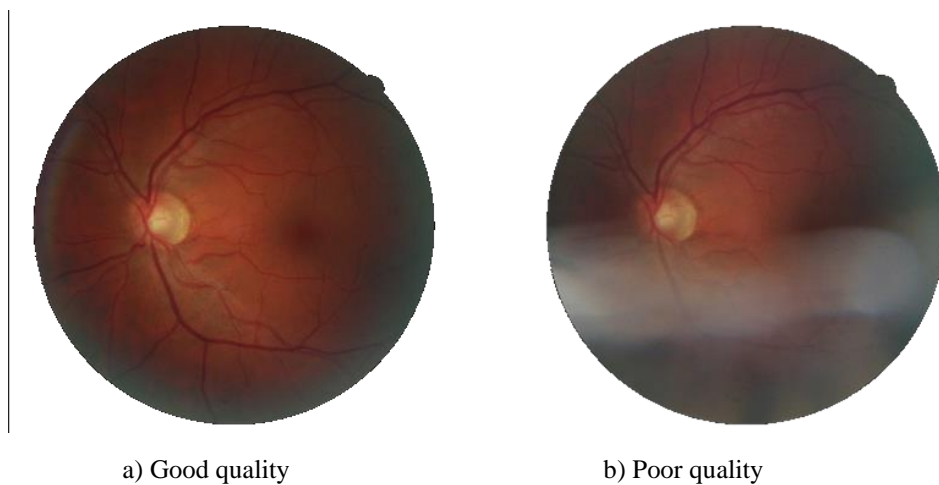


FIGURE 1.4 - 3: THE GOOD AND POOR QUALITY IN A RETINAL IMAGE.

### 1.5 Problem statement

The key research problem can be identified in **how to apply an image registration algorithm followed by change detection to retinal images automatically, efficiently, accurately, and robustly.** In other words, this study analyses retinal images to find differences between them, without losing any information that affects the diagnosis of the disease. Therefore, this research looks at answering the following question:

*Can an image registration algorithm be implemented between retinal images without losing their retina features?*

The problem of applying retinal image registration and the detection of differences can be focused on four issues: automation, efficiency, accuracy, and robustness. In terms of this research, automation means that all developed processes operate by themselves without any human intervention or control. Efficiency represents the optimal use of the available resources such as computer memory in the shortest possible time. Accuracy and robustness mean that the output of the registration process is a match between two images within overlap area and without being affected by their different characteristics, in particular the signs of illness.

Technically, as a result of the spherical surface of a retina, the registration of two images must take into account that the value of displacement needed for the second image to match the first image could have different values. In other words, each part of the second image may have to be shifted differently from the rest of the image to match with the first image. Other Technical issues are: how to make the two images have close colour range (colour gradient) ?, how to detect control points for registration?, how to measure the difference between two control points?, how to detect the best matching among control points in two retinal images?, and how to find the corresponding point in a retinal image for a point in another image ?

## **1.6 System Prototype**

An approach is developed in this research. It is to detect changes between two retinal images. The image registration is the key process in this approach. It depends on Bifurcations Intersection Points as control points. On the other hand, it uses the cross points, among branches or vessels in a retina. These points are used to calculate the transformation formula. by this formula, corresponding points can be derived. In addition, there are some preprocesses required for detecting bifurcations intersection points. Cross points are chosen as control points because they are one of main features in a retina. There must be some of these points even in the case of existence of illness symptoms or even if the image is in bad quality. However, the main reason for choosing them is the detection accuracy of their locations as proven in the evaluation results. In the early stages of this study, SURF method is used to extract features to be used as control points. An evaluation is achieved to compare the registration accuracy between using bifurcations intersection points and using SURF features. The results obtained by using cross points are better than those are by using SURF.

Accordingly, the cross points are used as control points in the developed algorithm in this research.

Regarding the used colour spaces, two colour spaces are used in the developed system. They are Green space and Gray Scale. The processes of control points detection depend on Green Channel within BGR space. In contrast, Gray Scale is used for similarity measurement. Green space has been used, because the results of edge detection in such space is better than those within Gray scale. The edge detection is one of the control points detection processes. In contrast, the usage of Gray Scale for similarity measurement has given noticeable accurate results as shown in the evaluation results of the whole developed algorithm.

All the processes of the developed system, for this study, are developed or chosen from existing algorithms with specific setting and arranged in a specific sequence according to the experimental results. These processes can be divided into three stages: Control Points Detection, Image Registration, and Change Detection.

These stages are as the follows:

### **Stage 1: Control points detection**

This stage involves some pre-processes followed by cross points detection.

#### **Part 1.1: The Pre-processes**

After loading the two retinal images that will be registered, some pre-processes are implemented. They are:

##### **Part 1.1.1: The first pre-processes for both images**

These pre-processes are applied on each of the two images. they include:

- 1) Retina Cropping
- 2) Image Resizing. It is to reduce the time required to detect control points (in the current developed algorithm, the image size is reduced to 500x500 pixels instead of the actual size: 2912 x 2912 pixels). Therefore, the image size is reduced approximately to a quarter of the original size.
- 3) Enlarging Image Background
- 4) Finding Foreground Mask
- 5) Retina Border Extending
- 6) Finding Foreground Mask

### **Part 1.1.2: The pre-processes for the second image**

They are applied on the second image. They include the following processes:

- 7) **ROI sizes Equalizing:** It is to equalize the size of the two retina areas. Retina size of both images must be the same.
- 8) **Colour Matching for Image2 with Image1:** It is achieved by applying a developed algorithm on the second image, considering the first image as reference. Actually, this operation is to equalize the histogram of the second image with the histogram of the first image. The whole image colours (of the second image) are matched with the corresponding colours in the reference image.

### **Part 1.1.3: The second pre-processes for both images**

They are some processes applied to each of the two images. They include the following operations:

- 9) Green Channel Separation
- 10) Deriving the potential retina area [ Retina Mask 1 ]
- 11) Reducing Bright Lesions By K-means Clustering
- 12) Background extension
- 13) Border Extending
- 14) Deriving the potential retina area [ Retina Mask 2 ] From extended image
- 15) Image Smoothing (using Gaussian Blur algorithm and kernel size is 11)
- 16) Colour Normalization in the range between 0 and 255
- 17) Bifurcation sharpening (using Modified Unsharp Masking technique)
- 18) Bifurcation edges sharpening

### **Part 1.2: Detecting of Control Points**

The processes of this sub-stage are applied to each of the two retinal images. They are divided in two parts.

#### **Part 1.2.1: Bifurcations Segmentation**

It includes three sub-processes which are:

- a. Identifying of the expected Bifurcations Area: Such area is

defined by three methods: Laplacian, Adaptive Threshold, and Morphological Operations (Erosion and Dilation).

- b. Detection of Bifurcations' skeleton: Such skeleton is a structure of bifurcations in a thin form, 1-pixel wide. This process involves some corrections on the expected Bifurcations Area, followed by an image thinning approach.
- c. Bifurcations segmentation: It is a process of applying image segmentation using the Watershed algorithm with innovative (proposed) marker

### **Part 1.2.2: Locating of intersections between bifurcations**

These points represent the cross points in the thinned bifurcations form. These points are required for aligning the two images in the registration process.

### **Stage 2: Image Registration**

It is the process of the matching of the two retinal images according to the best similarity values and the locations among the control points.

It involves the following processes:

#### **Part 2.1: The Pre-processes for both images**

They include the following four processes:

- 1) Converting images to Gray Scale
- 2) Invert colours in both images (NOT operation)
- 3) Colour normalization between the two tested images
- 4) Finding Foreground Mask for both images

**Part 2.2:** Deriving the right matches between the detected control points

**Part 2.3:** Finding of the corresponding point in a retinal image for a point in another image.



### **Stage 3: Change Detection**

It is the detection of dissimilarities between two images. Typically, it is a subtraction operation between the two registered images with specific thresholding within their overlap.

#### **1.7 Contributions**

The contributions that are obtained from this study can be listed as follows:

- ✓ A study of the existing algorithms regarding colour distance measurement, colour normalization, vessel segmentation, retinal image registration.
- ✓ A new approach for pre-processing of retinal images before registration.
- ✓ A new approach for colour distance measurement between images.
- ✓ A new approach for colour normalization between two images.
- ✓ A new approach for bifurcation detection and their cross points.
- ✓ A new approach for the registration of retinal images.
- ✓ An approach for detection of changes between two registered retinal images.

All the developed algorithms in this research involve a combination of processes, some of them are combinations of existing algorithms, taken from published scientific resources, and used with a specific setting in this research, whereas others are new methods developed in this study.

#### **1.8 Thesis overview**

The Thesis of this research presented here, is broken into a number of separate chapters. These chapters are listed as the following:

##### Chapter 1 – Introduction

This chapter is concerned with the introduction that shows the importance, motivations, aims and objectives, work stages, problems, and the proposed system prototype.

## Chapter 2 – Medical Background

This chapter provides a medical background regarding registration and segmentation techniques, retina and its diseases, and retinal images. In addition, this chapter clarifies the medical requirements that motivates this research.

## Chapter 3 – Colour Distance Measurement

This chapter illustrates how to calculate colour difference between digital images. It explains the method developed in this research for calculating colour difference between retinal images. At the end of this chapter, overall discussion and conclusion are presented.

## Chapter 4 – Colour Mapping

This chapter explains the proposed normalization operation which equalizes the colours of the two images in the way that the colours of the second image become the same or very close to the colours of the first image. This process is a solution to the problem of the presence of different colours between the images to be compared. This chapter includes the colour mapping concepts, the Histogram Specification algorithm, and the developed algorithm and its results and evaluation.

## Chapter 5 – Preprocesses

This chapter describes the required processes before registration to ensure the best results. Such processes involve image resizing, retina cropping, background extension, green channel separation, the derivation of the retina mask, Weber space transformation, bright lesions reduction, and border extension.

## Chapter 6 – Control Points Detection

This chapter explains the required processes for extraction of bifurcations in a retina. The chapter presents a summary about the previous approaches in vessel segmentation. Then, it presents the algorithm developed in this research for bifurcations detection and their cross

points. These points are used as Control Points in this research. Next, another method is shown for detecting other Control Points by SURF algorithm.

#### Chapter 7 – Registration and Changes Detection

The developed processes in this study for registration and change detection are illustrated in this chapter. Such processes are: image partitioning, image matching, and the identification of changes location. In addition, this illustration includes the evaluation and the results of the developed algorithm, suggestions for future work, and the overall conclusion.

#### Chapter 8 – Thesis Conclusion

The overall research findings from this study are listed and discussed in this chapter. These findings are presented as a summary of the whole thesis followed by the results of the developed algorithm. In addition, the technical problems of the developed algorithm, the contributions and the achievements of this research are presented. Finally, suggestions for future work and the overall conclusions are presented at the end of this chapter.

## **Chapter 2 – Medical Background**

### **Overview**

This chapter describes the fundamental medical concepts regarding this research. It starts with an introductory explanation for registration and segmentation of medical images, then it provides a medical background about the retina and its diseases, such as Diabetic Retinopathy. Furthermore, this chapter shows the features of retinal images that are used in this research. At the end of this chapter, the reasons for the necessity of an automatic system that supports ophthalmologists in their diagnosis are clarified.

### **2.1 Medical Image Computing for registration and segmentation**

Medical image computing (MIC), the field of this research, concentrates on the computational analysis of medical images to extract clinically relevant information. Image registration and image segmentation are two common processes used in such analysis. This research focuses on image registration applying where there is necessity to align or match some images taken at different times. However, image registration is still obstructing the development of the medical imaging technology. The reason of that is due to its complexity concerning its operations such as feature extraction and image mapping. As illustrated by Ferreira (2012), image registration is an operation that associates each element, or a feature, in an image with a corresponding one in another image. Furthermore, Brown (1992) describes it as a process of transforming different sets of data into one coordinate system. Data may be multiple photographs, data from different sensors, times, depths, or viewpoints. Registration is necessary in order to be able to compare or integrate the data obtained from these different measurements. A change detection or tumor monitoring is an example of an application of medical image registration, for the data of the same patient taken at different points in time. Daniel Rueckert (Rueckert, 2013) presents an overview of techniques and applications regarding medical image registration. In recent years, there are numerous studies regarding the registration of images. The key issue in the majority of academic scientific publications is the automation of the operations required for the image registration.

Image segmentation is the process of partitioning a digital image into multiple segments, sets of pixels,. The goal of segmentation is to simplify and/or change the representation of an image into something that is more meaningful and easier to analyze (Shapiro & Stockman,

2001). Image segmentation is typically used to locate objects such as optic disc and vessels in retinal images.

## **2.2 The Retina and the anatomy of human eye**

One of the most vital organs in the human body is the eye due to its responsibility for the sense of sight. It connects directly with the brain via the optic-nerve. The Mangawhai Optometrists (2015), Macula Center (2015), and WebMD (2015) present a detailed explanation relating to the human eye, for example, its Anatomy or Structure , and the Vision.

### **2.2.1 The Retina**

It is the essential examining area in this research. It is a layer at the back of the eyeball containing cells that are sensitive to light and that trigger nerve impulses that pass via the optic nerve to the brain, where they are interpreted as an image. By analogy with a camera, the retina's function is similar to the film in a camera. It captures the light rays and converts them to light impulses through millions of tiny nerve terminals. Subsequently, these impulses are sent to the optic nerve by millions of retinal nerve fibers. In a retinal image, the major components that can be perceived are the fovea , optic head, vessels, and macular (Macula Center, 2015) .

### **2.2.2 The Optic disc**

Optic disc, sometimes also referred to as the optic nerve head, is one of the significant parts in the retina. It is usually the brightest partition in a retinal image. The optic-head is the place from where all the vessels emerge and to where the brain connects. It has a circular shape. It is a blind spot where there is not any captured data. Furthermore, it is a crucial location to investigate several ophthalmological diseases such as Glaucoma.

### **2.2.3 The Vessel Network**

It is a significant retinal landmark that consists of branches of blood vessels, arteries or veins, in a tree shape. For instance, in the case of diabetic retinopathy, there will be notable changes in vascular structure. There are two types of vessels, an artery and a vein. A vein is the smaller vessel whereas an artery is the larger.

#### **2.2.4 Retinal Conditions**

The most important cases of ophthalmology in this research are those affecting the retina. Diabetic retinopathy is one of the most common types of infection. This disease is the main cause of blindness (Kumara, et al., 2012) (Mangawhai Optometrists, 2015) (Macula Center, 2015) (Specialists, 2015) (WebMD, 2015).

##### **2.2.4.1 Diabetic Retinopathy**

Diabetic Retinopathy causes serious damage to blood vessels which nourish the retina. This disorder can lead to blindness. There are two types, diabetes type 1 and diabetes type 2. The worst case is when there is a bleeding in the retina. There is not effective treatment for this situation. Diabetes causes a deterioration in the retinal vessels leading to change in the structure of the retina (Kumara, et al., 2012) (Mangawhai Optometrists, 2015) (Macula Center, 2015) (Specialists, 2015) (WebMD, 2015).

The typical symptoms of Diabetic Retinopathy appear because of damage in blood vessels in the retina. They can occur anywhere throughout the retina including the macula. They may involve bulges (microaneurysms) and connections with each other (intraretinal microvascular anomalies) and/or swelling (edema), protein deposits (exudates), blood (hemorrhage), or puffy white patches on the retina (cotton wool spots) as shown by Ang (2010-2015) and Dr.Neuhoff (2015).

#### **2.2.5 Diagnosing Techniques**

The common approach is by repetitive examination of a collection of images to assess the presence of abnormalities and monitor their progression.

#### **2.2.6 Retinal Abnormalities and Artefacts**

Continuous and regular screening is very necessary to ensure the health of the eyes. Such examinations check the presence of abnormalities and monitor their progression. The abnormalities within a retina can be pathological abnormalities or artefacts. Pathological abnormalities are such as micro-aneurysms and hemorrhages. In contrast, artefacts are not as a result of disease progression or retinal damage. They are usually introduced during the capture process. They are illustrated through common four exemplifications which are: floater

supervening when robbing on the eye, eyelashes, grease or dust on camera lens, and camera artifact causing unwanted and unintentional changes within an image, as a result of wrong camera settings.

### 2.3 Retinal Images

Recently, retinal images have become widespread, as a result of availability of cheap digital fundus cameras, and they are stored in digital formats. The next figure shows an example of a healthy retinal image with high resolution. This example is characterized by very high contrast and clear visibility of its common structures such as vessels and optic disc.



*FIGURE 2.3 - 1: AN EXAMPLE OF A RETINAL IMAGE (FROM FIRE DATASET, CODE: S59\_1) IN A NORMAL CONDITION (HERNANDEZ-MATAS, ET AL., JUL. 2017).*

### 2.4 The necessity of an automatic system that supports ophthalmologists in their diagnosis

Overall, the necessity of developing an automatic system, that aids ophthalmologists in their diagnostic process, is as a result of the following issues:

- ✓ The necessity of automation, speed and accuracy of retina examination
- ✓ The shortage of professional ophthalmologist in some countries
- ✓ The urgent necessity of accurate and early discovery of diseases causing blindness;  
this issue is as results of the following facts:
  - The large and growing number of visually impaired people in the world
  - The variety of illnesses causing blindness

- The cost of sight loss

By the existence of a tool for automatic and reliable detection of changes in a retina, the performance of eye-care specialists will be improved in practice of ophthalmic examining and subsequently their diagnosis will be more accurate, and besides, it will potentially provide an effective facility for tracking the progression of pathological conditions in the long term.

Furthermore, there is a lack of professional ophthalmologists in poor and some developing countries, as stated in VISION 2020 report (WHO Press, 2007), which is the action plan for the period between 2006 and 2011 of a global initiative for the elimination of avoidable blindness.

Another consideration is the errors in diagnosis and lack of ophthalmological follow-up. Such case may lead to a vision loss. For instance, according to the result of the research of Garfield and Neil-Dwyer (1975) regarding the delay that is in a diagnosis of optic nerve and chiasmal compression, there are a few patients, 5 out of 29 patients who presented with failing vision in one eye due to optic nerve or chiasmal compression, which have been initially diagnosed with such disease. The errors in diagnosis and lack of ophthalmological follow-up, led to delays of up to many years with serious deterioration in acuity of vision. The major causes of such errors were lack of charting of the visual fields, the acceptance of the diagnosis of the neuritis in the absence of essential features, and the infrequent use of skull radiographs. Another proof of the existence of medication mistakes, as mentioned by Ophthalmic Mutual Insurance Company, in USA, which has shown, in its report (OMIC, 1995), entitled "Medication Errors Result in Costly Claims for Ophthalmologists", that "The review of data collected on 117,000 claims and lawsuits by the Physicians Insurers Association of America (PIAA) reveals that medication errors are the second most frequent reason for claims against physicians and result, cumulatively, in the second highest indemnity paid behind faulty diagnosis and evaluation. The high frequency and severity of claims involving medication errors prompted the PIAA to study the problem in 1993". Its report has cited some of the findings from that PIAA study. For instance, "Jerome W. Bettman's review of Seven Hundred Medicolegal Cases in Ophthalmology indicates that medication errors are the third most frequent complaint against ophthalmologists following claims arising from cataract surgery and treatment of retinal detachments". Consequently, the existence of such mistakes shows the great need for the establishment of a system that relies on the computer and be more accurate to overcome these human errors.



According to the key information and statistics of Royal National Institute of Blind people (RNIB, 2016), over two million people in the UK are living with sight loss. And the number of people in the UK with sight loss is set to increase dramatically in the future, It is predicted that by 2050, the number of people with sight loss in the UK will double to nearly four million. Therefore there is pressing demand for accurate and early detection of the diseases causing blindness, as a result of the increasing number of vision-impaired patients as described in RNIB (2016) and the variety of illnesses causing blindness. For example, the main diseases which cause blindness in adults (RNIB, 2016) are Age-related macular degeneration ,glaucoma, cataracts and diabetic retinopathy. Regarding diabetic, for instance, nearly one person in 25 in the UK has diabetes mellitus. At least 20 per cent of people with diabetes will develop some sort of diabetic retinopathy (RNIB, 2016). As stated in Diabetes information of RNIB (2016), the most sight loss due to diabetes is preventable if treatment is given early. In addition to the Cost of sight loss. As mentioned in RNIB (2016), the cost of sight loss to the UK economy in 2008 was at least £6.5 billion, and this is likely to increase as long as the number of people with sight loss increases. This statistic does not include the cost of sight loss in children. This cost consists of:

- £2.14 billion in direct health care costs, such as eye clinics, prescriptions, and operations.
- £4.34 billion in indirect costs, such as unpaid carer costs and reduced employment rates.

All the mentioned statistics are considered as evidence of the need for an automatic system that supports ophthalmologists in their diagnostic process. Furthermore, the research titled “Comparison of Diagnosis of Early Retinal Lesions of Diabetic Retinopathy between a Computer System and Human Experts” (SC, et al., 2001) presents another proof of the necessity of such system. It aims "to investigate whether a computer vision system is comparable with humans in detecting early retinal lesions of diabetic retinopathy using colour fundus photographs" (SC, et al., 2001). They have concluded that "the performance of such computer vision system in diagnosing early retinal lesions was comparable with that of human experts. Therefore, this mobile, electronically easily accessible, and noninvasive computer system, could become a mass screening tool and a clinical aid in diagnosing early lesions of diabetic retinopathy" (SC, et al., 2001).

Besides, the presence of tens of published researches, related to this research. The key issues of the most such publications, are limited to retinal image registration, optic disc

segmentation, and vessel segmentation. For instance, there are many examples of researches regarding image registration such as temporal registration for low-quality retinal images of the murine eye (Andreou & Achim, 2010), MSc. dissertation: algorithms for ophthalmology image (Ferreira, 2012), retinal fundus image registration via vascular structure graph matching (Deng, et al., 2010), retinal image matching using hierarchical vascular features (Bhuiyan, et al., 2011), retinal image registration using bifurcation structures (Chen, et al., 2011), accurate and robust image registration based on radial basis neural networks (Senol, et al., 2011), a robust hybrid method for nonrigid image registration (Yang, et al., 2011), temporal registration for low-quality retinal images of the murine eye (Andreou & Achim, 2010), a method for automatic image registration through histogram-based image segmentation (Gonçalves, et al., 2011), and image registration by compression (Bardera, et al., 2010). In addition, there are further instances of researches relating to vessel segmentation such as vessel segmentation in retinal images using multi-scale line operator and k-means clustering (Saffarzadeh, et al., 2014), real-time retinal vessel mapping and localization for intraocular (Becker & Riviere, 2013), fast retinal vessel detection and measurement using wavelets and edge location refinement (Bankhead, et al., 2012), a new supervised method for blood vessel segmentation in retinal images by using Gray-level and moment invariants-based features (Marin, et al., 2011), and retinal vessel segmentation using the 2-d Gabor wavelet and supervised classification (Soares, et al., 2006). Furthermore, there are other examples concerning optic disc segmentation such as combining algorithms for automatic detection of optic disc and macula in fundus images (Qureshi, et al., 2012), application of principal component analysis in automatic localization of optic disc and fovea in retinal images (Mudassar & Butt, 2013), automatic detection of optic disc in digital retinal images (Wisaeng, et al., 2014), the automatic detection of the optic disc location in retinal images using optic disc location regression (Abràmoff & Niemeijer, 2006), extraction of the contours of optic disc and exudates based on marker-controlled Watershed segmentation (Eswaran, et al., 2008), and automatic detection of optic disc based on PCA and stochastic (Morales, et al., 2012).

Overall, all the mentioned facts, statistics, and publications have highlighted the importance of this research, demonstrated the need for an automatic system, and provide a great motivation to study the subject of this research.

## 2.5 Conclusion

The field of this research is Medical image computing (MIC). This field focuses on the computational analysis of medical images to extract clinically relevant information. The image segmentation and the image registration are two examples of The methods of this analysis. These two methods are a part of the study in this research. One of the typical applications of such analysis is the computer-aided diagnosis. The automatization is the key issue for applying such analysis in all its related image processing techniques such as the image registration.

Regarding image registration, it is a process that associates each element, or a feature, of an image with corresponding feature of another image. Although there are many existing researches or studies related to this process, this process is still obstructing the development of the medical imaging technology due to its complex operations such as feature extraction and image mapping, and due to various medical images, even in one type of images, for example, retinal images have different colours and structures making the retinal image registration become difficult. One example of the applications of medical image registration is the tumor monitoring which is a change detection process.

Concerning the image segmentation, it partitions an image into multiple segments, to simplify the image into something that is more meaningful and easier to analyze. This process has been exemplified in this research in the segmentation of the optic disc and vessels in retinal images.

The significant parts in the human eye structure are retina, optic disc, and blood vessels. The retina's function is similar to the film in a camera. The optic-head is the place from where all the vessels emerge and to where the brain connects. There are two types of vessels, an artery and a vein. A vein is the smaller vessel whereas an artery is the larger.

Diabetic Retinopathy is the major reason of blindness. Its main signs include bulges (microaneurysms) and connections with each other (intraretinal microvascular anomalies) and/or leak fluid (edema), protein deposits (exudates), blood (hemorrhage), or puffy white patches on the retina (cotton wool spots). The Diagnosing of this disease depends on the repetitive examination of retinal images to assess the presence of abnormalities and monitoring their progression.

The Retinal Abnormalities can be classified into two groups, pathological abnormalities and artefacts. For instance, the pathological abnormalities of diabetic retinopathy include micro-

aneurysms, hemorrhages, exudates, cotton wool spots, abnormal blood vessels and edema. In contrast, the common artefacts are eyelash, floater, and grease.

The retinal image is a picture taken of the back of the eye. Its clarity depends on a camera resolution and the surrounding lighting. The high contrast and clear visibility of the common structures of a retinal image are the most significant factors that distinguish among different images.

There are many issues regarding developing an automatic system that aids ophthalmologists in their diagnostic process. This shows the reason or the importance of this research. These issues include the necessity of an auto, fast and accurate retina examination; the shortage of professional ophthalmologist in some countries; the errors in diagnosis and lack of ophthalmological follow-up; the urgent necessity of the accurate and early discovery of the disease causing blindness, as a result of the large and growing number of visually impaired people around the world, the variety of illnesses causing blindness, and the cost of sight loss; The development of such system is still under study and continuous.

## **Chapter 3 – Colour Distance Measurement**

### **Overview**

The chapter explains the process of colour difference calculation in digital images. It starts with clarification of some basics of colour science such as colour attributes, colour spaces, opponent colours, examples of common colour spaces such as LAB and HSV, Euclidean distance, and maximum colour difference. Then, it presents an introductory explanation for colour image difference, followed by some examples of some of its applications. Next, it shows some issues or considerations that should be taken into account during the development of such methods. Subsequently, the algorithm, developed in this research, is illustrated. At the end of the chapter, the overall discussion and conclusion are given.

### **3.1 Introduction**

The process of calculating colour difference is one of the important studies in colour science. Such studies are continuing to develop an efficient way to calculate the colour difference between two materials each material has several different colours as in the digital images.

The measurement of colour difference between retinal images is required in this research. It is one of the key processes needed to achieve image registration to find the best displacement or match between two points, each one in an image. Therefore, finding an effective method for such measuring is worthy of study and development.

### **3.2 Colour Science Principles**

According to what are reported in the doctoral dissertation of Matković(1997), it is necessary to have sufficient knowledge that enables to understand the methods of calculating colour difference. This knowledge must include at least the basic principles of colour science, radiometry, human vision, and photometry. There are many resources regarding these conceptions such as the books of Hunt (1992, cited in Matković, 1997), Boynton (1992, cited in Matković, 1997), and Wyszecki and Stiles (1982, cited in Matković, 1997). There are three factors that influence the principle of human vision of the things surrounding the human being. These factors are object characteristics, the human observer, and lightness. First of all, it is the characteristics of a material. For example, some of materials have a yellow colour,

whilst some of the others are white. The second factor, the human observer, is a person who notices or watches an object. It is difficult to describe how human beings feel a colour. A person can distinguish among the different colours and recognize the similarity or difference among the colours of the materials and determines the extent of this similarity or difference, to be large, small, or medium. The last of these factors, it is a lightness. In the case of the absence of light, the human being can not see. Under different lighting conditions, the perception of things varies from person to person. For instance, the same material could be seen with more than one colour from several people in different lighting conditions. Some of them may see it red in daylight, whereas others could see it blue in a dim light in the dark of the night.

Furthermore, as stated by Matković(1997), the light is known as electromagnetic waves ranging from low to high frequency waves. The low frequency waves are such as visible light, microwaves, ultraviolet light, and infrared. In contrast, gamma rays and x-rays are examples of high frequency ones. The human eye only distinguishes visible light while the rest of the waves need special devices to identify them. The wavelengths of the visible spectrum ranged from 380 to 770 nm. The science of light measurement is known as radiometry. In comparison, the photometry is the science of visible light measurement depending on the sensitivity of the human eye. Both of radiometry and photometry do not take into account colour measurement. However, colour measurement is done through colourimetry which is the science of colour measuring.

Colour Science is full of many techniques, concepts, and scientific subjects that must be aware of, to understand this science and to be able to conduct scientific researches regarding this science. Some of these concepts are Colour Attributes, Colour Spaces, Opponent Colour Spaces,  $L^*A^*B^*$  Colour Space, HSV Colour Space, Colour Difference Metric, Euclidean Distance, and Maximum Colour Difference.

### **3.2.1 Colour Attributes**

As clarified by Bora, Gupta, and Khan (2015), the colour is identified by some colour appearance parameters. The main of these parameters can be listed as the following:

- Colourfulness: It is the attribute that determines how much the amount of colour is apparent. Is It more or less chromatic?

- Hue: It is the visual sense in which the colour is described as similar to or different from that of the red, yellow, green and blue.
- Brightness: It can be defined as the attribute that determines how much light is displayed in the visible colour.
- Saturation: It is another main property of a colour. it is the chromatic amount relative to the brightness amount.
- Lightness: It is a feature that determines how bright the colour is, relative to the white colour.
- Chroma: It is the degree of colour fullness which is relative to white luminous brightness.

### 3.2.2 Colour Spaces

The range of colours are represented in a colour space. A colour space is an abstract mathematical model. It is also called a colour model or a colour system. It describes the representation approach of colours. The range of colours are represented as tuples of numbers, typically as triples such as in RGB, Lab, and HSV or as quadruples such as in CMYK (ArcSoft, 2016 ). Each of these tuples represent one of colour attributes

such as Red level, Green level, Blue level in RGB colour space, or Hue, Saturation, and Value in HSV colour space. There are many resources illustrating different colour spaces and conversion methods among them such as in the documentation of OpenCV(2015). In addition to the paper of Saffarzadeh, Osareh, and Shadgar (2014) which clarified Weber Space.

Furthermore, there are many researches regarding developing new colour space. For example, the colour space of Johnson, Song, Montag, and Fairchild (2010) and the oRGB colour space of Bratkova, Boulos, and Shirley (2009). At the same time, there are some studies looking for the best colour space that can be used for a particular application. For example, Bora, Gupta, and Khan (2015) compared the performance of  $L^*A^*B^*$  and HSV colour spaces. The aim of their study is to see which colour space is better for the process of colour image segmentation. The result of the study found that HSV was better than Lab for colour Image Segmentation by using Watershed algorithm. And HSV is more suitable for dealing with segmentation of noisy colour images. Furthermore, there are other studies looking for the best components, that are in colour spaces, have the best representation of a colour. The common components include Red R, Green G, Blue B, Hue H, Saturation S,

Value V, Intensity I, Luminosity L, Chromaticity a, Chromaticity b, Chromaticity u, and Chromaticity v. For instance, Zhou, Li, Lin, Liang, and Liu (2014) concluded that the best colour components for representing a colour are Saturation, Intensity, and Value, S,I, and V, respectively. Also, they found the colour components of Intensity I and Luminosity L are very close because their correlation coefficient approximates to one.

### **3.2.3 Opponent Colour**

At the end of the nineteenth century, Hering (1964) proposed the principles of opponent colours. Hering assumed that there are six primary colours which can be seen. He categorized to two sets. The former is achromatic colours, whereas the latter is chromatic ones. Achromatic colours include black and white. Whilst chromatic colours are green, red, blue, and yellow. These colours are the basis of the formation of opponent colours which are represented in three pairs of colours, white and black, red and green, and yellow and blue (Johnson, et al., 2010). The principle of opponent colours can be proved by that the colours of redish-greens, or bluish-yellows cannot be perceived by the human eye.

There are several researches that have proven the importance of using the opponent colour concept in various applications or processes. For instance, Johnson, Song, Montag, and Fairchild (2010) addressed this technique during their experiments related to their research entitled “Derivation of a colour space for Image colour Difference Measurement”. They presented a review of opponent colour spaces. In addition to developing new opponent colour space. Johnson, Song, Montag, and Fairchild (2010) clarified the need for orthogonality, opponent colour spaces, in image difference calculations. There are many attempts to create a new opponent colour space such as the colour space invented by Johnson, Song, Montag, and Fairchild (2010) and the oRGB colour space that is proposed by Bratkova, Boulos, and Shirley (2009). One of the widespread opponent colour spaces is L\*A\*B\* colour space. It is commonly used in image analysis techniques.

### **3.2.4 L\*A\*B\* Colour Space**

L\*A\*B\* colour space is defined by CIE in 1976. In fact, there is two Lab colour space. The former is created by Hunter according to his two published papers (Hunter,1948a, cited in Bora, Gupta, & Khan, 2015) (Hunter,1948a, cited in Bora, Gupta, & Khan, 2015). The latter is the colour space that is commonly used these days. The stars were placed in the



abbreviation to distinguish it from the term of Hunter. Also, it is known as CIE L\*a\*b\* 1976 colour space or CIELAB. This colour space is made of three dimensions. The first one, L-component, determines the degree of luminance, lightness. While other dimensions are chromaticity layers. A-component specifies the degree of colour in the range between the red colour and green colour, whilst B-component indicates the degree between the blue and the yellow. Lab colour Space is one of the colour spaces that depend on opponent colours. It contains two dimensions, a-component and b-component, representing opponent colours. The a-component represents green and red opponent colours, whereas b-component is for blue and yellow. When the value of A is positive, it means that the colour is approaching the red colour, while if it is negative means that the colour is approaching green. In comparison, B-value will be negative when the colour approaches the yellow and be positive when is close to the blue colour. In contrast, L-value is always positive. Its value ranges from 0 to 100. A zero indicates the black colour, whilst a hundred indicates the white. One of the most significant features of L\*A\*B\* colour space, is that, it is considered as a device independent (Bora, Gupta, & Khan, 2015) (OpenCV,2015). Furthermore, OpenCV (2015) shows the conversion methods from L\*A\*B\* colour space to other colour spaces.

### **3.2.5 HSV Colour Space**

It consists of three dimensions. The first one is H-component. It stands for Hue. The hue value represents an angle ranging from 0 to  $2\pi$  for the red colour axis. Its value is zero or  $2\pi$  at the red,  $2\pi/3$  at the green, and  $4\pi/3$  at the Blue. The next dimension is S-component which indicates the saturation of a colour. The saturation expresses the amount of hue relative to white colour. It can be considered as the purity of a colour. Its values are in a radial measurement. The value of saturation ranges from zero to one. At the centre of axis, S-value equals zero, whereas at the outer surface it is one. The third channel is V-component. The letter V is the first letter of the word value. It expresses the value of the luminous light of the colour. It is measured in percentage, from 0 to 100. For instance, the colour is bright when the value is high and the hue is red, whereas the colour is dark in the case of the value is low (Bora, Gupta, & Khan, 2015) (OpenCV,2015). The formulas of conversion from HSV to other colour spaces are illustrated in documentation of OpenCV (2015).

### 3.2.6 Colour Difference Metric

One of important metrics in the colour science is the difference or distance between two colours. This metric is used to quantify the perceptual difference between colours.

### 3.2.7 Euclidean Distance

The Euclidean distance is the standard and basic equation for calculation of the colour difference within a colour space. The RGB colour space is represented as a 3-tuple. Each colour has three values, Red, Green, and Blue values. Basically, Euclidean distance can be used to compute the colour difference in such RGB colour space between these two colours. By knowing the values of colour component: r for red, g for green and b for blue, the formula of Euclidean distance is as the following:

$$\text{diff} = \sqrt{(r_2 - r_1)^2 + (g_2 - g_1)^2 + (b_2 - b_1)^2}$$

For instance, by using Euclidean equation, the calculation of the difference in colour between (0, 0, 0) and (1, 1, 1), is

$$\text{diff} = \sqrt{1 + 1 + 1} = \sim 1.73$$

This difference cannot be distinguished by human eye,

### 3.2.8 Maximum Colour Difference

Technically, maximum colour difference is the permissible distance between two colours so that they can be considered as similar; in other words, if the difference between two colours is greater than this distance, they are not similar. For instance, by using Euclidean distance, the colour difference between black and white colours is  $\sim 441.67$ . So, if a solid black image is compared with a white one and the Max colour Difference is set to be 441.67, the result will be positive, that means the images match.

### **3.3 Colour Image Difference**

In some applications, there is a need to calculate the difference between all colours of two images. This difference shows how close or different the two images are. At the same time, such difference clarifies that there are changes in one of the two images compared to the other. For instance, some medical systems need to identify the colour distance between specific area in both medical images. The value of this distance indicates the illness progress or existence of an abnormal object. In some other systems, this technique is used as a feature extraction method or as a filter; for example, in pattern recognition systems such as detecting a face of a person among huge dataset of stored faces. Nevertheless, the approaches for these requirements, are still under research and study.

As mentioned in the dissertation of Matković (1997), an effective photo scale is needed with digital image technology. For instance, this measure is used to assess the progress in the development of digital image processing methods. The other use of it, is in comparison of images taken from several different devices. This comparison clarifies whether there are details existing in one of the images and not in the others. Another example is searching for a specific image. This process involves searching for the best image similar to the target image among a huge database of stored images. Matković (1997) reported that the human way of comparing images is not by calculating the average of differences between each pixel in both images. He also stated that the scale that will be used in the comparison of images must distinguish the difference among images as distinguished by the human eye. Another finding of him, the use of luminance pixel data alone will result in inaccurate calculation of the differences between the colours.

### **3.4 The Related Works of the Calculation of the Colour Difference between two Colour Images**

The process of colour difference calculation is still under research and development, as stated in the book of Zhan, Zuo, and Li (2016, p.61): “Currently, there is not any formula to measure the colour difference between two colour images directly, while there is only formula to calculate the colour difference between two specific colour tristimulus values”. Tristimulus values are the values that together represent a particular colour and are three values.

The works regarding the colour difference among images, can be classified into four groups depending on the used techniques.

First group depends on using some approaches related to signal processing. The examples of this are the two studies carried out by Jacobs et al. (1995, cited in Matković, 1997) and Gaddipati et al. (1997, cited in Matković, 1997) which use wavelet transform. In addition to the approach of Rushmeier, Ward, Piatko, Sanders, and Rust (1995, cited in Matković, 1997) which is an example of using Fourier transformation. An image is broken up into some chunks, and each chunk gets split up separately. Fourier transforms split a chunk up into its frequencies. These frequencies refer to some fundamental properties of the image. For instance, a set of frequencies could be used to determine how light or dark each pixel is, and other sets for the colour, for example one for red-green, and another for blue-yellow. The number of frequencies used for each chunk determines the image quality. For colour image, it can be cleaved to three different images, its Red, Green, and Blue components. Each of those can be processed with a Fourier Transform independently. The colour difference is measured by comparing the corresponding frequencies calculated by Fourier Transform.

The second one depends on computing of an average, for example, as in the proposed methods of Matković (1997), Zhan, Zuo, & Li (2016)'s algorithm, and the approach of Hong and Luo (2006).

The next category includes those which are based on Histogram such as in the work of Hong and Luo (2006), and the paper titled "Comparison of histograms of data banks" (Smirnov, 1996), this paper presents a developed correlation method for histograms comparison of meteorological data banks.

The last group contains the works of those that use Delta-E formula. This is exemplified in the work undertaken by Bubak, Albada, Sloot, and Dongarra (2004).

### **3.4.1 The Related Works based on Techniques of Digital Signal Processing**

Some of the processes of digital signal processing are used in some proposed algorithms that are relevant to image processing. In particular to those related to frequency analysis such as Fourier or Wavelets Transform. Matković (1997) presented, in his Phd dissertation, some examples involving image transformation to Fourier (Rushmeier, Ward, Piatko, Sanders, & Rust, 1995, cited in Matković, 1997) or wavelet space (Gaddipati, Machiraju, & Yagel, 1997, cited in Matković, 1997). Subsequently, complex comparisons will be performed. Rushmeier, Ward, Piatko, Sanders, and Rust (1995, cited in Matković, 1997) presented several algorithms for luminance images comparison depending on image compression techniques and

developing new metrics calculated in Fourier space. These developed measures can be used only for Gray scale images as they rely on luminance images that do not contain all colour information. For colour image, it can be divided to three Gray scale images, its Red, Green, and Blue components. The transformation to wavelet space has been exemplified in a paper by Jacobs, Finkelstein, and Salesin (1995, cited in Matković, 1997), and in a paper by Gaddipati, Machiraju, and Yagel, 1997, cited in Matković, 1997). Jacobs et al. (1995, cited in Matković, 1997) presented a querying method depending on the wavelet transform, whereas Gaddipati et al. (1997, cited in Matković, 1997) proposed a wavelet based metric. This metric is computed from an image. Then it is converted to CIE LUV. The L-component of this metric is only used in their proposal. Overall, signal processing-based approaches for image comparison use frequency analysis techniques such as Fourier or Wavelets Transform. They convert an image to a set of frequencies. These frequencies refer to some fundamental image pixel properties such as a contrast and a colour. In other words, instead of dealing with image pixels, frequencies will be used.

### **3.4.2 The Related Works based on Average Calculation**

Some suggested methods depend mainly on the calculation of the average to compute colour difference. The process of calculating of the average varies from one method to another. Some methods calculate the average of the entire image while the other calculate it in specific areas of an image. Each method depends on a certain colour space.

#### **3.4.2.1 The Matković 's Algorithm (1997)**

Matković (1997) proposed a Colour Image Difference algorithm in his PhD thesis, entitled "Tone Mapping Techniques and colour image Difference in Global Illumination". The concept of this method is to calculate the weighted average of colour difference for pairs of parts of an image. These parts are in the form of randomly selected rectangles of various sizes with taking into account some considerations. The average calculation process for each rectangle is in the CIE XYZ colour space. Then, the final form of the average colour is converted to CIE LUV space. In the end, the colour difference is computed by using the CIE LUV colour difference formula as following:

$$\Delta E^* = \sqrt{(\Delta L^*)^2 + (\Delta u^*)^2 + (\Delta v^*)^2}$$

Matković (1997) reported that the reason of using CIE LUV space rather than other colour space, is due to its characteristic of colours uniformity, in particular, it is more uniform than CIE XYZ colour space. And any noise in the image that cannot be highly distinguished by the

human eye will automatically be ignored by using the contrast sensitivity function suggested by Mannos and Sakrison (1974, pp. 525-535, cited in Matković, 1997)

#### **3.4.2.2 The Zhan, Zuo, & Li (2016)'s Algorithm**

This is an algorithm proposed in Zhan, Zuo and Li's book (2016, pp. 53-61). The main idea of this algorithm is to calculate the Euclidian distance of two average colours in CIE XYZ colour space. This algorithm is designed to be used as evaluation criteria. Their book explains some approaches of colour correction on tongue images, and then it shows their evaluation results. These tongue images are shown before and after correction, therefore the colour difference can be recognized by the human eye. Nevertheless, as declared in this book, the assessment of the subjective evaluation, which is based on the human sight sense, is hard to quantify. Consequently, other quantized assessment methods must be devised to calculate the colour distance among these tongue images. The proposed algorithm, in this book, depends on computing the average colour in each image. Subsequently, the colour difference is measured by calculating the difference between two average colours. Actually, this algorithm involves three operations. Firstly, the colour space transformation of the images from RGB to CIE XYZ. Then, the calculation of colour centre. Finally, the colour difference is computed by calculating Euclidian distance to the calculated colour centre.

#### **3.4.3 The Related Works based on Histogram Calculation**

A histogram is diagram representing a distribution of numerical data. Its horizontal line represents the range of values (bin). The entire range of values are divided into a series of intervals. The vertical line of the histogram chart is number of values fall into each interval (frequency) (Pearson, 1895) (Howitt & Cramer, 2008) .

There are some approaches depending on Histogram data to calculate the colour difference. These methods have been exemplified in the algorithm of Hong and Luo (2006), the algorithm of Lee and Plataniotis (2014), and the five methods of Histogram Comparison algorithm (OpencvDev.Team, 2017) (Doxygen, 2017).

### 3.4.3.1 The Approach of Hong and Luo (2006)

The title of the paper for this method is “New algorithm for calculating perceived colour difference of images”. This algorithm is reported in the survey of (Mokrzycki & Tatol, 2012). It is the approach of (Hong & Luo, 2006). They proposed an algorithm to compute the perceived colour distance. The suggested method was developed depending on their experiments with comparing of image colours. They reached four conclusions. Firstly, the value of the difference between the colour of the image can be computed from the calculation of the average of the sum of the colour differences between the corresponding points in both images. Second finding is that the colour that fills a larger area, must has a larger weight than the colour that occupies less space. Thirdly, the large colour differences between image pixels should be calculated in a better and accurate way. The last conclusion is that the colour shade should be taken into an account because it is one of the significant characteristics in the graphic technique. The proposed algorithm involves seven operations. At first, every pixel is converted from Lab colour space to  $LC_{ab}H_{ab}$  colour space. The image histogram for channel  $H_{ab}$  is then calculated. This graph, histogram, represents the number of occurrences of each hue value. The histogram data are stored in in the table  $hist[hue]$ . Subsequently, the hist table is sorted in ascending order. Next, the sorted table is divided into four parts according to the following conditions:

- The first  $n$  of the hue values in the hue table, in the case of  $\sum_{i=0}^n hist[i] < 25\%$  , will be  $hist[i] = hist[i] / 4$
- The next  $m$  of the hue values in the hue table, in the case of  $\sum_{i=n+1}^{n+m} hist[i] < 25\%$  , will be  $hist[i] = hist[i] / 2$ ;
- The next  $L$  of the hue values in the hue table, in the case of  $\sum_{i=n+m+1}^{n+m+L} hist[i] < 25\%$  , will be  $hist[i] = hist[i]$ ;
- The rest of the hue values in the hue table, will be  $hist[i] = hist[i] * 2.25$ ;

The colour difference average is calculated for each hue value in an image. These averages are stored in table  $CD[hue]$ . Then  $CD_{image}$  , the overall colour difference average, is computed by the equation:

$$\sum hist[hue] * \frac{CD[hue]^2}{4}$$

### 3.4.3.2 The Approach of Lee and Plataniotis (2014)

In this paper, a new evaluation method is proposed based on the value of colour hue. This method involves initial processing using CSF filtering. CSF stands for contrast sensitivity function. Then, deriving hue histogram for each of the two images that will be tested to compute the colour difference between them. Subsequently, calculating the colour difference between the two images by computing the distance between the derived hue histograms. This distance, the overall difference, is calculated by using the suggested formula of this proposed method. The proposed equation is defined as the following:

$$CD_H(\mathbf{X}, \mathbf{Y}) = \frac{1}{M \times N} \sum_{i=1}^M \sum_{j=1}^N CD_H(x_{i,j}, y_{i,j})$$

Where  $CD_H(x, y) = d(\text{hist}(x), \text{hist}(y))$ , and  $d(\cdot)$  is a histogram Quadratic-Form (QF) distance measure. The Quadratic-Form distance is defined as:

$$QF^A(P, Q) = \sqrt{(P - Q)^T A(P - Q)}$$

Where P and Q be two histograms and A the bin-similarity matrix (Hafner, et al., 1995).

QF distance was used for two reasons. The former is that similarity or dissimilarity among hue values can be modelled. And the latter is that it is a cross-bin distance that can be calculated effectively and without depending on the size of quantization. According to experiments, it was concluded that this proposed measurement is particularly effective against colour distortion in image.

### 3.4.3.3 The Histogram Comparison algorithm

This algorithm is one of the common approaches to compare two histograms. It is to calculate a numerical parameter expressing how closely the two histograms, H1 and H2, are matched. This parameter is defined as  $\mathbf{d}(\mathbf{H1}, \mathbf{H2})$ . This algorithm has five different metrics used to compare two histograms. These metrics or methods are Bhattacharyya or Hellinger, **Chi-Square**, **Alternative Chi-Square**, Correlation, and Intersect (OpencvDev.Team, 2017) (Doxygen, 2017). The formulas of these metrics are as in the following table:



Metric	Formula
Bhattacharyya	$d(H_1, H_2) = \sqrt{1 - \frac{1}{\sqrt{\bar{H}_1 \bar{H}_2 N^2}} \sum_I \sqrt{H_1(I) \cdot H_2(I)}}$
Chi-Square (Chisqr)	$d(H_1, H_2) = \sum_I \frac{(H_1(I) - H_2(I))^2}{H_1(I)}$
Alternative Chi-Square (ChisqrAlt)	$d(H_1, H_2) = 2 * \sum_I \frac{(H_1(I) - H_2(I))^2}{H_1(I) + H_2(I)}$
Correlation	$d(H_1, H_2) = \frac{\sum_I (H_1(I) - \bar{H}_1)(H_2(I) - \bar{H}_2)}{\sqrt{\sum_I (H_1(I) - \bar{H}_1)^2 \sum_I (H_2(I) - \bar{H}_2)^2}}$
Intersect	$d(H_1, H_2) = \sum_I \min(H_1(I), H_2(I))$

Table 3.4.3.3 – 1: The formulas of the Histogram Comparison metrics.

where

$$\bar{H}_k = \frac{1}{N} \sum_J H_k(J)$$

and N is a total number of histogram bins.

For the resulting value from Correlation or Intersection method, where the value is greater, the matching is greater. Conversely, for the rest of the method, where the value is close to zero, there is more matching (OpencvDev.Team, 2017).

#### 3.4.3.4 The Evaluation of Histogram Comparison metrics within different colour spaces for retinal images

The Histogram Comparison algorithm is used in this research within an evaluation method.

Such method is to evaluate the colour mapping approach developed in this study.

Histogram Comparison algorithm have five methods. Thus, it is necessary to know the best method from them and the best colour space which can be used together to calculate the color difference between two retinal images. To accomplish this, eight different retinal images have been selected, on the basis of the difference in the color of retina background, from Messidor dataset. On other words, eight images having different retina colour have been used. These images are as in the following figure.



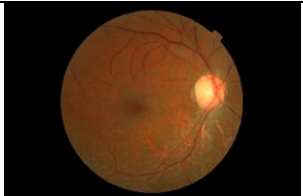





Image number	Image	Image number	Image
1		5	
2		6	
3		7	
4		8	

FIGURE 3.4.3.4 - 1: THE SELECTED EIGHT RETINAL IMAGES FROM MESSIDOR DATASET

Subsequently, two tests are achieved. In both of these tests, each selected image is tested with itself and with other selected images. The second test involves applying Histogram Specification algorithm (Wang, 2013). This is to make the colours of both tested images are close. On other words, second image's colours of each pair are converted to the colours of the first image with the same pair. In contrast, the first test uses the actual images without any modification. Therefore, the colour distance between a pair in test-2 must be less than that between the same pair in test-1.

The following three table show the overall results of implementing the two tests for the evaluation of Histogram Comparison algorithm in its five metrics. Each table represents the results implemented in a specific colour space: BGR, Lab, and HSV. These results have been

obtained by using a computer with a Processor: Intel core (TM) i5 at 2.4GHz, and memory (RAM) of 8 Gigabyte.

The letter “T” is Elapsed Time Average in second for implementing a method and D is Colour Distance Average calculated by a method. The small letter “w” refers to the Average is calculated without considering or taking the results of the tests between the same image, an image with itself. While, the small word “all” indicates the all results are included in the calculation. Therefore, both  $T_w$  and  $D_w$  are computed without testing for the same image. While,  $T_{all}$  and  $D_{all}$  are computed for all tests. D1 is either  $D_w$  or  $D_{all}$  from test1, whereas D2 is from test2. T2 is either  $T_w$  or  $T_{all}$  from test1, whereas T2 is from test2. The maximum Colour Distance is indicated by  $D_{max}$ .

To determine the success of a tested method, three conditions are specified. The first one is that there is a noticeable difference between each two corresponding results in test-1 with test-2. The second requirement is that each result in test-1 must be greater than the corresponding result in test-2, except for Correlation and Intersection methods. The second condition for Correlation and Intersection is that each result in test-1 must be less than the corresponding result in test-2. The reason for this difference regarding Correlation and Intersection is due to whenever the value of the test result is the biggest whenever there is more matching, whereas the opposite in the other metrics which is where the value is close to zero, there is more matching. In the last condition, the result of self-testing, an image with itself, must equal zero.

The first next table is for BGR colour space. Its results clarify that the Histogram Comparison algorithm in all its metrics has failed or is unsuccessful for the calculation of colour distance. All metrics have a number of failed tests as shown in the table. In contrast, for Lab colour space, Bhattacharyya and ChisqrAlt do not have any number of failed tests, as shown in the next second table. However, the corresponding results, by Bhattacharyya, are very close. The difference between colour distance average is 0.15 for  $D_w$  and 0.12 for  $D_{all}$ . Consequently, Bhattacharyya is not suitable for using as a colour distance metric. ChisqrAlt is the only metric that can be used to calculate colour difference in Lab colour space. While, ChisqrAlt and Intersect metrics are the successful methods for computing colour difference in HSV colour space, according to the third table results.

Metric	Test-1					Test-2					Number Of Failed Tests	Notes
	D <sub>w</sub>	D <sub>all</sub>	D <sub>max</sub>	T <sub>w</sub>	T <sub>all</sub>	D <sub>w</sub>	D <sub>all</sub>	D <sub>max</sub>	T <sub>w</sub>	T <sub>all</sub>		
Bhattacharyya	0.69	0.52	0.72	8.26	13.23	0.65	0.48	0.91	22.85	20.93	4	D1>D2, T1<T2
Chisqr	55737.02	41802.77	104357.31	8.73	8.44	7588451.21	5691338.41	64281990.96	18.45	19.21	18	D1<D2, T1<T2
ChisqrAlt	175174.95	131381.21	192881.34	4.93	9.74	170954.31	128215.73	311970.21	24.98	21.02	4	D1>D2, T1<T2
Correlation	0.91	0.93	1	7.44	7.44	0.75	0.81	1	20.74	20.74	7	D1>D2, T1<T2
Intersect	41212.95	53177.03	90000	9.70	9.70	40557.9	52685.75	90000	21.15	21.15	4	D1>D2, T1<T2

Table 3.4.3.4 - 1: The comparison among the results of the Metrics used in Histogram Comparison algorithm in BGR colour space.

Metric	Test-1					Test-2					Number Of Failed Tests	Notes
	D <sub>w</sub>	D <sub>all</sub>	D <sub>max</sub>	T <sub>w</sub>	T <sub>all</sub>	D <sub>w</sub>	D <sub>all</sub>	D <sub>max</sub>	T <sub>w</sub>	T <sub>all</sub>		
Bhattacharyya	0.68	0.51	<b>0.72</b>	10.38	16.71	0.53	0.39	<b>0.61</b>	20.46	26.69	0	D1>D2, T1<T2
Chisqr	9802707.94	7352030.95	28324322.08	8.72	7.44	3193481.85	2395111.39	28368765.69	17.32	14.93	10	D1>D2, T1<T2
ChisqrAlt	174024.32	130518.24	190630.08	5.57	7.14	119607.19	89705.39	160505.28	19.90	22.31	0	D1>D2, T1<T2
Correlation	0.95	0.96	1	11.61	11.61	0.94	0.95	1	24.00	24.00	11	D1>D2, T1<T2
Intersect	42094.33	54070.75	90000	10.63	10.63	51735.57	61301.67	90000	24.77	24.77	1	D1<D2, T1<T2

Table 3.4.3.4 - 2: The comparison among the results of the Metrics used in Histogram Comparison algorithm in Lab colour space.

Metric	Test-1					Test-2					Number Of Failed Tests	Notes
	D <sub>w</sub>	D <sub>all</sub>	D <sub>max</sub>	T <sub>w</sub>	T <sub>all</sub>	D <sub>w</sub>	D <sub>all</sub>	D <sub>max</sub>	T <sub>w</sub>	T <sub>all</sub>		
Bhattacharyya	0.87	0.65	<b>0.91</b>	9.07	9.58	0.70	0.53	1	20.09	22.70	1	D1>D2, T1<T2
Chisqr	61549.25	46161.94	148444.22	7.20	10.17	504838.74	378629.05	2174394.57	21.05	28.40	19	D1<D2, T1<T2
ChisqrAlt	169138.85	126854.13	185982.87	7.28	8.52	110742.32	83056.74	140139.03	19.56	22.65	0	D1>D2, T1<T2
Correlation	0.68	0.76	1	10.63	10.63	0.65	0.73	1	22.41	22.41	5	D1>D2, T1<T2
Intersect	10983.24	21914.82	61773	7.06	7.06	18965.76	27901.71	61773	20.01	20.01	0	D1<D2, T1<T2

Table 3.4.3.4 - 3: The comparison among the results of the Metrics used in Histogram Comparison algorithm in HSV colour space.

According to the results shown in the three previous tables, the minimum processing time is 4.93 seconds in BGR by ChisqrAlt, 5.57 seconds in Lab by ChisqrAlt, and 7.06 seconds in HSV by Intersect. Consequently, these approaches could be considered as fast methods comparing with other Histogram Comparison methods with different color spaces.

The next figure expresses the findings from this study. It presents the most proper metrics of Histogram Comparison algorithm that can be used as a colour distance measurement within

specific colour space. This conclusion has been reached according to their evaluation tests results as shown in the averages of the colour distances and processing times. *It can be concluded that Histogram Comparison algorithm by ChisqrAlt within Lab colour space is the most accurate and the fastest comparing with other four Histogram Comparison methods, and Lab is the most convenient colour space through which the colour difference between images can be calculated more accurate and faster by using Histogram Comparison techniques comparing with other colour spaces such as BGR and HSV.*

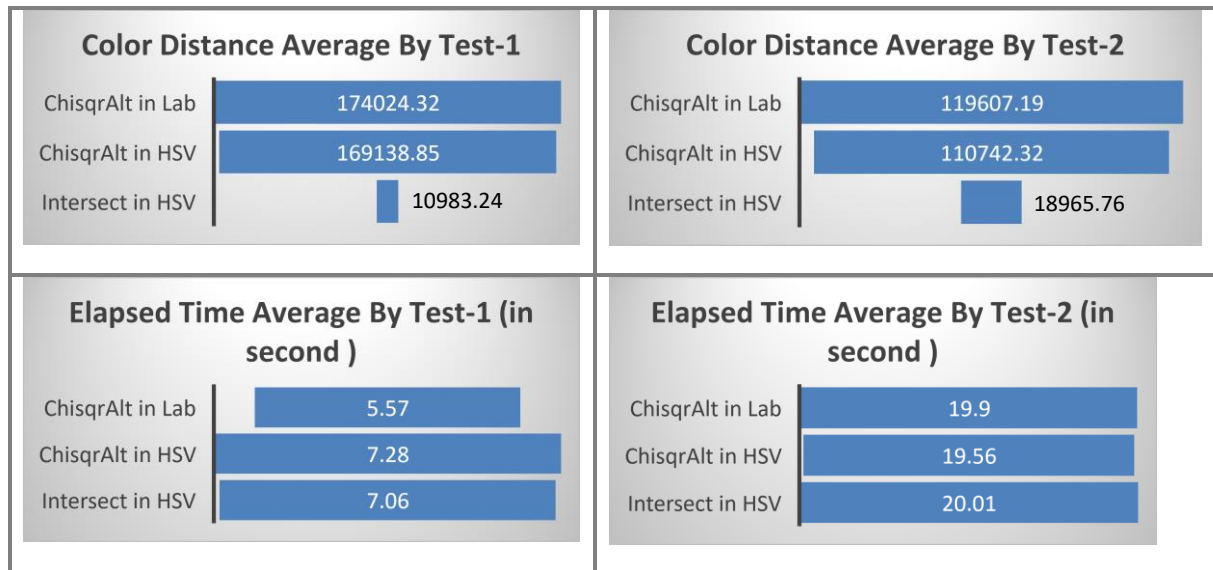


FIGURE 3.4.3.4- 2: THE AVERAGES OF THE COLOUR DISTANCES AND PROCESSING TIMES IN THE TWO TESTS BY THE PROPER METRICS OF HISTOGRAM COMPARISON ALGORITHM WITHIN SPECIFIC COLOUR SPACE.

### 3.4.4 The Related Works based on Specific formula

These works depend on using specific formula. This formula is either common or proposed equation. The common formulas, that are used in some approaches are, Delta-E or EMD. The usage of EMD has been exemplified in two proposed algorithms: The former is by Orlova and et al.(2016) and the latter is by Shishibori, Koizumi, and Kita (2011). Orlova and et al.(2016) presented a flow cytometry data analysis depending on EMD, to measure biomarkers changes. The measurement of such changes is considered as one of the methods used to diagnose or treat several diseases or to study the growth of living cells. In contrast, Shishibori, Koizumi, & Kita (2011) introduced a EMD-based technique for quick retrieval of similar elements from a huge database.

Despite, Delta-E is mainly used as a common method for calculating the colour difference between two uniform colour s, there are some other methods using it for calculating the

chromatic difference between images. One of these approaches is suggested by Bubak, Albada, Sloot, and Dongarra (2004, pp. 37-40).

#### **3.3.4.1 The Measurement of the Accuracy of an Image Processing Operation (Bubak, et al., 2004)**

The conference proceedings by Bubak, Albada, Sloot, and Dongarra (2004, pp. 37-40), in the experiments section, highlighted another example of an application that requires the computation of colour distance. This application aims at measuring the accuracy of a filter. The experiment involves three processes. Adding some noise on an image, obtained from a public image data set. Then applying a specific filter on the corrupted image, to get rid of the noises in this image. In the end of this application, the filtered image is compared with the original image by computing the accuracy of this filter. The filter accuracy is calculated by using signal-to-noise ratio, SNR. For a pair of colour images, this ratio is defined by the following equation:

$$\text{SNR} = 10 \log_{10} \frac{E[\mathbf{f}_i^T \mathbf{f}_i]}{E[\mathbf{n}_i^T \mathbf{n}_i]}$$

Where  $\mathbf{f}_i$  is a colour vector, and  $\mathbf{n}_i$  is the noise vector calculated by the vector distance between two pixels. Therefore, it requires calculating colour distance between two pixels to compute the noise vector,  $\mathbf{n}_i$ , of this ratio. The formula of CIE94 is used for this requirement. CIE94 is used to quantify the colour difference between two colours. It is a CIELAB-based color-difference formula, developed by the CIE Technical Committee (CIE Central Bureau, 1995).

#### **3.3.4.2 The Template Matching algorithm**

Template matching (Brunelli, March 2009) “is a technique for finding areas of an image that match (are similar) to a template image (patch). While the patch must be a rectangle it may be that not all of the rectangle is relevant. In such a case, a mask can be used to isolate the portion of the patch that should be used to find the match.” (OpenCV, 2020).

There are six comparison methods used for Template Matching. They are: Square Difference (SQDIFF), Normalized Square Difference (SQDIFF\_NORMED), Correlation coefficient (CCOEFF), Normalized Correlation coefficient (CCOEFF\_NORMED), Cross Correlation (CCORR), Normalized Cross Correlation (CCORR\_NORMED) (OpenCV, 2020).

The Square Difference method uses Euclidian distance concept. It is the sum of squared differences between each pair of pixels. In contrast, Cross Correlation approach is a dot product operation. It is the sum of products between each pair of pixels, whereas, Cross Coefficient method is similar to Cross Correlation, except each pixel value is subtracted by a specific value before computing the dot product operation. A normalized method result equals the result of the corresponding non-normalized method divided by a specific factor.

### 3.5 The issues required to develop a new method for calculating a colour distance

The main issues or considerations required to develop a new method for calculating the colour distance between two retinal images can be listed into five items. These issues are colour space, accuracy, performance time, Image Details, and measurement formula.

The issue of colour space is concentrated on identifying the best colour space for the images in order to perform such calculation. Meanwhile, the developed algorithm should have accurate results obtained in the shortest possible time. Regarding Image Details, all data of image features must be included in colour distance measurement. The last point is what is the best equation can be used to compute the difference between two image data.

### 3.6 The Developed Similarity Measurement Algorithm

At the beginning, the two retinal images are converted to Gray scale following by Bitwise-Not operation. After that, the colours of the two images are normalized so that their colour values become between 0 and 255. Such image enhancement technique improves the clarity of image features or details. Subsequently, the similarity value is computed between two tested regions. The similarity is measured by Template Matching algorithm using normalized Cross Correlation method (Brunelli, March 2009) according to the following equation:

$$R(x, y) = \frac{\sum_{x',y'} (T(x', y') \cdot I(x + x', y + y'))}{\sqrt{\sum_{x',y'} T(x', y')^2 \cdot \sum_{x',y'} I(x + x', y + y')^2}}$$

Where I denotes image, T template, R result. The method compares the overlapped patch against template. The size of the overlapped patch is  $w \times h$ . The summation is done over template and/or the image patch:  $x'=0...w-1$ ,  $y'=0...h-1$  (OpenCV, 2020).

The similarity measurement is achieved within the overlap between the two tested areas. Taking into account, overlap area must be detected so that it does not include any background points. The presence of a black dot or a background point very negatively affects the outcome. Before measuring the similarity, colours of the tested area in the second image is normalized to the colours of the tested area in the first image (reference image). The computed Similarity Value is percentage value, ranged between 0 and 1. The number 1 means: the two areas are 100% matched.

Three different sizes are used for the test region within the developed algorithm. Firstly, the size: 157 x 157 pixels is used for calculating similarity value for each control point in the first image with each point in the second image. This calculation ignores small overlap. The number of pixels in the overlapped area must be greater than a quarter of the number of points in the tested area of the reference image, otherwise the Similarity Value equals -1 (not matched). In another meaning, in the case of there is small overlap, the similarity measurement will be ignored. The other two sizes are 97 x 97 and 177 x 177 pixels, which are used for the registration correction process. Such process does not ignore small overlap cases. The size of the test area is increased. Before similarity is measured, the overlap area is detected between the two tested areas. Then the height and width of the overlap are computed. If one of its dimensions is less than Small Dimension Limit, Feature (test area) Dimension will be increased as follows:

$$\text{FeatureDimension} = 2 * \text{FeatureDimension} - \min(h,w), \text{ where } h \text{ and } w \text{ are height and width of the overlap respectively.}$$

Through experiments, the best value of Small Dimension Limit is 95. That means the height and width of the overlap must be at least 95 pixels.

### **3.7 Discussion**

In terms of colour space, the argument regarding choosing a suitable colour space, in fact, depending on the type of application, for instance, food or medicine application. Some of colour spaces, such as RGB, are considered as not perceptually uniform. Therefore, the approach using Euclidean RGB distance metric, will not give results matching the human-perceived difference between colours. In contrast, Lab is designed to be a perceptually uniform colours space. Lab colour space is the most common colour space used to measure the colour distance. However, there are many developed colour spaces compatible with human cognition. It is noted that there are several colour spaces have been repeated in many methods developed to calculate the colour difference. These colour spaces include Lab, LCH,



HSV, and XYZ. Another example, Bora, Gupta, and Khan (2015) found that HSV colour space is better than  $L^*A^*B^*$ . However, this comparison is achieved only for colour image segmentation by using Watershed algorithm. One criticism of the approach of this comparison is that the obtained results may be unreliable or require further testing. Because of their dependence on testing only one image and they did not show that they tested more other images.

In addition, Zhou, Li, Lin, Liang, and Liu (2014) found that the best colour elements that can define a colour are Saturation S, Intensity I, and Value V. The strongest element is S followed by I and V. Furthermore, they concluded that the colour Intensity I and colour Luminosity L are very close. Although Zhou, Li, Lin, Liang, and Liu (2014) did not consider hue property of a colour to be one of the important colour characteristics, there were some algorithms that only relied on this feature with ignoring the other colour characteristics in their operations. Among these algorithms are the approach of Lee and Plataniotis (2014) and the approach of Hong and Luo (2006) which have been published in certified scientific papers. Consequently, the property of Hue must be taken into account.

On the question of digital images, there are many applications that require analyzing a whole image to identify the colour distance between images. The concept of the most existing developed works involves at least three key processes. The first one is a colour space conversion to specific colour space. The second operation is a calculation of specific parameter such as an average. The last one is a colour difference calculation using the computed parameters. This difference is calculated by using a specified formula. This formula can be one of the common equations such as Euclidian distance, or Delta-E, or it can be a new proposed formula. One consideration regarding image processing, is that the process of converting an image from one format to another can be another matter of argument, the original features of an image could be lost during this process.

With respect to Histogram, a Histogram diagram represents the number of repetitions of each colour in the image. This makes it use in statistical calculations such as computing the colour average such as in the approach of Hong and Luo (2006). The data of this graph can be used in such calculation, instead of dealing with each pixel in the image. In the case of there are many statistical calculations, there is no doubt that the performance of calculations based on the Histogram data is faster than those that depend on dealing with the image pixels in each process.

In terms of taking advantage of other techniques, some methods of electrical signals processing are used within the image processing technology. For example, some of the previous works for calculating colour difference have included converting the image to Fourier or Wavelets space. This motivates for further study and research to develop the processing and analysis of images. However, the converting of an image to Fourier or Wavelets space, could make the subsequent operations become more complex than if the image is in a colour space. Matković (1997) reported, in his Phd dissertation, that after transformation to Fourier or Wavelets space, the subsequent comparisons will be complex.

As regards shortcomings, there are notable drawbacks in some previous methods such as using part of the colour data as in the suggested method of Gaddipati et al. (1997, cited in Matković, 1997) and the approach of Hong and Luo (2006, cited in Mokrzycki & Tatol, 2012). The former just use L-component of a colour, whereas the latter only use H-component. The rest of the colour data was never used in both algorithms. Consequently, the results obtained from these proposed methods are expected to be not entirely accurate.

In case of average calculation, there is a criticism of how to calculate the colour average of an image to compute the colour difference. If the average is calculated by taking the overall mean of the colours of an image, the colour difference could be inaccurate. One of the suggestions for developing this process is as stated by Hong and Luo (2006, cited in Mokrzycki & Tatol, 2012). They proposed to calculate the average of the colour differences between the corresponding points in both images. This concept has been applied in the method of Bubak, Albada, Sloot, and Dongarra (2004, pp. 37-40). Therefore, it is expected, if the algorithm proposed in the book of Zhan, Zuo and Li (2016) is developed according to this suggestion, the result could be more accurate.

In contrast, the developed method, in this study, is based on calculating of the sum of multiplications between each pair of pixels values. It uses Normalized Cross Correlation method for Template Matching. The main difficulty of developing such a method is to find an algorithm that can accurately calculate similarity. This can only be reached after many experiments. This difficulty could be due to unclear image features, different colors or contrast, the presence of features in an image that is not present in other image, or the same features in both images could be different due to an illness, lighting, or camera setting for image capture. The developed approach is identified after many experiments and tests. It measures the colour differences or the similarity between two tested images. This measurement is one of the fundamental processes in the developed algorithm. The whole

algorithm is evaluated by using 710 pairs of points from FIRE dataset within S-category. The average of registration errors was around 1.2 pixels, as a result of this evaluation. Accordingly, such result demonstrates the accuracy of the developed method.

### **3.8 Conclusion**

In conclusion, it is difficult to identify which colour space is the best. Because it depends on a specific application. However, some components such as Saturation, Intensity or Luminosity, Value, and Hue are assumed to be more common than the other components.

The ideal use of Histogram is when it is needed to perform several calculations based on the frequency of each pixel in an image.

The colour difference between two images, according to this research, is a calculation process of the similarity value between two images. For precise result of this operation, the calculations should include computing the colour difference between each pixel in one of the two images with the corresponding pixel in the other image instead of calculating the colour difference between the colours average of one image and the colours average of the other image. And the repetitions number of each colour must be taken into account, so the colour, which is repeated more than the other colours, should be weighed or considered more than those of the less frequent colours. In addition, all colour data must be entered in the calculation equation, for example, not only the lightness or hue value is considered and the rest of colour data is ignored.

The background colour of an image could be the prevalent colour, because it is the most visible colour in images. However, some images such as some medical ones have one background colour, mostly is either Gray, black or white. In this case, it is inefficient to use background colour as a feature. Therefore, for such medical images, the dominant colour should be the most visible colour in an image except the image background colour.

Regarding Template Matching algorithm, all its six methods depends on either the sum of differences or the sum of multiplying between each couple of pixels values.

Concerning the developed approach, it involves using all values of the pixels within the overlap area between the two tested images. It does not test background of the tested images (the black pixels that are outside a retina). Colour normalization has been implemented to

ensure the two tested images have close range of colours. It is based on calculation of the sum of multiplication between each pair of pixels values. Consequently, the concepts of using all pixels, excluding of a background, the comparison between each pair of pixels, and normalization are exemplified into the developed method.

## **Chapter 4 – Colour Mapping**

### **Overview**

This chapter clarifies the colour mapping process which is a solution to the problem of normalization or equalization of colours between two images. Firstly, the chapter presents an introduction to this process. It shows the concepts of this operation and its usages in this research. Then, the chapter explains an existing algorithm for colour mapping, which is called “Histogram specification algorithm”. This explanation includes the algorithm and its outcomes through various experiments. Next, the chapter describes the algorithm which is developed in this study. This description includes the algorithm, its results compared with the existing algorithm of Histogram specification through various experiments, and its evaluation. Three proposed evaluation approaches, with their results, for this developed method are presented in this chapter. At the end of this chapter, the evaluation results are discussed and compared to show which evaluation approach is the best and if the overall evaluation result proves the validity of the developed algorithm for colour mapping process.

### **4.1 Introduction**

Colour Mapping is a normalization operation to equalize the colours of two images, so that the colours of the second image become the same or very close to the colours of the first image. In this operation, the first image is known as a reference image and the second image is a source or an input image. The output image of this process is the transformed, equalized or colour mapped image.

In this research, this process has been used in two ways. The first application scenario is to equalize the colours of the tested images, all the dataset images, with the colours of a specific reference image. Such process enables the subsequent operations to use the same values of the parameters of those processes that have been applied on a reference image. Consequently, this enables any subsequent processes to be more automated. This application scenario has been exemplified in vessels segmentation (bifurcations detection).

In contrast, the second application scenario is to equalize the colours of a pair of image partitions, the colours of the source image partition with the colours of the reference image partition in this pair. The process of the image registration explained in this research is an example of this application scenario. It is expected that by making the colours of the two

image partitions equal or similar, the results of the image registration process will be more accurate.

There are several operations achieved in this research. which are affected by the difference of the colours between two images. These operations require specific values or parameters such as thresholds to implement efficiently according to the colours range existed in the tested images. In other words, without colour mapping processes, many operations cannot be automatic. Because in each specific colours range, these operations require some different parameters. Such operations are exemplified in this research in ROI detection, Skeletonization, Edge detection by Canny, Circle detection by Hough, and Image Segmentation by Watershed.

In this study, a Colour Mapping algorithm is developed. This algorithm is actually a development of the existing algorithm called Histogram specification algorithm (Wang, 2013). This new algorithm involves the development of additional ten operations to the existing algorithm. As a result, the developed algorithm has given more accurate results than those of the existing method.

#### **4.2 Histogram specification algorithm**

In the first stages of this research, the Colour Mapping process is achieved in by using the Histogram specification algorithm (Gonzalez & Woods, 2002). The outcome of this process is shown in following figure.

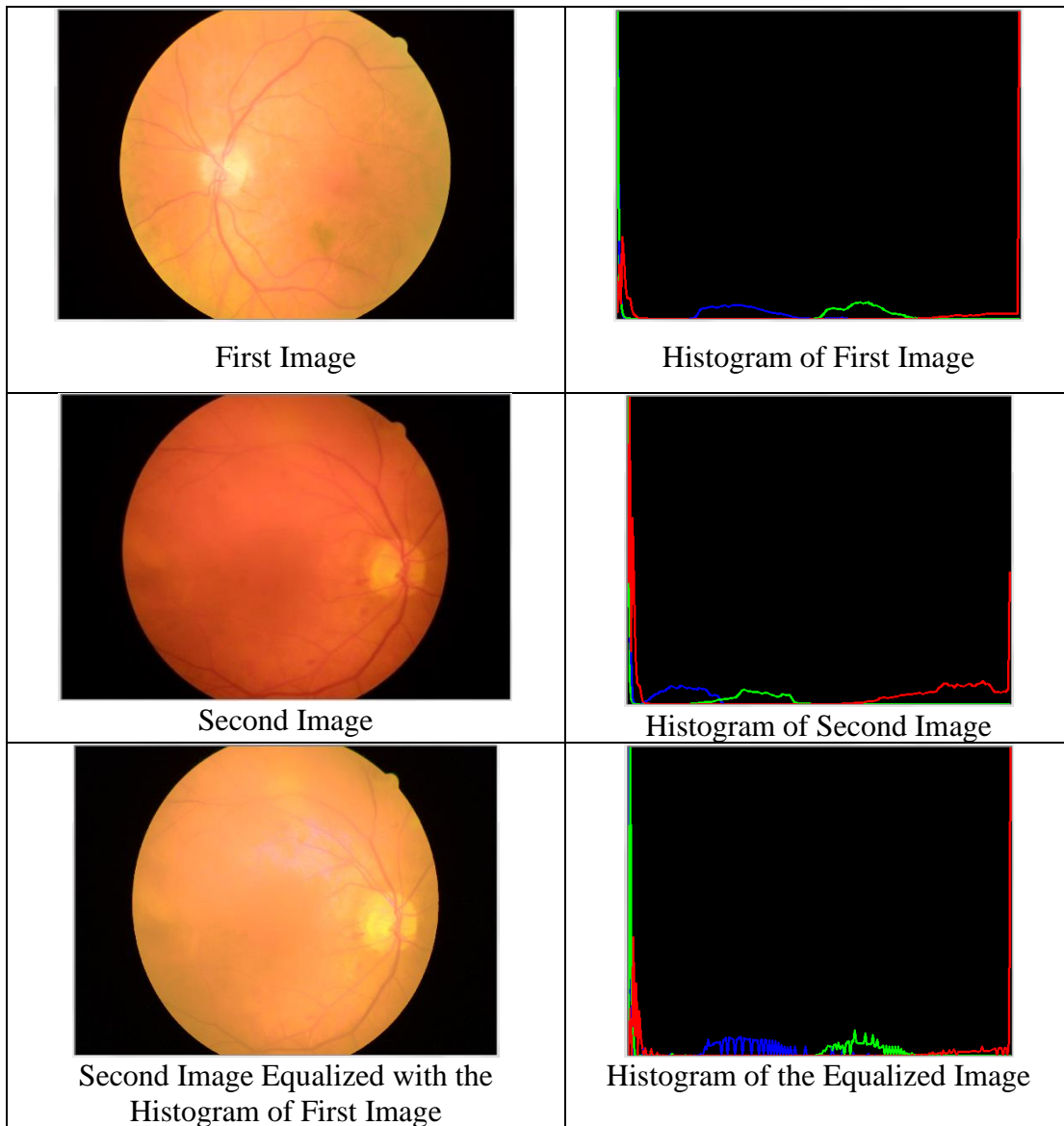


FIGURE 4.2 - 1: HISTOGRAM SPECIFICATION ALGORITHM

#### 4.2.1 The algorithm

The algorithm of Histogram specification (Gonzalez & Woods, 2002) can be described in the next operations (Wang, 2013):

- 1) Derive the histogram of input image, the source image. Then the cumulative of this histogram is calculated by the following formula:

$$H_x[j] = \sum_{i=0}^j h_x[i]$$

Where  $h_x$  is the histogram of the source image and  $H_x$  is its cumulative.

- 2) Derive the histogram of reference image. Then the cumulative of this histogram is calculated by the following formula:

$$H_z[j] = \sum_{i=0}^j h_z[i]$$

Where  $h_z$  is the histogram of the reference image and  $H_z$  is its cumulative.

- 3) Derive the lookup table that represents the mapping function to transform the colours of source image to the colours of reference image. It is derived by finding an output level  $j$  for each input level  $i$  so that  $H_z[j]$  has the best match with  $H_x[i]$ . In this case the element of  $\text{lookup}[i]$  equals  $j$ . In other words, the value of  $\text{lookup}[i]$  equals the value of  $j$  at which the difference between  $H_z[j]$  and  $H_x[i]$  is as small as possible.

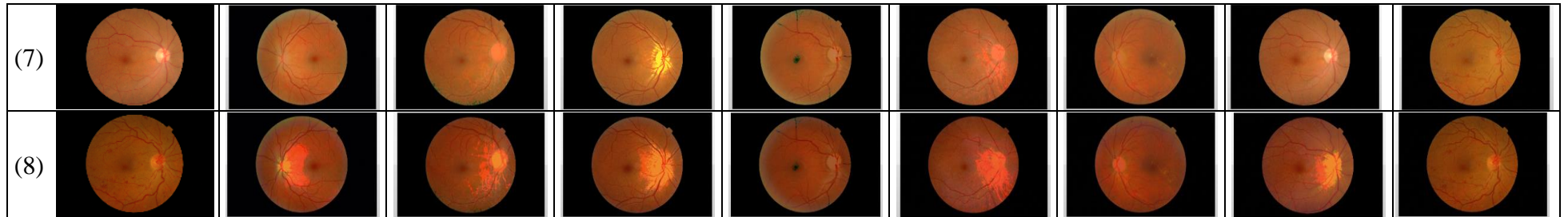
This algorithm is implemented in each corresponding channel of both two images, reference and source image. Therefore, it involves three implementations in Gray scale. It is applied individually through blue, green, and red channels. subsequently, the three resulted images will be merged in one colour image in BGR space.

#### **4.2.2 The Results and Discussion**

In order to evaluate this algorithm, eight retinal images that have different retina backgrounds are chosen from the Messidor dataset (ADCIS-SA, 2017). Each image is tested against the other seven. Therefore, there are sixty-four experiments including testing of an image against itself. Their results are shown in the following table.



Image Number		(1)	(2)	(3)	(4)	(5)	(6)	(7)	(8)
Image Number	Tested Image								
	Reference Image								
(1)									
(2)									
(3)									
(4)									
(5)									
(6)									



*Table 4.2.2 - 1: The outputs of Histogram Specification algorithm, the resulted images, through sixty-four experiments.*

As shown in the previous two tables, most of the transformed images, the output images of the algorithm of Histogram Specification, are distorted, or some of their features have disappeared. In particular in the area of optic disc in a retina, for example, the transformed image from image 3 according to image 1. It could be in some cases, the process of colours converting has been successful, however, with losing of some of the image features such as the images transformed from images 4 and 5 to be similar to image 1; the optic disc of these images is not clear or its light colours have been changed to be darker. According to these results, it is required to develop a new method for colour mapping that gives better results than the ones by the Histogram Specification algorithm.

### **4.3 The Developed Colour Mapping Algorithm**

According to the unsatisfactory results of the existing algorithm of Histogram Specification, there is a need to develop a new algorithm for the colour mapping. Through this research, a successful developed colour mapping method has been derived and evaluated, after several attempts and experiments to develop this new method.

#### **4.3.1 The algorithm**

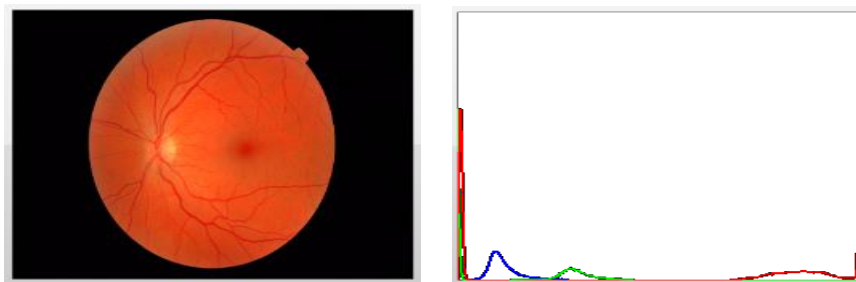
The existing Histogram Specification algorithm applies the process of colour mapping in all image points. In contrast, the concept of this algorithm is to apply the Histogram Specification algorithm, a colour mapping process, only in the similar parts between the two histograms, the histogram of a tested image and the histogram of a reference image.

The idea of the developed algorithm is to convert the point colour in a tested image to a colour similar to the colour of the corresponding point in a reference image, in condition of that this point has been modified in all conversions applied to all channels of the image histogram. The idea of this conversion, for each channel in both images, is to normalize the colours that are in each two similar curves, that have a similar width, in each histogram channel of a tested image and a reference image. In other words, or with more details, this algorithm depends on extraction of the curves in each channel, blue, green, and red channel, from the histogram of each image, a tested image and a reference image. Then, matching the similar curves, that have a similar width, in each histogram channel of both images. Next, for each channel, converting the colour of any point that its colour value is in the range of the matched curves. This conversion is performed by modifying the extracted histogram curve of

a tested image according to the extracted reference histogram curve by using the Histogram Specification algorithm. Finally, if any point has not been modified in all the three channels, it will be returned to its original value.

Overall, the developed system can be illustrated in the next five steps. The first four steps are preprocesses. Then the fifth step is the method developed in this research for colour mapping process, which will be clarified in ten processes later.

1) Load image 1, the Reference image, and derive its histogram, as shown in figure 4.3.1 - 1 as an example.



*FIGURE 4.3.1 - 2: THE REFERENCE IMAGE AND ITS HISTOGRAM.*

2) Find the mask of Image1, ReferenceMask. Then invert it, white colour becomes black and black becomes white, as clarified in figure 4.3.1 - 3.



*FIGURE 4.3.1 - 4: THE REFERENCE MASK.*

3) Load image 2, the Source image, and derive its histogram, as shown in the next image as an example.

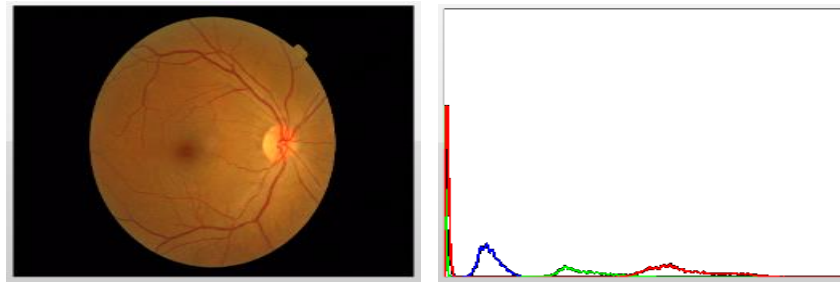


FIGURE 4.3.1 - 5: THE SOURCE IMAGE AND ITS HISTOGRAM.

4) Find the mask of Image 2, SourceMask. Then invert it, white colour becomes black and black becomes white. The next example clarifies this operation.



FIGURE 4.3.1 - 6: FIGURE DERIVING OF SOURCE MASK

5) Transform the colours of Image2 to be equal or similar to the colours of Image1. This is a colour mapping process. For instance, the output of this transformation is as in Figure 4.3.1 - 7 as an example. This example shows the result of the colour transformation of Image2 according to the Image1's colours. Furthermore, the histogram of this transformed image shows that the histogram of Image2 becomes similar to the histogram of Image1.

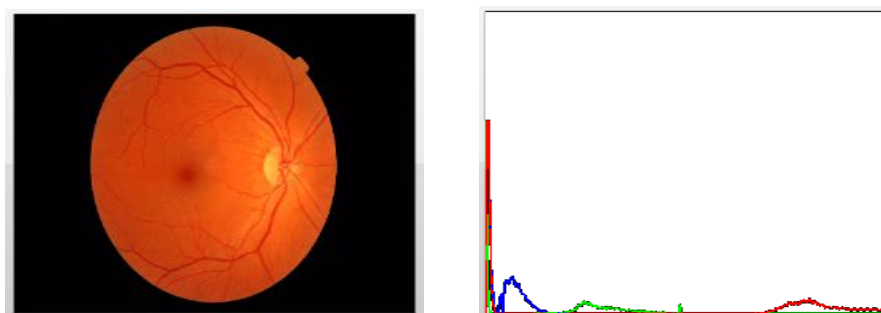


FIGURE 4.3.1 - 8: THE TRANSFORMED IMAGE AND ITS HISTOGRAM

The colour mapping process, mentioned in the previous fifth step, is achieved by the developed algorithm which involve ten operations. Taking into consideration, a histogram consists of three main curves, each curve represents one of the three image channels: blue,

green, and red channel. If the main curve is irregular, then it can be considered to be composed of some different sub-curves. The developed algorithm processes are as follows:

1) Set the following parameters:

$HistSize = 256$ , where  $histSize$  is the number of Bins in a histogram.

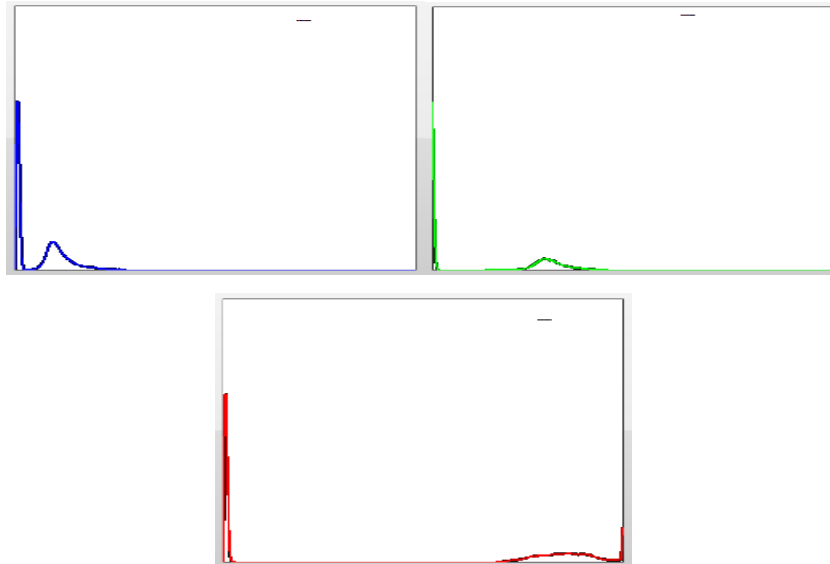
$HistRange = \{ 0, 255 \}$ , this range is the values of histogram bins. The bin value ranged from 0 to 255.

$Threshold = 21$ . This threshold expresses the limit that if a bin value is greater than it, this indicates the presence of a curve or a sub-curve in the histogram. In other hand, if a bin value is less than or equals  $Threshold$ , this means that this bin value is in a horizontal line in the histogram. The value of this  $Threshold$  is concluded through the study of various histograms for a number of different retinal images.

2) Derive Histogram Curves List for each channel in the reference image, Image1. The list includes the information of each curve in the Histogram. This information consists of the first bin number ( $f_i$ ), the last bin number ( $e_i$ ), and the number of bins ( $n$ ) in a Histogram curve. There are three lists, for blue, green, and red channel. If the number of elements, curves, in any of these lists is less than one, stop the algorithm, this means the histogram is empty. The list for a channel is derived by checking the data of the histogram. By starting from  $i=0$  to 254, if  $Bin_i$  is not greater than the  $Threshold$ , set  $i=i+1$  and continue checking of  $Bin_i$ . Otherwise, set  $n = 1$  and  $f_i = i$ . Then continue to check  $Bin_j$  where  $j=i+1$  to 255. If  $Bin_j$  is greater than the  $Threshold$ , set  $n = n+1$  and  $j = j+1$ , otherwise stop checking  $Bin_j$  and set  $e_i=j-1$ . Subsequently, add this curve information,  $f_i$ ,  $e_i$ , and  $n$ , to the list. Set  $i=j$  and repeat the previous checking starting by checking of  $Bin_i$ , however starting from last value of  $j$  not from zero,  $i=j$  to 255.

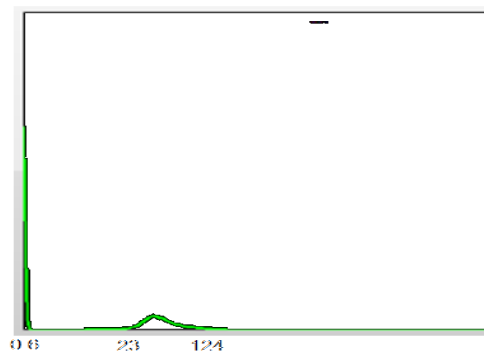
3) Sort, in descending order, the derived Lists of the Histogram Curves of the reference image according to the value of the number of bins,  $n$ , in a curve. The number of bins of the first item in the sorted list is the largest value whereas the number of the last item is the smallest.

For instance, the following three charts show the histogram of each channel, blue, green, and red channel for the reference image.



*FIGURE 4.3.1 - 9: THE HISTOGRAM OF EACH CHANNEL, BLUE, GREEN, AND RED CHANNEL FOR THE REFERENCE IMAGE.*

The next histogram of green channel for the reference image, as an example, shows the first bin number ( $f_i$ ) and the last bin number ( $e_i$ ) in each curve or change in the histogram. Therefore, the sorted List of the Histogram Curves for the green channel of the reference image consists of two items, the first item expresses the information of the largest curve which has the largest number of bins ( $n$ ). According to the results of the two processes of the deriving of Histogram Curves List and its sorting for the next green channel histogram, the first list item's information is  $n=102$ ,  $f_i=23$ , and  $e_i=124$ ; and the second list item's information is  $n=7$ ,  $f_i=0$ , and  $e_i=6$ .



*FIGURE 4.3.1 - 10: THE GREEN HISTOGRAM OF THE REFERENCE IMAGE, SHOWING THE FIRST AND THE LAST BIN NUMBER IN EACH CURVE OR CHANGE IN THE HISTOGRAM.*

4) Repeat the derivation procedure of Histogram Curves List for each channel but in the source image, Image2.

5) Sort, in descending order, the derived Lists of the Image2 Histogram Curves according to the value of the number of bins.

6) Identify the common number of items,  $K$ , that will be checked between the reference image lists and the source image lists. This number is the minimum number of the items in all derived lists for both of the reference and the source image. It can be defined as in the following formulas:

$K1 = \text{Minimum}(\text{number of the items in blue channel of source image, number of the items in blue channel of reference image})$

$K2 = \text{Minimum}(\text{number of the items in green channel of source image, number of the items in green channel of reference image})$

$K3 = \text{Minimum}(\text{number of the items in red channel of source image, number of the items in red channel of reference image})$

$K = \text{Minimum}(K1, K2, K3)$

7) Modify all the three source channels according to the reference derived list corresponding to each channel. There are two outputs from this operation, a modified source channel and the mask that specifies the locations of the pixels that have been changed. In other words, after applying this process on all three source channels, there will be six resulted images, modified source blue channel, modified source green channel, modified source red channel, Mask1 which specifies the locations of the modified pixels in source blue channel, Mask2 which is for source green channel, and Mask3 which is for source red channel. This process can be described by repeating the following steps for each image channel for each  $ii$ , where  $ii$  is the curve number and  $ii=0$  to  $K-1$ .

1- Set  $f_i = \text{ReferencList}[ii].f_i$  and  $e_i = \text{ReferencList}[ii].e_i$ .

Where  $f_i$  is the first bin number and  $e_i$  is the last bin number.

2- Extract the curve between the two bin values,  $f_i$  and  $e_i$  in the histogram of the reference channel. By remove all the curves in the histogram before  $f_i$  and after  $e_i$  in the histogram of the channel.

3- Set  $f_i = \text{SourceList}[ii].f_i$  and  $e_i = \text{SourceList}[ii].e_i$ .

4- Repeat step 2 to extract the curve that is in the source channel histogram.

5- Modify the extracted source histogram curve according to the extracted reference histogram curve by using the Histogram Specification algorithm.

6- Derive the mask that shows which pixels are changed in the modified image channel, be set  $\text{Mask}_{ij}=255$  for each modified pixel  $ij$ .



8) Find the common mask, CommonMask, among the SourceMask, Mask1, Mask2, Mask3. This operation aims to find the pixels that are modified in all the three channels of the source image and they are within the SourceMask. The white colour in CommonMask indicates the corresponding pixel is modified in all the three channels, whereas the black colour refers to the pixel is not modified in all channels. The next figure is an example showing this process.

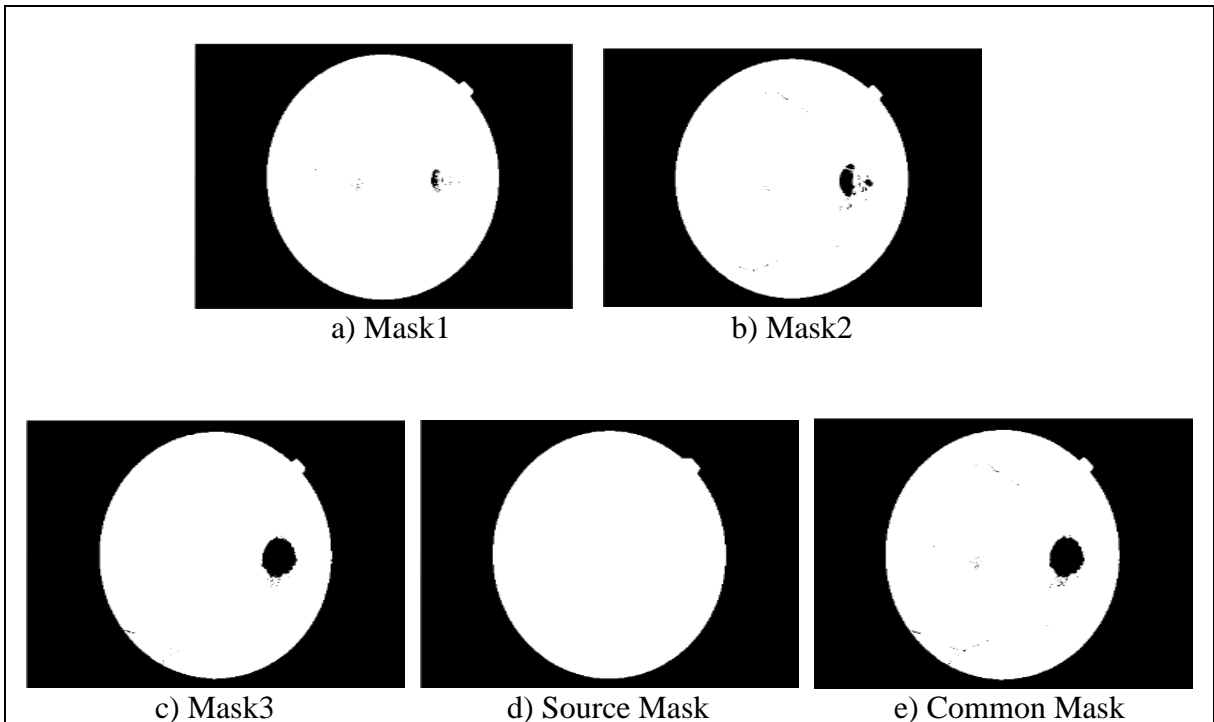


FIGURE 4.3.1 - 11: DERIVING OF COMMON MASK

9) If the number of nonzero pixels in the derived common mask is greater than Threshold, merge all the three modified source channels in one colour image.



FIGURE 4.3.1 - 12: THE OUTPUT OF THE MERGING OF THE MODIFIED THREE CHANNELS

10) According to CommonMask, copy only the pixels that are modified in all the three channels to the modified image which is the overall output of the developed algorithm. In

other words, the pixels that are not modified in all the three channels during all cases of  $i$  which ranges from 0 to  $K-1$ , remain equal to their original values as in the source image.



FIGURE 4.3.1 - 13: THE FINAL OUTPUT OF THE PROPOSED ALGORITHM FOR THE COLOUR MAPPING.

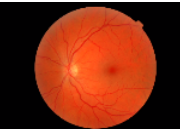
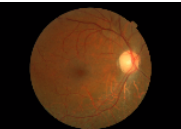
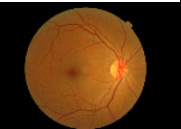
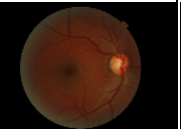
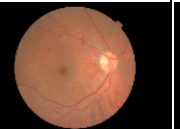
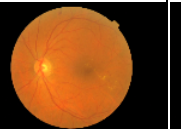
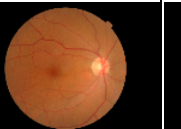
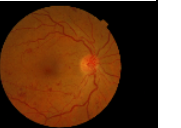
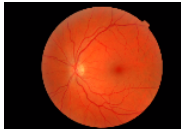







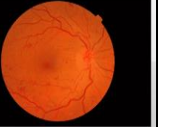



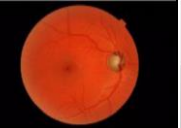




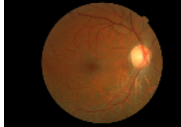


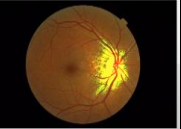


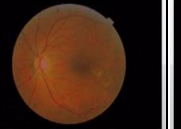









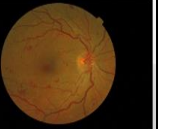
### 4.3.2 The Results of the Developed Algorithm compared with the Histogram specification algorithm

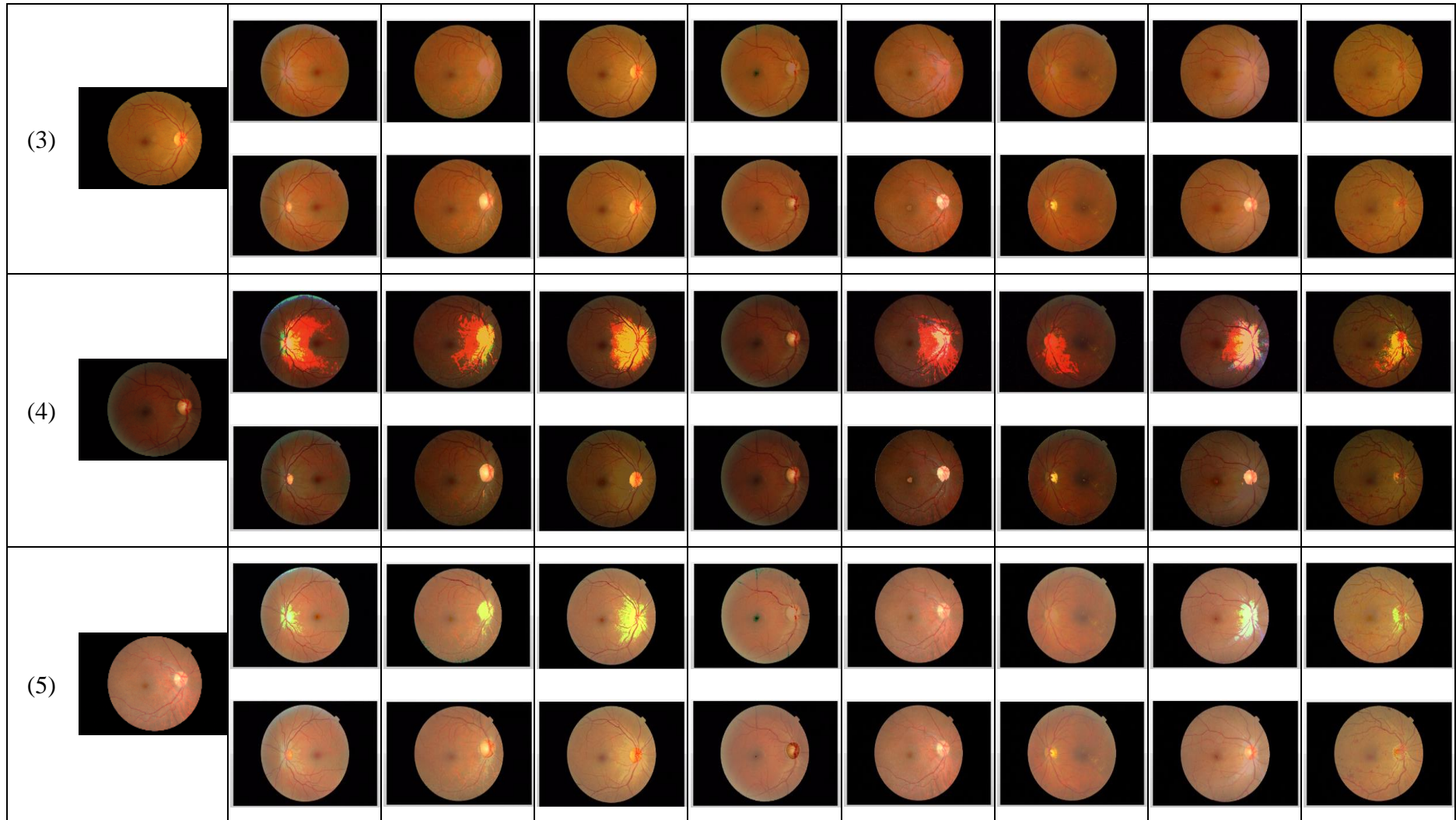
In order to evaluate the developed algorithm, sixty-four tests are achieved by using eight retinal images, that have different retina background, from Messidor dataset (ADCIS-SA, 2017). Keeping in mind, these tests involve testing of an image against itself. The next table shows an example of the transformed image by both of the Histogram specification algorithm and the developed algorithm. For more clarification, the Histograms of both resulted images have been derived as shown in the table. The Histogram of the image resulted by the developed method appears as closer to the Histogram of the reference image, comparing with the Histogram of the transformed image by Histogram specification algorithm. There is a noticeable rise at the end of the green curve in Histogram resulted from using specification algorithm. The colour value where this rise is far away from the green colours gradient range of the reference image.

Reference Image	Tested Image	The results of the developed algorithm (The resulted image and its histogram)	The results of the Histogram specification algorithm (The resulted image and its histogram)

Table 4.3.2 - 1: An example of the resulted image and its histograms by the Developed Algorithm compared with the Histogram Specification Algorithm.

The following table presents the results of sixty-four experiments for testing the developed method and comparing it with the existed algorithm: Histogram Specification. It shows the transformed images by both methods. In each result, the top image is transformed by Histogram specification whereas the bottom one is the output of the developed algorithm.

Image Number		(1)	(2)	(3)	(4)	(5)	(6)	(7)	(8)
Image Number	Tested Image								
	Reference Image								
(1)									
									
(2)									
									



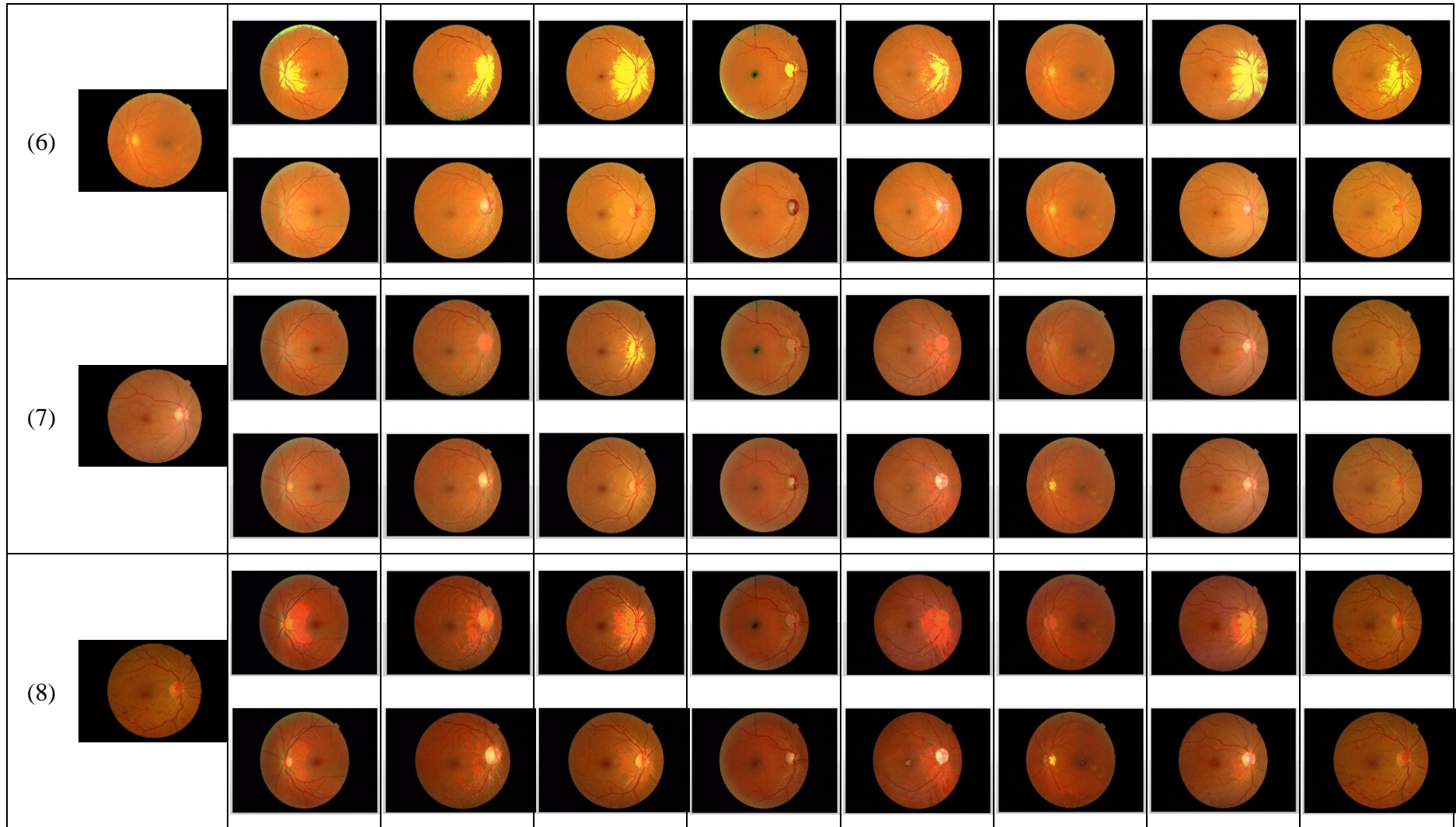


Table 4.3.2 - 2: The resulted images of the Developed Algorithm compared with the Histogram Specification Algorithm.



### **4.3.3 The Colour-Distance-and-Edge-Matching-Rate-Based Evaluation**

An evaluation algorithm is developed for testing the Colour Mapping algorithm developed in this research. This evaluation involves sixty-four tests. It uses eight retinal images that have different retina background. They are from Messidor dataset (ADCIS-SA, 2017). The developed evaluation algorithm consists of two parts. The first one is Colour Distance Calculation, whereas the second part is Calculation of Edges Matching Rate.

The criteria of this evaluation approach are by comparing each colour distance regarding Histogram specification algorithm with the corresponding one from the developed algorithm and comparing each matching rate regarding Histogram specification algorithm with the corresponding one from the developed algorithm. If the matching rate regarding the developed algorithm is less than that is related to Histogram specification and the colour distance regarding Histogram specification is less than that is related to the developed algorithm, this indicates the developed algorithm is invalid or unsuccessful.

The evaluation experiments have been implemented by using a computer with a Processor: Intel core (TM) i5 at 2.4GHz, and memory (RAM) of 8 Gigabyte.

#### **4.3.3.1 Part1: The Colour Distance Calculation for Evaluation**

According to the evaluation results of Histogram Comparison metrics within different colour spaces for retinal images, in this research, It is concluded that Alternative Chi-Square (ChisqrAlt) (OpencvDev.Team, 2017) (Doxygen, 2017) within Lab colour space is the most accurate and the fastest comparing with other four Histogram Comparison methods. Consequently, they will be used to calculate the colour distance (or difference). The colour distance is calculated between the reference image and modified image by the developed colour mapping algorithm.

#### **4.3.3.2 Part2: Edges Matching Rate Calculation for Evaluation**

It is a computing of matching rate between the derived edges of the two images, the source image and its modification by the specific algorithm of colour mapping. In other words, this evaluation part computes the number of matching between the pixels of the edges that are extracted from both of the source image and its modified image by a colour mapping algorithm. This evaluation part does not involve testing the reference image. Edges are detected by using Canny algorithm on Green Channel of an image and with auto threshold

detection. The computing of the matching rate between the detected edges can be clarified in the next six steps:

1) Find the edges of Image1, Edges1.

The applied algorithm for auto detecting of the edges can be described as in the following five operations:

1- Create new black image, Edges1, in Gray scale with the same size of Image1.

2- Copy the green channel of Image1 to Edges1. In other words, Edges1 equals Image1[1], the green channel of Image1. Through various experiments, the best results of edges deriving were in green space comparing with other colour spaces such as Gray or BGR.

3- Smooth the image, Edges1, by using Smooth Gaussian algorithm with kernel size equals three.

4- Detect automatically the two thresholds that will be used for Canny algorithm for edges detection. The second threshold, Threshold2, is identified by using Otsu algorithm which chooses the optimal threshold value between 0 and 255. The first threshold is calculated from Threshold2 by the next formula:

$$\text{Threshold1} = 0.5 * \text{Threshold2}$$

The number 0.5 is concluded through many tests on various retinal images.

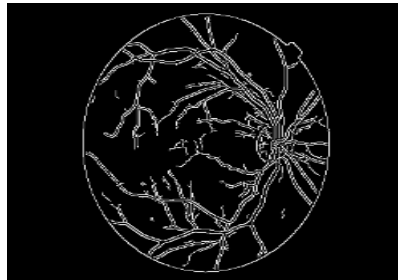
5- Apply Canny algorithm with the two parameters, Threshold1 and Threshold2. For instance, the output of this algorithm is as in the following image.



*FIGURE 4.3.3.2.1 - 1: EDGES OF IMAGE1, REFERENCE IMAGE*



2) Find the edges of Image2, Edges2, by applying the same five operations of edge detection that is applied for detecting Edges1 with using Image2 instead of Image1. The next image is an example of Edges2.



*FIGURE 4.3.3.2.1 - 2: EDGES OF IMAGE2, SOURCE IMAGE*

3) Set the following variables:

$$\text{MatchingNumber} = 0 \quad , \quad \text{NumberOfEdges2} = 0$$

Where MatchingNumber is the number of white pixels matching between Edges1 and Edges2, and NumberOfEdges2 is the number of white pixels in Edges2.

4) Determine MatchingNumber by counting the cases that Edges1[i,j] and Edges2[i,j] equal 255 in the same time. Where i ranges from 0 to the height of Edges1 and j ranges from 0 to the width of Edges1. With taking into consideration that the sizes of the both of Edges1 and Edges2 are equal.

5) Find NumberOfEdges2 by counting the cases that Edges2[i,j] equal 255. where i ranges from 0 to height of Edges1 and j ranges from 0 to width of Edges1. With taking into consideration that the sizes of the both of Edges1 and Edges2 are equal.

6) Calculate the percentage of the matching, MatchingRate, by the subsequent equation:

$$\text{MatchingRate} = 100 * \text{MatchingNumber} / \text{NumberOfEdges2};$$

#### **4.3.3.3 The Evaluation Results of Histogram Specification algorithm**

The next two tables show the tests results of the Colour Distances Calculation and their processing time for the Histogram specification method by using Alternative Chi-Square (ChisqrAlt) method of Histogram comparison within Lab colour space.

Image Number	(1)	(2)	(3)	(4)	(5)	(6)	(7)	(8)
(1)	0.00	253890.36	156484.37	306867.66	277753.15	230208.95	257052.36	316181.99
(2)	269287.88	0.00	162485.73	120210.35	272405.78	240658.39	255437.90	311261.83
(3)	170241.60	157913.29	0.00	183939.46	289816.32	265286.31	279684.58	293296.19
(4)	317860.36	122904.19	195838.43	0.00	262138.01	231185.55	271110.06	311011.18
(5)	383696.89	250455.43	386683.49	237976.71	0.00	167386.74	163767.82	280978.00
(6)	330996.85	208407.08	355952.64	195827.82	162005.24	0.00	174230.42	270410.56
(7)	358302.08	227340.02	371492.57	242185.00	160508.96	176322.40	0.00	279363.80
(8)	415227.30	284152.93	387434.38	282185.93	277738.08	271443.96	278259.07	0.00

Table 4.3.3.3 – 1: The tests results of Colour Distance Calculation for the Histogram specification method by using ChisqrAlt method of Histogram comparison within Lab colour space

Image Number	(1)	(2)	(3)	(4)	(5)	(6)	(7)	(8)
(1)	9.09	0.89	8.66	1.03	0.80	3.46	4.42	8.35
(2)	8.58	0.72	1.72	3.32	7.65	0.92	0.91	0.86
(3)	0.94	0.73	0.67	0.64	0.67	0.77	0.72	0.72
(4)	0.97	0.72	0.80	0.64	0.70	0.73	0.61	0.84
(5)	1.17	0.86	0.78	0.69	0.72	0.72	1.34	2.39
(6)	1.06	0.90	0.84	0.89	0.76	0.70	5.49	1.58
(7)	1.23	0.69	0.67	0.69	0.69	0.72	0.66	0.78
(8)	5.82	0.62	0.67	0.64	0.81	0.95	0.80	0.75
Processing Time Average							1.73 seconds	

Table 4.3.3.3 – 2: The processing time in second for the tests results of Colour Distance Calculation for the Histogram specification method by using ChisqrAlt method of Histogram comparison within Lab colour space

The following table shows the tests results of Edges Comparison, Edges Matching percentages (%), for the Histogram specification method within Green colour space. The Edges Comparison is achieved by calculating the number of edges matching between the extracted edges of the two tested images.

Image Number	(1)	(2)	(3)	(4)	(5)	(6)	(7)	(8)
(1)	100.00	88.47	92.92	66.79	91.30	92.60	94.44	86.90
(2)	88.86	100.00	90.64	60.37	93.21	90.83	91.93	83.16
(3)	85.45	81.18	100.00	53.70	90.56	91.62	94.13	74.79
(4)	88.76	83.44	58.64	100.00	85.20	94.87	85.92	91.55
(5)	69.44	59.69	71.05	31.28	100.00	92.18	72.80	63.59
(6)	66.51	50.40	65.95	30.09	80.11	100.00	66.16	57.82
(7)	80.28	77.33	87.29	49.33	89.81	90.60	100.00	69.93
(8)	94.23	94.20	92.03	76.64	95.14	93.27	91.09	100.00

Table 4.3.3.3 – 3: The tests results of Edges comparison, Edges Matching percentages (%), for the Histogram specification method within Green colour space.

#### 4.3.3.4 The Evaluation Results of the Developed Colour Mapping Algorithm

The next two tables show the tests results of the Colour Distances Calculation and their processing time for the colour mapping method developed in this research. the Colour Distance is computed by using ChisqrAlt method of Histogram comparison within Lab colour space

Image Number	(1)	(2)	(3)	(4)	(5)	(6)	(7)	(8)
(1)	0.00	201588.83	231389.35	178310.05	213482.92	254871.09	194865.15	314566.76
(2)	219687.36	0.00	160893.91	215960.92	229965.70	219015.42	237620.94	238087.18
(3)	242220.31	157823.62	0.00	253477.06	278385.06	269472.37	259517.43	173559.39
(4)	189254.77	215618.49	253620.46	0.00	234889.34	183735.15	236474.70	305197.19
(5)	228719.79	229400.02	280161.32	235108.92	0.00	169311.37	168784.30	233807.46
(6)	259060.55	210600.01	265512.43	177256.98	163908.00	0.00	184719.68	223792.95
(7)	207024.72	234015.03	260338.87	232062.93	164172.44	188194.15	0.00	232048.90
(8)	317155.40	233579.52	173089.35	303656.30	229193.04	224334.58	228643.41	0.00

Table 4.3.3.4 – 1: The tests results of Colour Distance Calculation for the developed method by using ChisqrAlt method of Histogram comparison within Lab colour space

Image Number	(1)	(2)	(3)	(4)	(5)	(6)	(7)	(8)
(1)	6.02	1.09	1.16	1.26	1.11	1.30	1.19	10.31
(2)	1.42	3.31	1.84	1.47	1.97	1.51	11.56	1.90
(3)	3.74	2.00	1.90	1.65	2.12	1.67	2.23	1.28
(4)	2.75	1.87	1.34	1.45	1.64	1.61	1.58	5.21
(5)	2.09	1.90	1.92	1.45	1.83	1.53	1.92	0.98
(6)	1.37	1.69	1.39	1.36	1.34	1.34	1.45	1.11
(7)	8.94	2.28	3.24	7.89	6.16	1.83	1.98	1.31
(8)	8.33	8.24	8.38	4.60	3.87	2.96	13.42	0.86
Processing Time Average						2.99 seconds		

Table 4.3.3.4 – 2: The Elapsed Time in second for the tests results of Colour Distance Calculation for the developed method by using ChisqrAlt method of Histogram comparison within Lab colour space

The following table shows the tests results of Edges Comparison, Edges Matching percentages (%), for the developed method within Green colour space.

Image Number	(1)	(2)	(3)	(4)	(5)	(6)	(7)	(8)
(1)	100.00	92.11	95.71	67.44	88.27	87.53	94.78	87.14
(2)	93.27	100.00	92.79	63.10	90.60	88.74	94.28	82.47
(3)	85.21	83.85	100.00	54.81	89.95	90.14	96.39	74.60
(4)	90.46	91.40	86.57	100.00	86.28	86.18	88.71	92.51
(5)	69.84	59.62	75.41	34.09	100.00	94.20	78.38	58.89
(6)	67.73	58.75	72.87	34.30	90.70	100.00	75.16	60.33
(7)	79.93	77.68	91.16	51.10	91.72	89.89	100.00	68.64
(8)	95.96	96.16	93.73	75.58	87.34	87.80	92.63	100.00

Table 4.3.3.4 – 3: The tests results of Edges comparison, Edges Matching percentages (%), for the developed method within Green colour space.

#### **4.3.4 The Results and Discussion**

According to the evaluation criteria, there are only five errors or failures, therefore the error rate is 7.81% ( $5/64 * 100=7.81\%$ ), or the success rate equals 92.19%.

Regarding processing time, it is expected that the developed method of the colour mapping takes more execution time than that of the Histogram specification method, because the developed method involves the Histogram specification method as part of its algorithm. In other hand, the Histogram specification process is one of the processes of the developed method. According to the results of the colour-distance-based evaluation, processing time average of Histogram specification process is 1.73 seconds, whereas the developed method takes 2.99 seconds as an average. This means the processing time of the developed method is around 1.72 times of that required for Histogram specification method, where  $2.99/1.73\approx 1.72$ .

## **Chapter 5 – Preprocesses**

### **Overview**

This chapter describes the common required processes before image registration to get the best results. The explained preprocesses include image resizing, retina cropping, background extension, green channel separation, deriving retina mask, Weber space transforming, bright lesions reduction, borders extending, and sharpening of bifurcation and its edges.

### **5.1 Image Resizing**

The developed algorithm is working on the real size of the tested retinal images except in the control points detection stage. During this stage, the size of images is reduced (to 500 x 500 pixels) to speed up the detection operations. Such operation applies a generic geometrical transformation of remapping on an image, using resizing process that defined in EMGU library (EmguCV, 2016) that depends on bilinear interpolation method. The algorithm is clarified in the journal paper titled “Image Resizing using Bilinear Interpolation” (Kumar, et al., Sep 2011).

### **5.2 Retina Cropping**

It is the detection of the ROI, Region Of Interest. It is located by cropping the region that has the largest size of enclosing bounding rectangle among the detected contours as shown in the following figure.

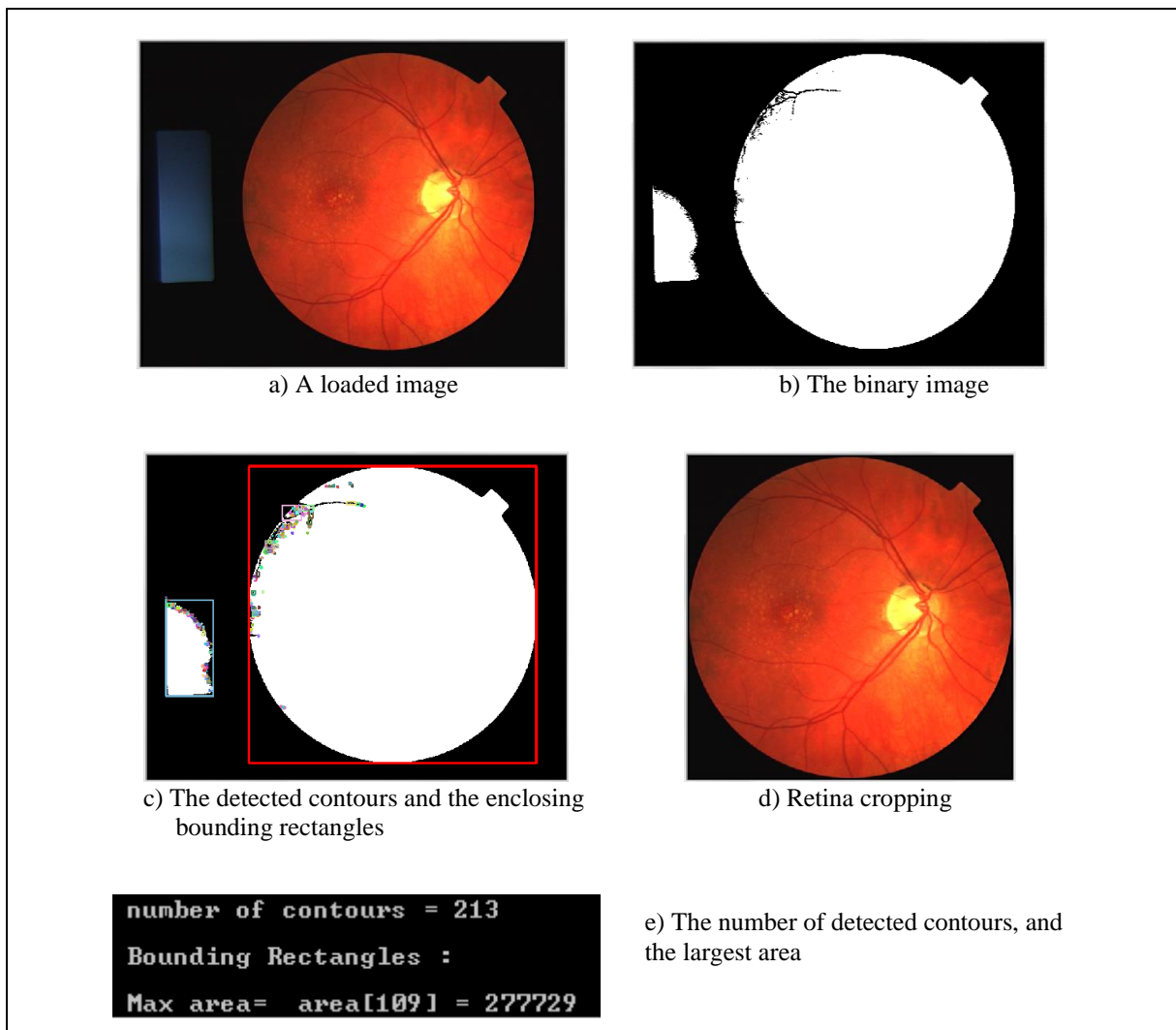


FIGURE 5.2 - 1: ROI CROPPING

The developed algorithm of this process can be illustrated in the next steps:

1- Convert the image to Gray colour scale

2- Find binary image by using Otsu method for auto thresholding and by using binary thresholding with the maximum value equals 255. The binary image in the previous figure (b) is an example of the result of this operation.

3- Find the contours within the binary image by using the implementation of EmguCV library (EmguCV, 2016, FindContours) which uses the algorithm of Suzuki (1985) with its Retrieval Mode is Tree and its Chain Contour Approximation Method is Simple. For example, in the last figure (e) shows that the number of the detected contours is 213 and the detected contours are shown in the figure (c).

4- Find the Bounding Rectangle around each detected contour. The result of this operation has been exemplified in the last figure (c) which shows a rectangle around each detected contour.

5- Find the largest area among the Bounding Rectangles, which is defined as the following:

The largest area =  $\text{Max}(\text{area}[i])$  , where  $i = 1$  to number of the detected contour

and  $\text{area}[i] = \text{boundRect}[i].\text{Width} * \text{boundRect}[i].\text{Height}$  , where  $\text{boundRect}[i]$  is the Bounding Rectangle of contour  $i$ .

For instance, in the previous figure (e) shows that the largest area equals 277729 of the contour number 109.

### **5.3 Background extension**

There is no gap between the retina and the border of an image after applying of the process of Retina cropping. It is required to insert a space between the retina and the image border, so that the edges of the retina do not overlap with the image frame through the edge detection process. In other words, without the separation between the retina and the image border, the image border will be considered as a part of the edges of the retina during edges detection process that is required for optic disc segmentation or for the evaluation approach of the colour mapping algorithm developed in this research.

As shown in the next figure, this process is an operation to enlarge an image background, black region, by increasing the gap, that is between the ROI (the circular shape of an image) and the border of an image, by specific length, 3 pixels length in each side of an image, so the image size [width \* height] becomes:  
 $\text{width}+6 * \text{height}+6$ .

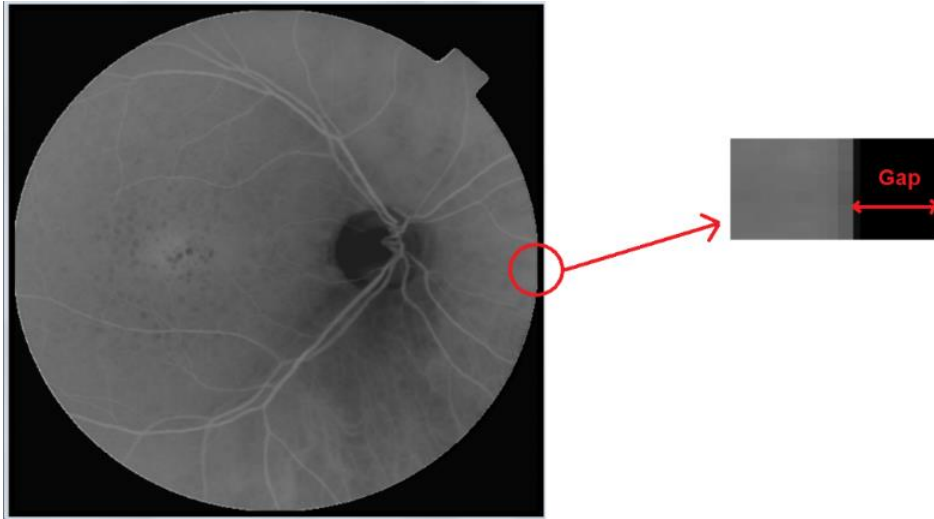


FIGURE 5.3 - 1: BACKGROUND EXTENSION

The algorithm developed for this process can be explained in the next steps:

- 1- Set EnlargeValue = 6.
- 2- Set SmallerImage= OriginalImage , where OriginalImage is the image that requires to enlarge its background.
- 3- Set height = SmallerImage.Height , width = SmallerImage.Width.
- 4- Set newWidth = Width + EnlargeValue , newHeight = Height + EnlargeValue.
- 5- Create new black colour image, LargerImage with the size of newWidth \* newHeight.
- 6- Set left = EnlargeValue / 2 , top = left.
- 7- Set rect = Rectangle(left, top, width, height).
- 8- Set the region of interest of LargerImage to be equal rect.
- 9- Set a= LargerImage.
- 10- Add SmallerImage to a.
- 11- Copy a to LargerImage.
- 12- Reset the region of interest of LargerImage.



## 5.4 Green Channel Separation

Several processes have been developed in this research. Some of them work better in specific colour space. For instance, edge detection is tested in some of colour spaces such as Green space and Gray scale. According to the results of this test, the Green space, green channel, is the colour space that is better than Gray scale for edge detection. The next figure shows an example of the green channel of a retinal image.



FIGURE 5.4 - 1: GREEN CHANNEL

The input image of Canny method, that is used for edge detection, must be 8-bit image (in Grayscale). The edge detection algorithm, used in this research, is tested in Green and Gray scale. It is found that there are more edges when using Green scale comparing with using Gray scale. The following figure is an example of the edges detection results in Green and Gray scale for the same image.

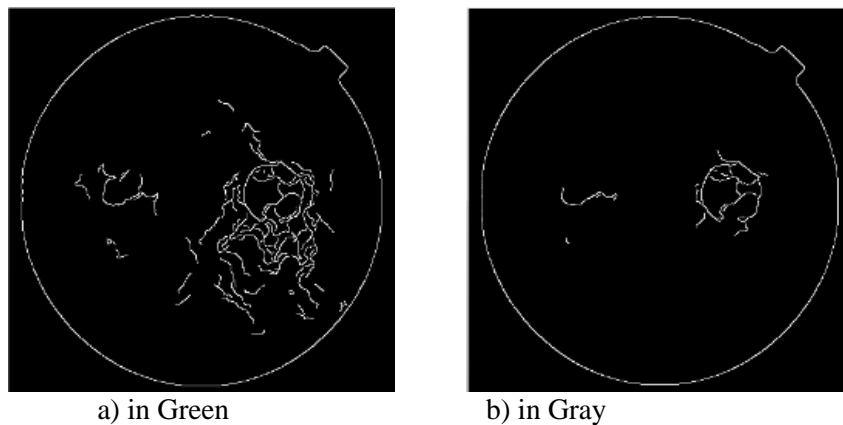
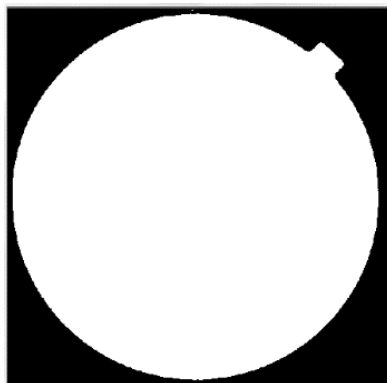


FIGURE 5.4 - 2: THE COMPARISON BETWEEN GREEN AND GRAY SCALE THROUGH APPLYING EDGES DETECTION ON THE SAME IMAGE.

## 5.5 Deriving Retina Mask

This process is a binary representation, in black and white colours. A human retina is located and represented in white colour, with black background, as shown in the next figure. In the developed approach of this research is referred to as Retina Mask or Mask.



*FIGURE 5.5 - 1: RETINA MASK*

The proposed algorithm in this research for deriving such Mask is clarified as in the following three steps:

- 1) Create black image as a Mask.
- 2) By starting at the left edge, column, of the image, from the top row to the bottom, check each pixel in each row in the source image, the image which requires to find its mask. If the value of a pixel,  $Src_{ij}$ , in all image channels is less than the specific threshold, the value of the Mask,  $Mask_{ij}$  becomes equal 255, the white colour. if so, after changing the Mask value to 255, the checking continues to check the next pixel to the right in the same row. In any case that the value of a pixel,  $Src_{ij}$ , in all image channels is not less than the specific threshold, the checking stops and move to the next row in the image starting from the left edge.
- 3) By starting at the right edge, column, of the image, from the top row to the bottom, check each pixel in each row in the source image. If the value of a pixel,  $Src_{ij}$ , in all image channels is less than the specific threshold, the value of the Mask,  $Mask_{ij}$  becomes equal 255, the white colour. if so, after changing the Mask value to 255, the checking continues to check the next pixel to the left in the same row. In any case that the value of a pixel,  $Src_{ij}$ , in all image channels is not less than the specific threshold, the checking stops and move to the next row in the image starting from the right edge.

Through many experiments on various retinal images, the best threshold for deriving the Mask is 32.

## 5.6 Weber Space Transforming

The algorithm of Weber Space transformation is clarified in the proposed method of vessel segmentation by Saffarzadeh, et al. (2014). It is used as an image enhancement method to reduce noise, in particular for vessels segmentation. The next figure shows an example of the Weber Space transformation.



FIGURE 5.6 - 1: TRANSFORMING TO WEBER SPACE

The Weber's law equation, transforming the input image  $I$  to output image  $O$ , can be expressed as:

$$O = \text{Ln}(1 + I) / k \quad (\text{Saffarzadeh, et al., 2014})$$

where  $k$  is a constant and is taken to be 0.0217 in this study ( $\ln(256)/255=0.0217$ ).

Actually, the value of  $k$  is obtained from the paper titled "Analysis of background detection and contrast enhancement of MRI images" (Sathya & Manavalan, Dec 2011). It is expressed as:

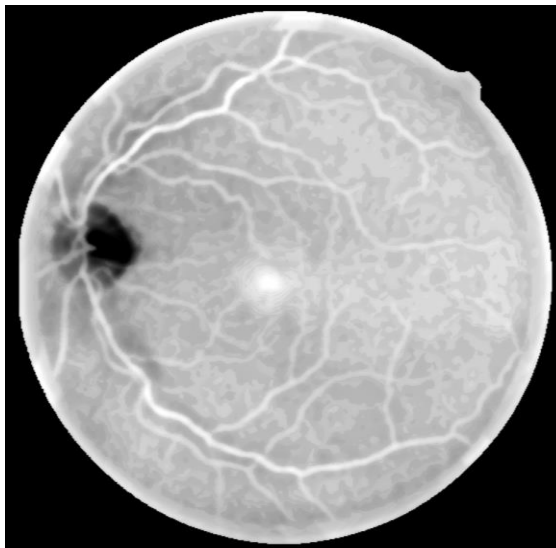
$$k = \ln(256) / (255 - m), \text{ where } m \text{ is the minimum intensity value.}$$

The minimum intensity value in a gray scale image is zero, so  $m$  is 0.

Therefore  $k = \ln(256) / 255 = 0.0217$ .

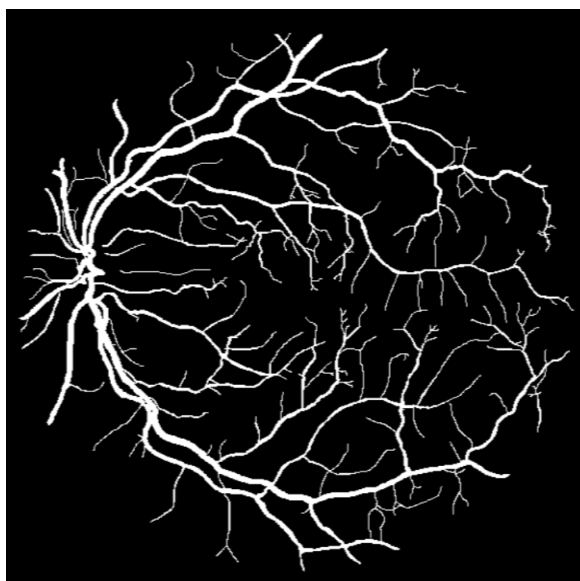
### 5.6.1 Evaluation of using Weber Space Transform in the developed algorithm

To decide to use Weber Space Transform in the developed algorithm or no, three comparisons are achieved. Two use thin bifurcation form, and another one uses thick form. The thin and thick bifurcations are two outputs of the developed approach to detect the control points. To achieve these comparisons, 20 retinal images with their vascular Ground Truths, from the Drive dataset, are used. Therefore, each comparison includes twenty tests. The following figure presents an example of the enhanced image, by the developed algorithm, that is used to extract the two forms, thin and thick ones, used for this evaluation.



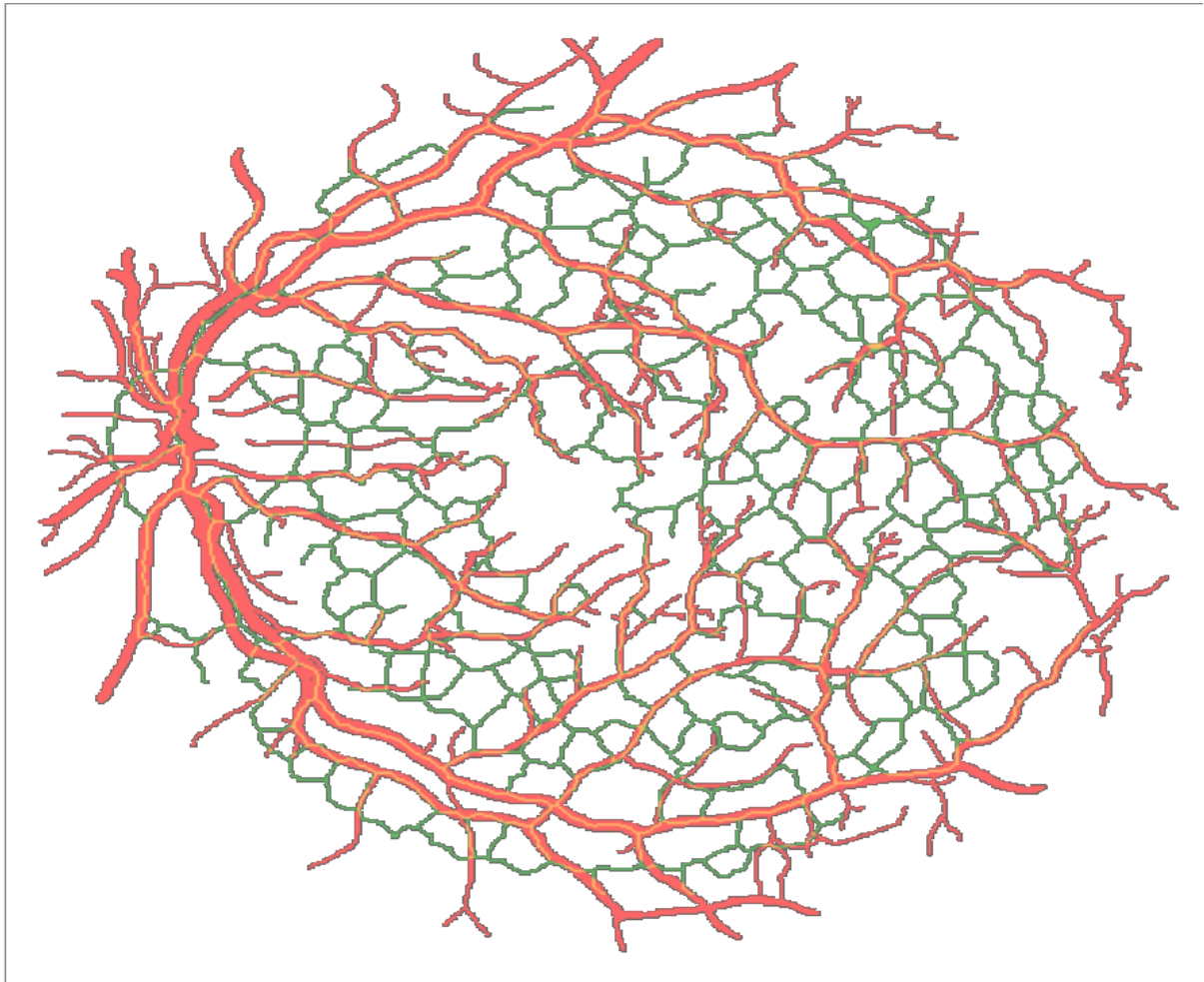
*FIGURE 5.6.1 - 1: AN EXAMPLE OF THE ENHANCED IMAGE BY THE DEVELOPED ALGORITHM*

The Drive Ground Truth for the previous image is described in the next figure.

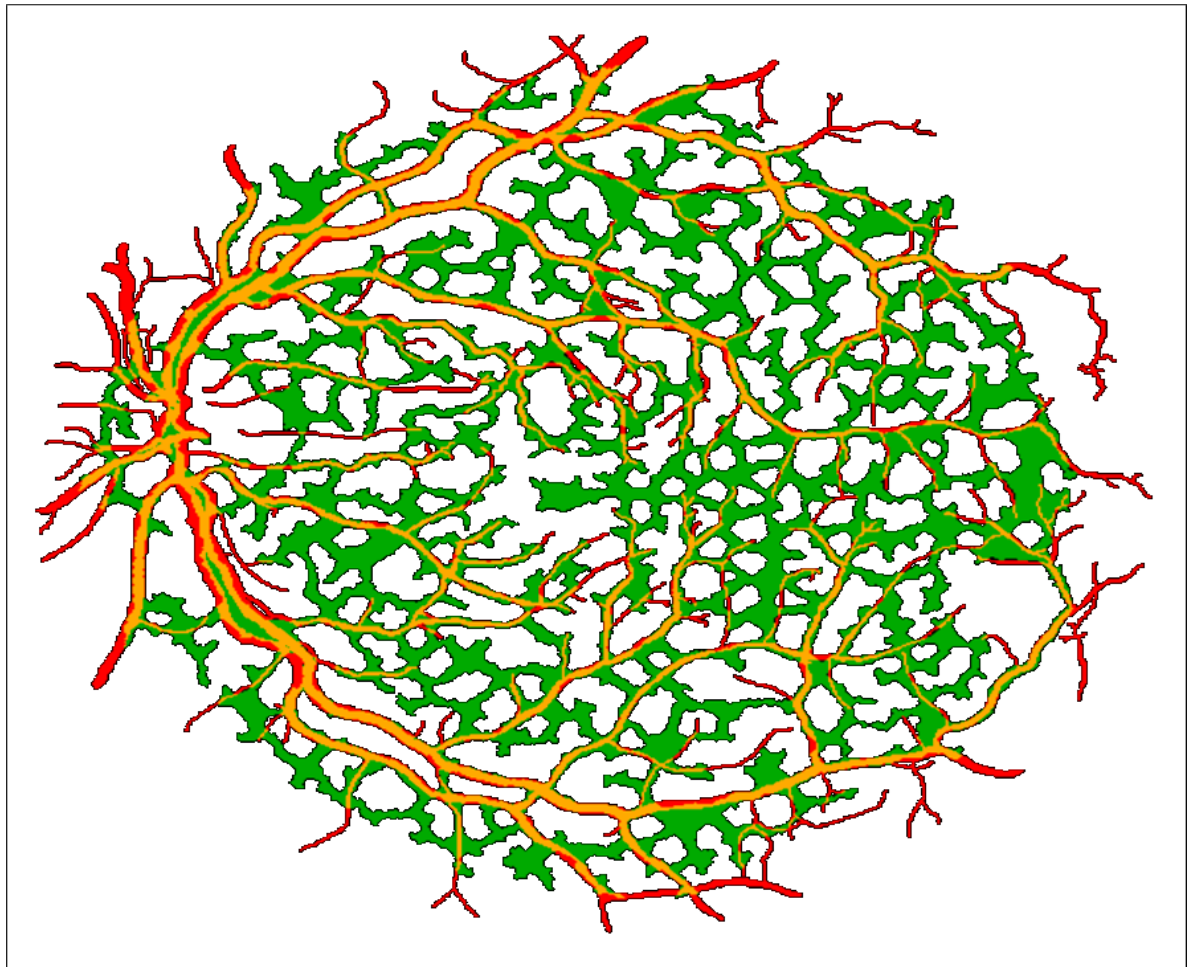


*FIGURE 5.6.1 - 2: A DRIVE GROUND TRUTH (IN WHITE COLOUR)*

The next two figures clarify the overlap (in orange colour) between the Ground Truth (in red) and the extracted bifurcations, either in thin or thick form (in green).

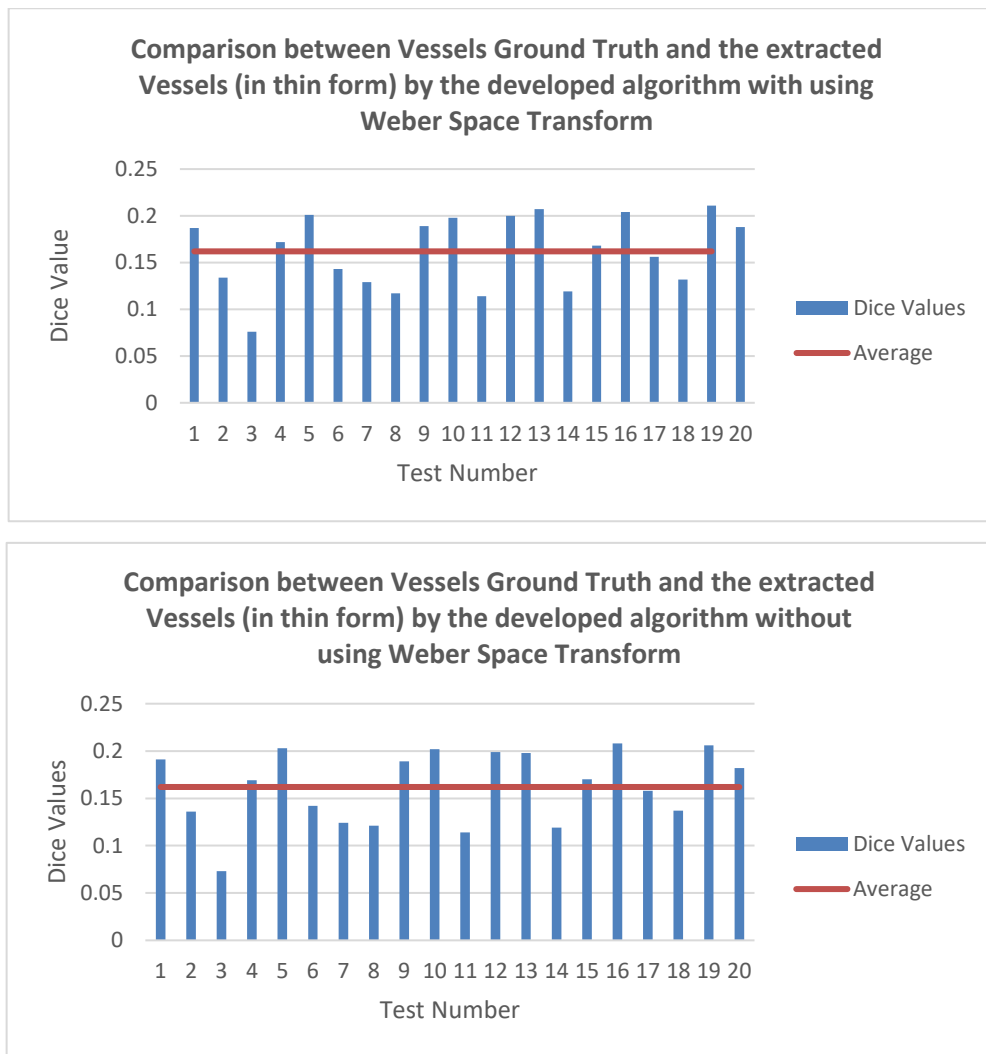


*FIGURE 5.6.1 - 3: A GROUND TRUTH (IN RED) + THE EXTRACTED BIFURCATIONS (IN GREEN) BY THE DEVELOPED ALGORITHM IN THIN FORM (THE OVERLAP IS IN ORANGE COLOUR)*



*FIGURE 5.6.1 - 4: A GROUND TRUTH (IN RED) + THE EXTRACTED BIFURCATIONS (IN GREEN) BY THE DEVELOPED ALGORITHM IN THICK FORM (THE OVERLAP IS IN ORANGE COLOUR)*

The first comparison is between Vessels Ground Truth of the Drive dataset and the extracted bifurcations (in thin form) by the developed algorithm with and without using Weber Space Transform. It is used Dice coefficient formula to compute the difference between detected bifurcations and the corresponding ground truth. The next two graphs show the Dice values as a result of this comparison.



*FIGURE 5.6.1 - 5: THE TWO COMPARISONS BETWEEN VESSELS GROUND TRUTH AND THE EXTRACTED VESSELS (IN THIN FORM) BY THE DEVELOPED ALGORITHM WITH AND WITHOUT USING WEBER SPACE TRANSFORM.*

The second comparison is between Vessels Ground Truth of the Drive dataset and the extracted bifurcations (in thick form) by the developed algorithm with and without using Weber Space Transform. Dice coefficient formula is used for this comparison. The following two charts are the outputs of such comparison.

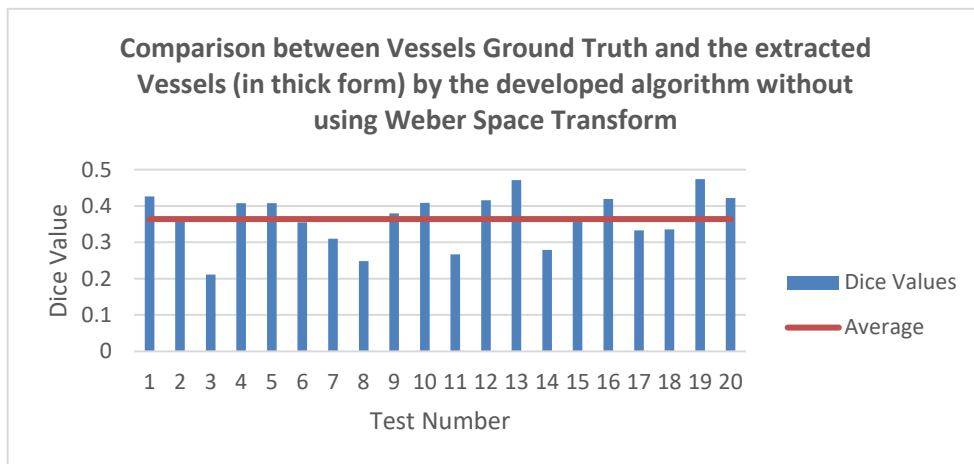
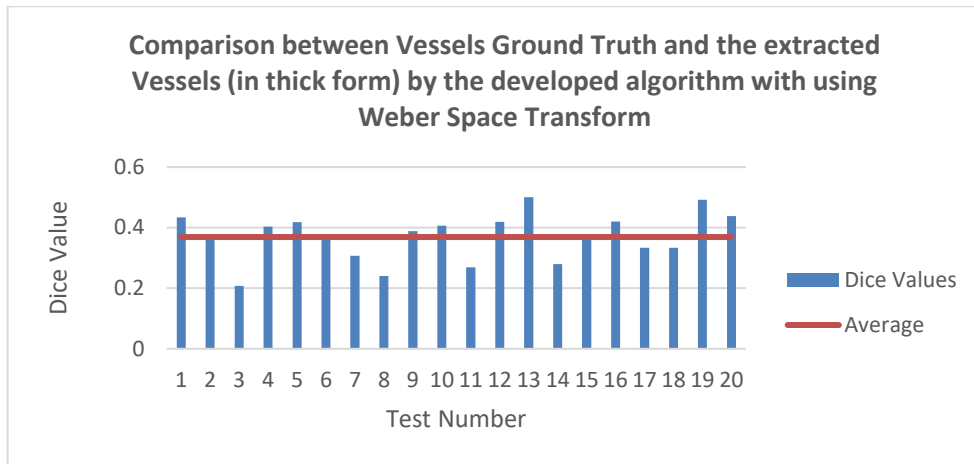
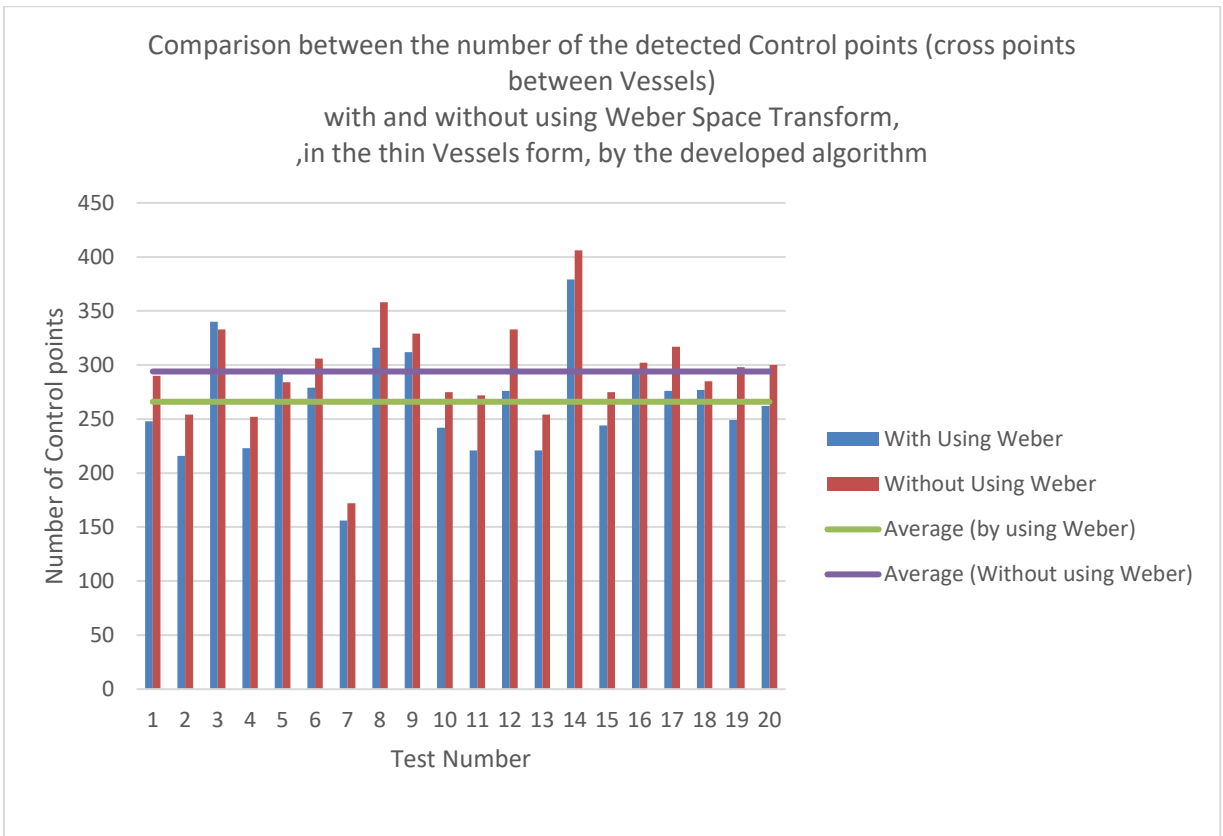


FIGURE 5.6.1 - 6: THE TWO COMPARISONS BETWEEN VESSELS GROUND TRUTH AND THE EXTRACTED VESSELS (IN THICK FORM) BY THE DEVELOPED ALGORITHM WITH AND WITHOUT USING WEBER SPACE TRANSFORM.

The third comparison is between the number of the detected Control points (cross points between Vessels) with and without using Weber Space Transform,

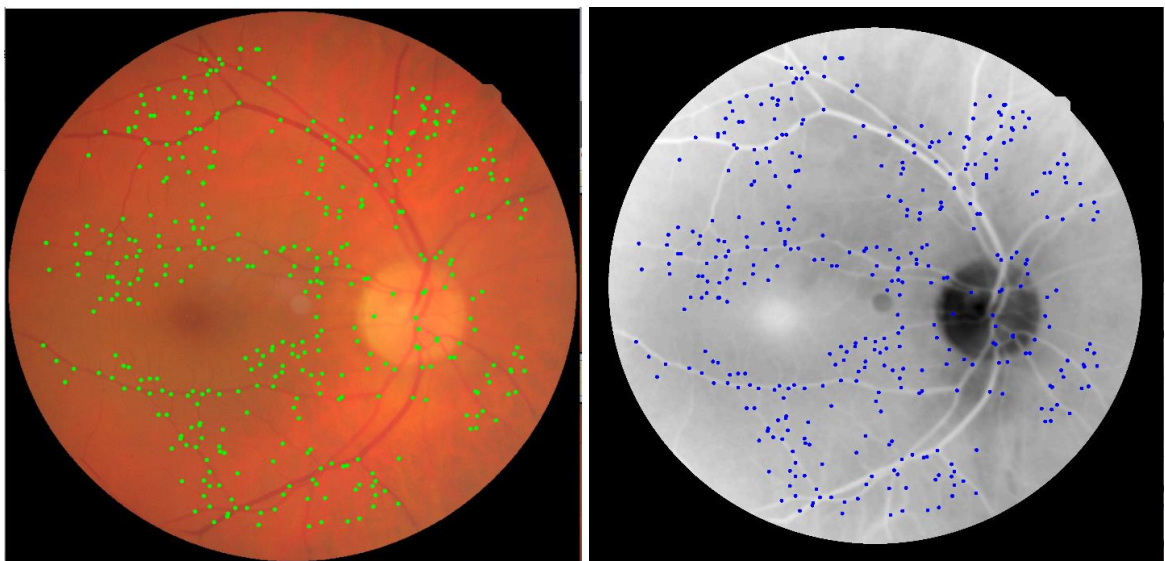
, in the thin Vessels form, by the developed algorithm. The results of this comparison are as shown in the next graph.



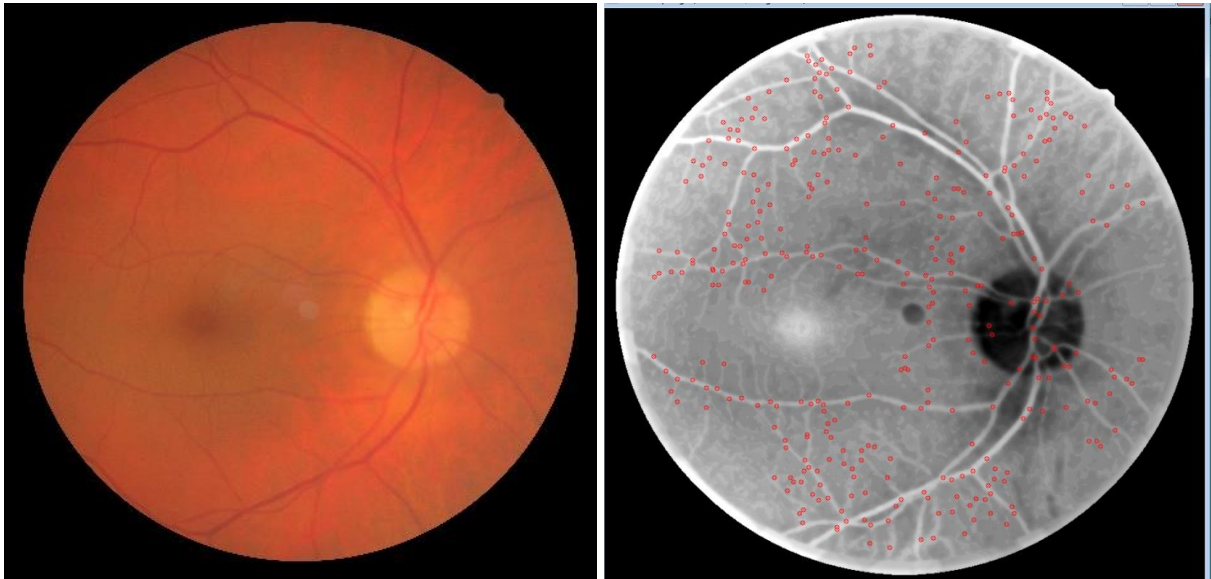


*FIGURE 5.6.1 - 7: THE COMPARISON BETWEEN THE NUMBER OF THE DETECTED CONTROL POINTS (CROSS POINTS BETWEEN VESSELS) WITH AND WITHOUT USING WEBER SPACE TRANSFORM, IN THE THIN VESSELS FORM, BY THE DEVELOPED ALGORITHM.*

The next two figures are examples of control points detection with and without using Weber Space, using image S03\_2 from FIRE dataset.



*FIGURE 5.6.1 - 8: AN EXAMPLE OF 390 DETECTED CONTROL POINTS FROM FIRE DATASET IMAGE CODE: S03\_2 (BY THE CURRENT DEVELOPED ALGORITHM WITHOUT USING WEBER SPACE)*



*FIGURE 5.6.1 - 9: AN EXAMPLE OF 349 DETECTED CONTROL POINTS FROM FIRE IMAGE CODE: S03\_2 (BY PREVIOUS DEVELOPED ALGORITHM WITH USING WEBER SPACE)*

The first two methods are based on Vessels comparisons, one in thin thickness, and the other in thick form. In the first method, with using Weber Space Transform, the Dice values average is 0.16225, whereas it is 0.16205 without Weber Space. In contrast, in the second method, with using Weber Space Transform, the average of Dice values is 0.3691, whereas it is 0.36465 without Weber Space. Accordingly, the averages are very close. Therefore, both methods have not provided a result helps to explain which is better, the use of Weber Space Transform or not. The reason for that, is the developed algorithm does not give the actual thickness of the vessels, in addition it detects any bifurcation which could not be a vessel. Actually, the developed algorithm does not aim to detect the vessels, Its goal is to discover location of intersection points between bifurcations. However, third comparison method has solved the issue. It depends on the number of the control points detected by the developed algorithm. And it is achieved in thin bifurcation form. It shows that the average of the number of the detected control points is 266 when using Weber Space Transform, whereas it is 294 without Weber Space. In other words, without using Weber Space, the number of the control points will be greater than the number with using Weber Space. No other comparison based on control points, in thick bifurcation form, has been performed. This is due to the number of control points obtained in either thin or thick form are equal.

In conclusion, according to the third comparison results, it is better to not use Weber Space Transform in the developed algorithm.

### 5.7 Bright Lesions reduction

It is another existing algorithm which is used as an image enhancement method in this research, particularly for Skeletonization and Retina Border Extending. It is achieved by using K-means Clustering algorithm (MacQueen, 1967). The next figure shows an example of the image segmentation by K-means Clustering.

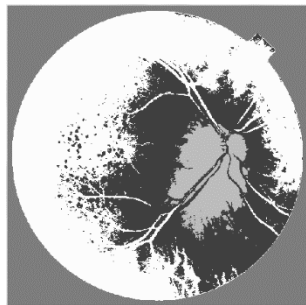
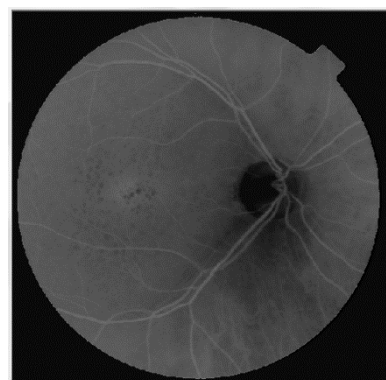


FIGURE 5.7 - 1: IMAGE SEGMENTATION BY K-MEANS CLUSTERING

The following figure presents the effect of applying K-means Clustering on the green channel of a retinal image, as shown in this figure, the bright regions become dark after applying such algorithm.



a) Before applying K-means Clustering

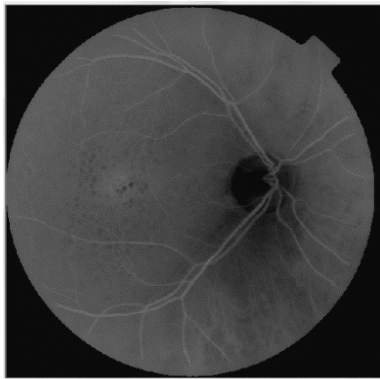


b) After applying K-means Clustering

FIGURE 5.7 - 2: THE EFFECT OF APPLYING K-MEANS CLUSTERING ON THE GREEN CHANNEL OF A RETINAL IMAGE

The process of Retina Border Extending aims to insert a space or a gap between the ends of vessels and the border of the retina. this process completely fails when it is applied without

performing K-means Clustering as in the results shown in the next figure, the vessels in first image (a) do not touch the edge of the retina, whereas there are not any spaces between them and the retina edge in the second image (b).



a) With applying K-means Clustering

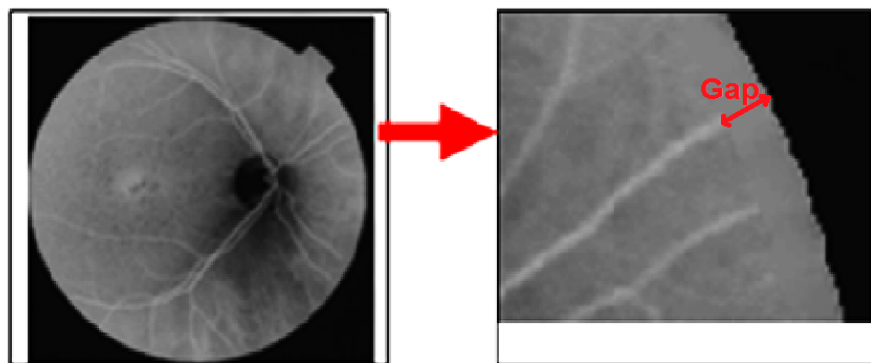


b) Without applying K-means Clustering

*FIGURE 5.7 - 3: THE RESULTS OF RETINA BORDER EXTENDING*

### 5.8 Retina Border Extending

This algorithm is performed to ensure more accurate results from the process of the vessel segmentation. It is the process of increasing the gap between the border of retinal circular shape, not the border of whole image, and ends of vessels. as clarified in the next figure. There could be some ends of vessels in a retina are very close to the border of the retina. In this case, the vessels segmentation will fail. The border of the retina could appear as an extension or a part of the segmented vessels. Therefore, it is required to separate between vessels ends and the retina border.



*FIGURE 5.8 - 1: BORDERS EXTENDING*

This process depends on morphology transformations, erosion and dilatation, as shown in the following figure.

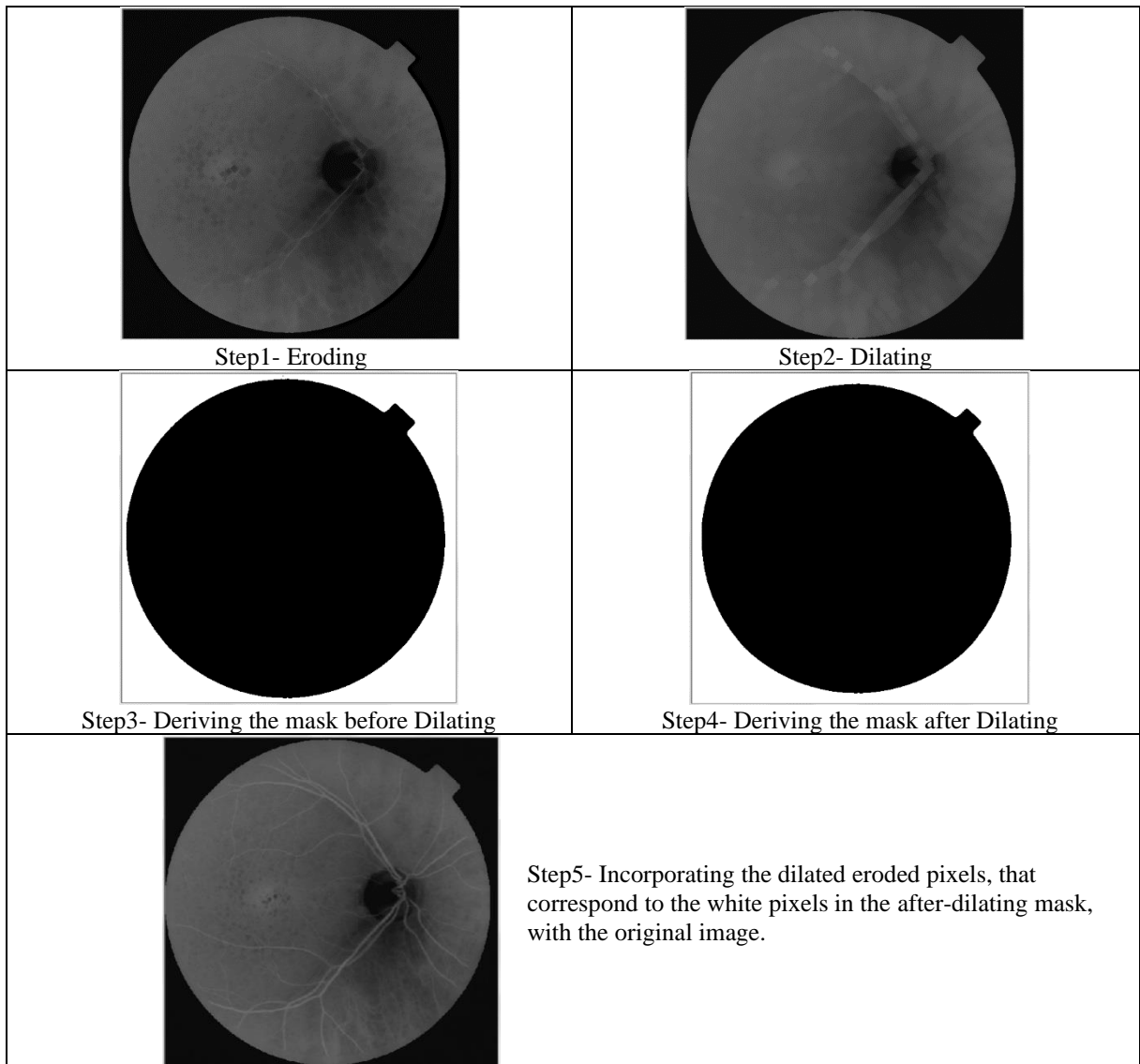


FIGURE 5.8 - 2: THE ALGORITHM OF RETINA BORDER EXTENDING

The dilating process is a stretching of the retina area towards the black background of a retinal image, whereas the eroding is an inverse process for dilating, it could be considered as shrinking process. However, when applying dilating on binary image, the mask, the white area is stretched towards the black area; in other words, the black area is shrunk, as shown in the dilatation result of step4 in the previous figure.

The algorithm developed for this process can be explained in the following operations:

1- Convert the Image to Gray scale, where Image is the image that requires to extend its retina border.

- 2- Derive the retina mask, RetinaMask1, using the method developed in this research, as shown in step-3 in the last figure which is the mask before any morphological transformations, Eroding or Dilating.
- 3- Create a new Gray blank image, ResultedImage, with the same size of the Image.
- 4- Set ResultedImage1 = Image.
- 5- Define a structuring element, Element, of the 5 x 5 kernel size and Cross shape for morphological operations, Eroding and Dilating (OpenCV dev.team , 2011-2014, Morphological Transformations).
- 6- Apply Eroding operation, only one time, (OpenCV dev.team , 2011-2014, Morphological Transformations) on the source image, Image, with using the structuring element, Element, and border value equals zero, black colour. The output of this operation, the eroded image, is stored in ResultedImage, as shown in step-1 in the last figure. The basic idea of erosion is illustrated in webpage of Morphological Transformations in the website of OpenCV documentation (OpenCV dev.team , 2011-2014, Morphological Transformations).
- 7- Apply Dilating operation, three times, (OpenCV dev.team , 2011-2014, Morphological Transformations) on the eroded image, ResultedImage, with using the structuring element, Element; border value equals zero, black colour; and constant border type. The last output of this operation, after its third implementation, is stored in ResultedImage, as shown in step-2 in the previous figure.
- 8- Create Gray blank image, RetinaMask2, with the same size of the source image, Image.
- 9- Set RetinaMask2 = RetinaMask1
- 10- Invert RetinaMask2 by changing white colour to black and black to white.
- 11- Apply Dilating operation, three times, (OpenCV dev.team , 2011-2014, Morphological Transformations) on RetinaMask2, with using the structuring element, Element; border value equals zero, black colour; and constant border type. The last output of this operation, after its third implementation, is stored in RetinaMask2.
- 12- Copy only the pixels of ResultedImage to ResultedImage1 that their locations are in the black colour area in RetinaMask2, as shown in step-5 in the last figure. The black colour area that is in RetinaMask2 is the retina area. The last output of this developed algorithm of the Retina Border Extending is stored in ResultedImage1.

The kernel size, used in this study for Retina Border Extending, has been chosen according to experiments results. Actually, this size is required for morphology transformations, erosion and dilatation. The kernel dimension must be an odd value. In this research, the size of 5 x 5 has been used as a kernel size. By this size, there will be a sufficient gap, between the retina border and a vessel end, whereas the greater size than 5 x 5 will give large gaps. In contrast, the size of 3 x 3 could give a small gap. The next figure presents examples of the Borders Extending results by using different kernel sizes: 3 x 3, 5 x 5, 7 x 7, and 9 x 9. The result of 3 x 3 size shows that there could be some ends of vessels in a retina are close to the border of the retina. As shown in the figure, the gaps by sizes: 7 x 7 and 9 x 9 are greater than those by 5 x 5 size; in addition, the gaps by 5 x 5 ensures that there is a noticeable separation between a vessel and the retina border.

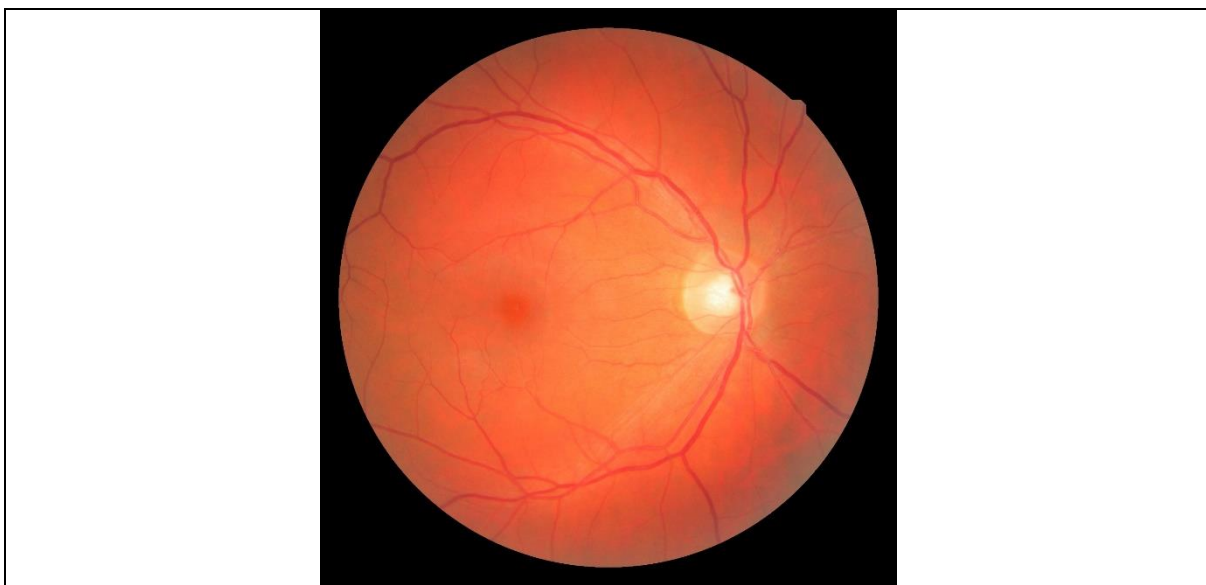
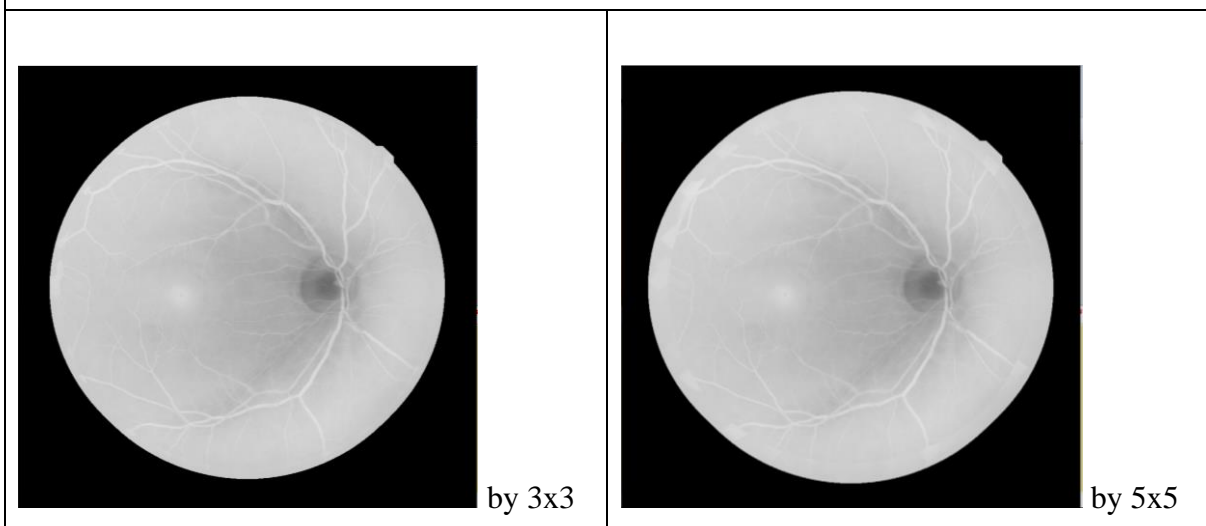
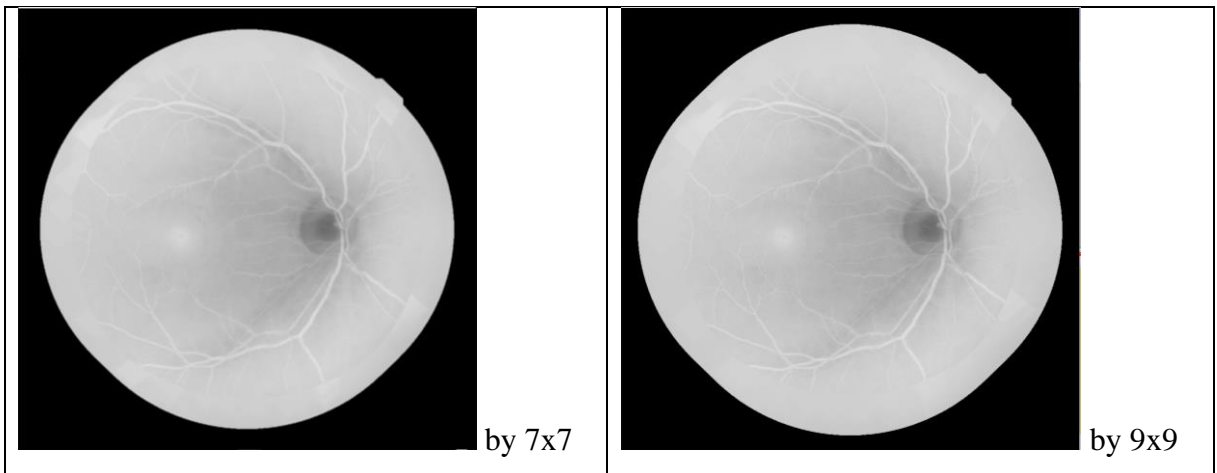


Image code: S58\_1 from FIRE dataset





*FIGURE 5.8 - 3: EXAMPLES OF THE BORDERS EXTENDING RESULTS BY USING DIFFERENT KERNEL SIZES: 3 X 3, 5 X 5, 7 X 7, AND 9 X 9.*



### 5.9 Sharpening of bifurcation and its edges (using Modified Unsharp Masking technique)

This method is developed by modifying in the Unsharp masking algorithm (Ramponi, et al., 1996). The aim of this developed method is to make any bifurcation in a retina clearer.

Unsharp masking algorithm is an image sharpening technique. It creates an image that is less blurry than its original. The resulting image is clearer; however, its details may not be as accurate as in the original image. It involves detecting of edges in an image, by subtracting of the image from its blurred copy. The blurred image is as a result of applying Gaussian Blur method with specific kernel size. Then, the mask is derived from the detected edges. Subsequently, the contrast is increased at the edge's location (or at the mask white area) in the original image.

In contrast, the developed method, in this research, uses the normalized image, instead of the original image, and Gaussian Blur method is implemented twice, in addition to removing of some unwanted pixels of edges. Edges are detected by subtracting of the normalized image (instead of the original image) from its blurred copy. The color normalization is applied on the original image so that its colours will be between 0 and 255. The blurred image is as a result of applying Gaussian Blur method with kernel size equals 33. Then, removing some noise pixels, by removing any pixel value ranged from 1 to 4 in the result of this subtraction. Followed by blurring in all image except the area of the removed pixels (noise area). Such blurring uses Gaussian Blur method with kernel size equals 17. The final result is added to the normalized image (not to the original image). The output of this developed method is shown in the following figure.

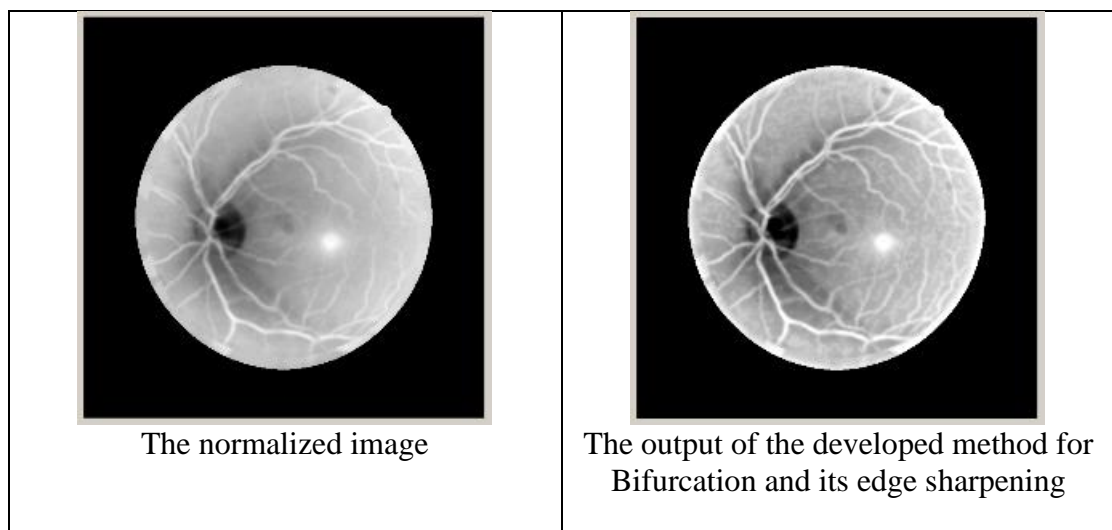


FIGURE 5.9-1: SHARPENING OF BIFURCATION AND ITS EDGE

## **5.10 Conclusion**

Despite all the existing studies regarding computer analysis of retinal images, this analysis requires more researching and development. One of the main reasons of that is the variety of these images, in particular in their structures, colours, and contrast. These differences lead to the need for special processes to deal with these variations. For instance, through the previous studies, such processes could be by using: a green channel and Weber's law space as the best representation for a retinal image, image enhancement, a border extension technique for vessel segmentation, K-means algorithm for reducing bright lesions. These methods can be considered as examples of the preprocesses that are required before any analysis process or in the first stage of any analysis regarding retinal images. Other examples of these methods are those used in this research, such as loading and displaying a retinal image, image resizing, retina cropping, background extension, and deriving retina Mask. All these examples of preprocesses are implemented in this research by developing them or by using the existing algorithms. They have been arranged in specific sequence to be as preprocess or the first processes of a specific tasks such as image registration or segmentation.

## Chapter 6 - Control Points Detection

### Overview

This chapter focuses on the process of control points detection. Firstly, this chapter presents an introduction of Feature-Extraction for Registration Control Points. Next, some previous approaches related to feature extraction are clarified. Then, it provides, in details, the algorithm developed in this study to achieve such operation. In addition, the chapter presents some previous approaches regarding vessel segmentation. Finally, the main future work and conclusion are presented at the end of this chapter.

### 6.1 Feature-Extraction for Registration Control Points

The significant stage of registration is the identification of control points. They are used to calculate the possible displacements for the registration process. Actually, these points are features in an image. There are several feature extraction methods. In the early stages of this study, SURF algorithm is used to extract features to be used as control points. The SURF is one of the most common feature extraction methods. Thereafter, in this study, the intersection points, between bifurcations within a retina, are used as control points. Where the results obtained from the use of intersection points are more accurate than the results obtained from the use of SURF features.

#### 6.1.1 Previous Approaches for Feature Extraction

One of the main processes required for image registration is feature extraction. It is one of the significant processes in computer vision technology.

According to the survey titled “A Review on Image Feature Extraction and Representation Techniques” (Tian, 2013), features are commonly classified to three categories: Colour, texture, and shape features. For instance, the **Hough transform** (Yuen, et al., 1990) (Fisher, et al., 2003 ) is the most widely used technique in the detection of geometric shapes such as ellipse, line ,and circle; Relating to this research, line detection is required for vessel extraction, whereas ellipse or circle detection is for Optic Disc localization.

Overall, the most common used algorithms for feature extraction are: colour histogram, FAST (Features from Accelerated Segment Test), SIFT (Scale Invariant Feature Transform),

PCA-SIFT (Principal Component Analysis-SIFT), F-SIFT (fast-SIFT) and SURF (speeded up robust features), as stated in the journal paper titled “a comparative study of image low level feature extraction algorithms” (El-gayar, et al., 2013), where these five feature detection methods have been evaluated. As a result of the findings of this evaluation, SURF and F-SIFT can be considered as the best two algorithms among these five methods, and SURF is fast and has good performance as the same as SIFT. However, F-SIFT suffers from detecting very few features comparing with other methods.

Actually, SURF is a speeded-up version of SIFT developed by three people, Bay, H., Tuytelaars, T. and Van Gool, L (Bay, et al., 2006). This algorithm is presented in their published paper titled “SURF: Speeded Up Robust Features”. The theory of SURF algorithm is clarified in OpenCV (OpenCV-dev-team, 2014,” Introduction to SURF”).

Accordingly, SURF algorithm is used in one of the developed registration methods in this research for detecting the control points required for matching between two images. Although F-SIFT has a good performance, it cannot be relied upon to carry out the registration operation because it detects a few features comparing with SURF as concluded by El-gayar, Soliman, and Meki (El-gayar, et al., 2013).

## **6.2 Retina-Bifurcation-based Detection of Control Points**

The developed algorithm, in this research for retinal image registration, involves detection intersection points among bifurcations within retina. These points are used as control points in the developed algorithm. A bifurcation could be any branch in retina including any vessel.

### **6.2.1 Optic Disc Centre**

Although the optic disc is unique in any eye retina, it cannot be used as a control point. This due to the difficulty of identifying its centre or its border accurately in the case of registration of two images. In other words, the centre or the border of the optic disc, derived by the developed algorithm, could be not the same in both of the two registered images. In the initial development stages of the registration algorithm in this study, the optic disc centre is proposed to be used as centre of rotation required in the registration. However, this proposal has failed through various experiments. This failure is as a result of variety of retinal images which are different in their colours and features structures.

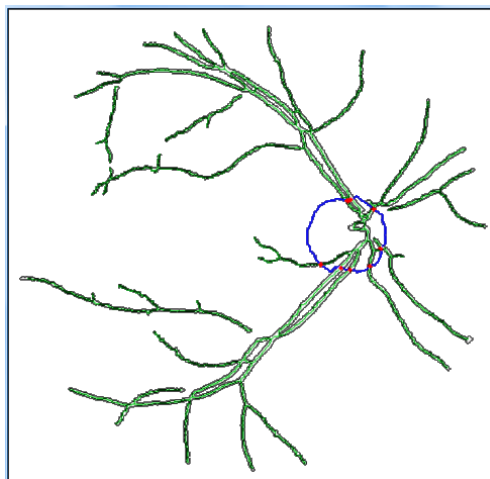
### 6.2.2 Cross Points between optic disc and vessels

In the initial development stages of the registration algorithm in this research, the intersection points, between optic disc and the retinal vascular network, are used as control points. The next three figures show an example for detection of such points. These points were difficult to determine precisely because of dependence on identification of the frame that is around an optic disc. This frame cannot be determined precisely due to various image colour contrast and the potential changes in the eye over time.



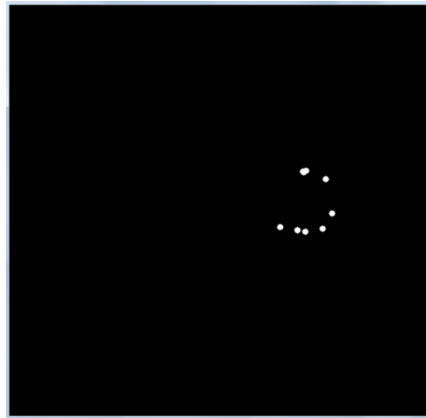
*FIGURE 6.2.2 - 1: THE INTERSECTION BETWEEN OPTIC DISC AND THE VESSELS NETWORK.*

*Where it is in red points, vessels are in green colour, and the boundary of optic disc is in blue colour.*



*FIGURE 6.2.2 - 2: THE CROSS POINTS BETWEEN OPTIC DISC AND THE VESSELS NETWORK.*

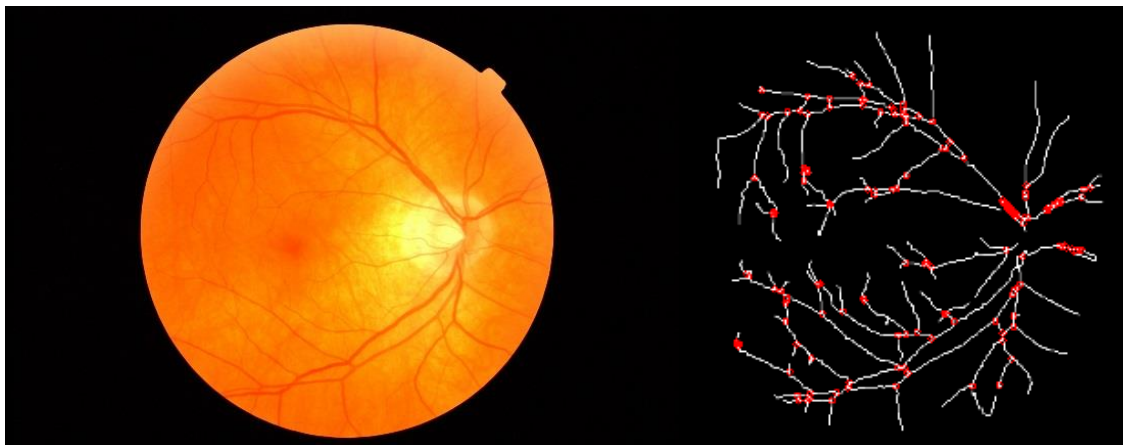
*Where they are in red colour, vessels are in green colour, and the boundary of optic disc is in blue colour.*



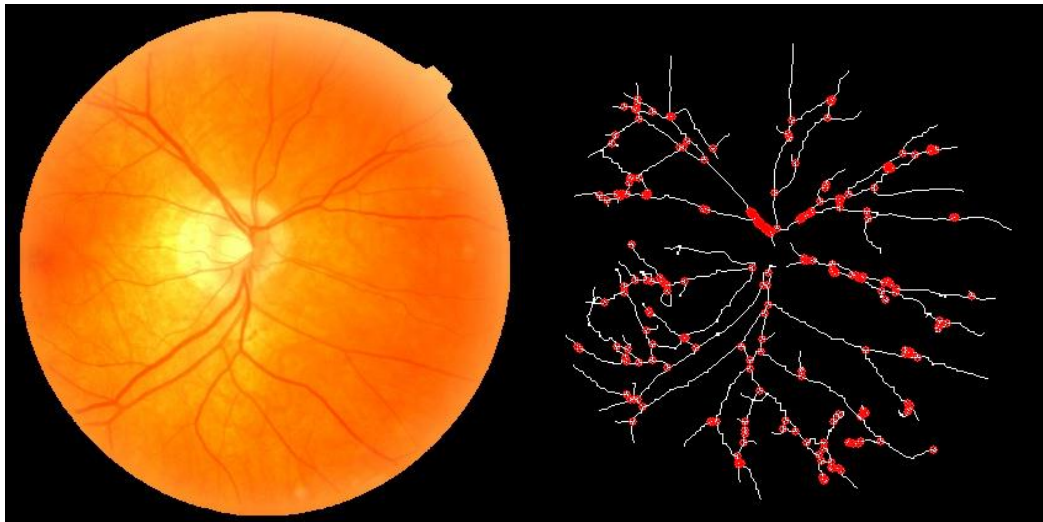
*FIGURE 6.2.2 - 3: THE DETECTED CROSS POINTS, INTERSECTION, BETWEEN OPTIC DISC AND THE VESSELS NETWORK.*

### **6.2.3 Cross Points between Bifurcations**

The control points, used in the developed method, are only intersection points among bifurcations in a retina. The optic disc centre and the cross points between the optic disc and vessels are not used, because they cannot be accurately detected. Such control points are exemplified in the next two figures. They show the output of the process of control points detection among bifurcations in a retina, where the detected cross points are shown in red circles and bifurcations (or retinal vessels) are in white colour.



*FIGURE 6.2.3 - 1: EXAMPLE 1: THE DETECTED CROSS POINTS, INTERSECTION, BETWEEN THE RETINAL VESSELS.*



*FIGURE 6.2.3 - 2: EXAMPLE 2: THE DETECTED CROSS POINTS, INTERSECTION, BETWEEN THE RETINAL VESSELS.*

#### **6.2.4 Previous Approaches in Vessel Segmentation**

The majority of existed retinal image registration methods involve vessel segmentation to extract the required features (or control points).

The methods for vasculature segmentation in retinal images are classified to two categories: supervised methods; and unsupervised methods. The former depends on a training process, whereas the latter does not. A training process requires vessel masks, the training set of labelled pixels, obtained from manual segmentation. Such sets are available in public databases, for example, DRIVE (Image Sciences Institute, 2001-2016) and STARE (STARE Project by Goldbaum MH, 1975 ).

The algorithms of (Saffarzadeh, et al., 2014) , (Becker & Riviere, 2013) and (Bankhead, et al., 2012) are examples of unsupervised methods, whereas (Marin, et al., 2011) and (Soares, et al., 2006 ) are examples of supervised ones.

The border extension technique that is introduced in (Soares, et al., 2006 ) is used in (Saffarzadeh, et al., 2014). Its function is to separate between the border and vessels of Retina. It is a repetitive approach depends on determining the calculation of the mean value of neighbours for each pixel.

In several approaches such as in (Saffarzadeh, et al., 2014), the green channel of the retinal image is used as the input of the method as it provides the best contrast between the vessels and the background. (Saffarzadeh, et al., 2014) enhanced the green channel by using Weber's

law transform, to re-represent it into a perceptive space for effective vessel segmentation as shown in the (Saffarzadeh, et al., 2014) 's results.

The algorithm of (Saffarzadeh, et al., 2014) can be applied on abnormal fundus images containing bright or dark lesions. It uses K-means segmentation to reduce bright lesions, and uses a multi-scale line operator in a way that detects vessels in the presence of dark lesions.

### **6.2.5 The Developed Algorithm for Retinal Bifurcation Detection**

The developed algorithm, in this research, for detecting of Bifurcation, involves the following nine main processes:

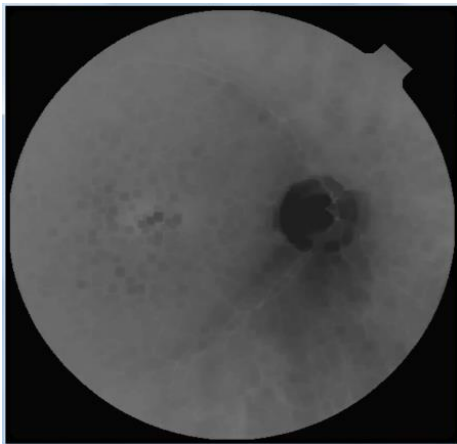
- 1) Skeletonization (which its output is in thick form)
- 2) Image thinning for Skeletonization
- 3) Small patterns removal
- 4) The verification of the Skeletonization Thinning
- 5) Image thinning for Improved Skeletonization
- 6) Cutting Small Branches
- 7) Removing the patterns with small dimensions
- 8) Creating of Watershed marker for vessel segmentation
- 9) Segmentation by Watershed

All these processes are developed or chosen from existing algorithms and arranged in the shown sequence according to experimental results, and the conclusions and results of published papers related to such operations. The existing algorithms that are used and taken from published scientific resources include Skeletonization for the first process, Image thinning for the second and fifth operations, and Watershed segmentation for the last step, whereas the other five processes are developed in this research. The five developed processes include: a) Small patterns removal; b) The verification of the Skeletonization Thinning; c) Cutting Small Branches; d) Removing the patterns with small dimensions; e) Creating of Watershed marker for segmentation.

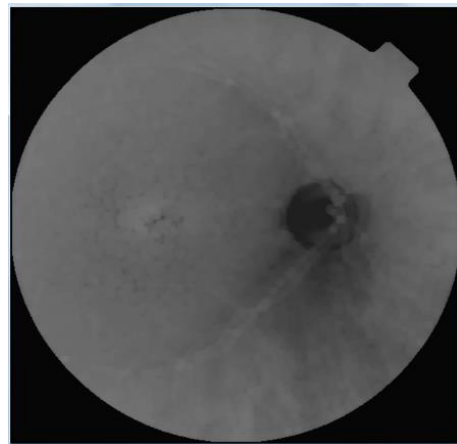


### 6.2.5.1 Skeletonization

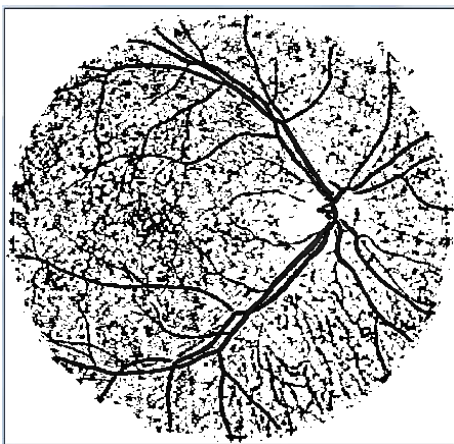
The concept of Skeletonization process depends on the erosion and dilation algorithms, It is shown as four steps in the next figure.



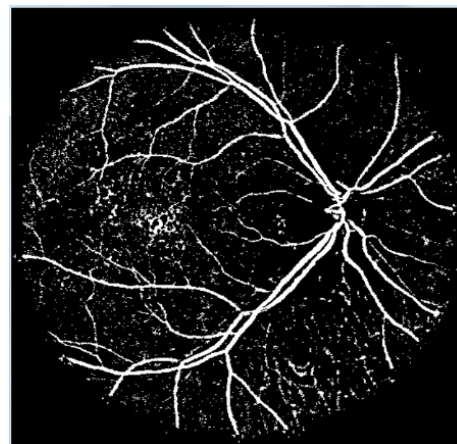
a) Step1: Eroding of Skeletonization



b) Step2: Dilating of Skeletonization



c) Step3: Subtracting of Skeletonization



d) Step4: The final Skeletonization result (vessels Mask)

*FIGURE 6.2.5.1 - 1: THE ALGORITHM OF SKELETONIZATION*

The following figure shows the preliminary result of Skeletonization before its modification by some developed corrections; As shown, there are some gaps among vessels in addition to some cuts in some of them. Consequently, the proposed algorithm has been updated to overcome such negative output, as shown in the previous figure in step4. It shows the black and white image of Skeletonization result without these gaps or cuts, according to the current developed algorithm of Skeletonization.

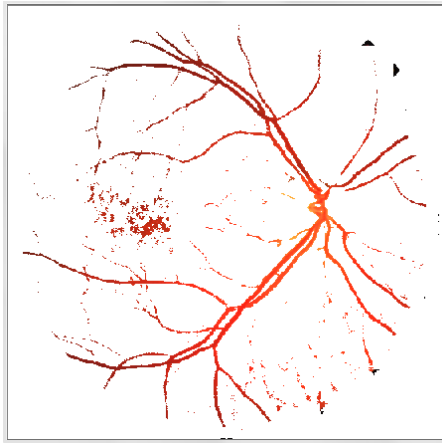


FIGURE 6.2.5.1 - 2: THE OUTPUT OF SKELTONIZATION BEFORE ITS UPDATING WITH SOME CORRECTIONS.

### 6.2.5.2 Image thinning for Skeletonization

It is a process to minimize the thickness of vessels to one pixel, to get vessels skeleton; Such operation is performed by applying eight common thinning filters with different structuring elements; These filters are:

$$\begin{aligned}
 & \{ 0, 0, 0 \}, \{ -1, 1, -1 \}, \{ 1, 1, 1 \} \\
 & \{ -1, 0, 0 \}, \{ 1, 1, 0 \}, \{ -1, 1, -1 \} \\
 & \{ 1, -1, 0 \}, \{ 1, 1, 0 \}, \{ 1, -1, 0 \} \\
 & \{ -1, 1, -1 \}, \{ 1, 1, 0 \}, \{ -1, 0, 0 \} \\
 & \{ 1, 1, 1 \}, \{ -1, 1, -1 \}, \{ 0, 0, 0 \} \\
 & \{ -1, 1, -1 \}, \{ 0, 1, 1 \}, \{ 0, 0, -1 \} \\
 & \{ 0, -1, 1 \}, \{ 0, 1, 1 \}, \{ 0, -1, 1 \} \\
 & \{ 0, 0, -1 \}, \{ 0, 1, 1 \}, \{ -1, 1, -1 \}
 \end{aligned}$$

Such operation represents generalization of Erosion and Dilatation filters, mathematical morphology, by extending flexibility of structuring element and providing different modes of its work. Structuring element may contain:

- 1 - foreground;
- 0 - background;
- -1 - don't care.

This process applies on the image resulting from previous operation, Skeletonization. The next figure presents an example of the result of this operation.

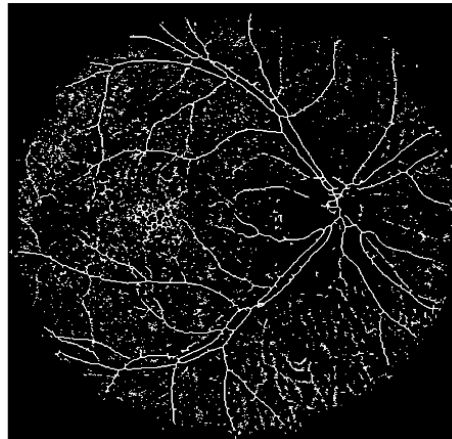
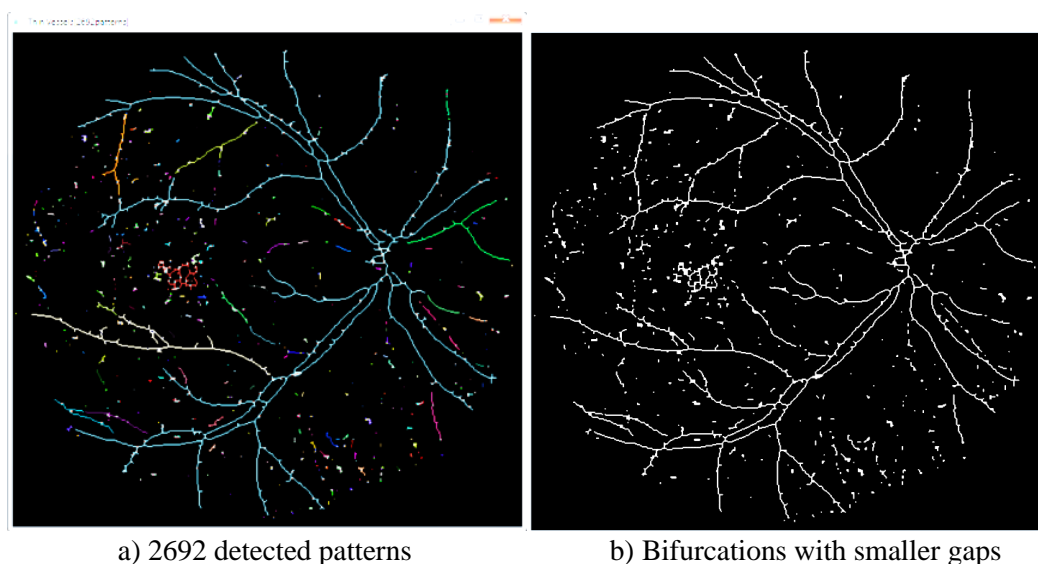


FIGURE 6.2.5.2 - 1: THINNING OF SKELETONIZATION

### 6.2.5.3 Reducing of gaps among bifurcations

It is a process to enhance the result of Skeletonization Thinning by Morphological operations, Dilating and Eroding, on each detected pattern, not on whole image. This operation aims to fill or reduce small gaps among bifurcations. The following figure presents an example of the pattern detection process which identifies 2692 patterns (branches) in vessels skeleton, and the enhanced bifurcations image resulted by this process. This image has smaller gaps than they were before.



a) 2692 detected patterns

b) Bifurcations with smaller gaps

FIGURE 6.2.5.3 - 1: PATTERN DETECTION OF BIFURCATION SKELETON AND REDUCING OF GAPS AMONG BIFURCATIONS

#### 6.2.5.4 The Verification of the Skeletonization Thinning

Some processes for Skeletonization depend on some mathematical morphology operations such as image Erosion and image Dilation. Such operations could erase some white pixels or insert new ones in the thin form of the vessel skeleton. Consequently, all pixels in the thin form of vessel skeleton must be verified. There are two outputs of Skeletonization process. One is in thin form, and the other is in thick form which is close to the actual thickness of the vessels in a retina. This verification is achieved by checking each pixel in the thin form, if it is white and the corresponding pixel in the thick form is white, it will be correct. Otherwise, it is incorrect and becomes black.

#### 6.2.5.5 Image thinning for Improved Skeletonization

This operation to ensure the vessel skeleton is still thin, thickness of one pixel, by reapplying the image thinning algorithm mentioned before.

#### 6.2.5.6 Cutting of Small Branches

This operation is the correction of the previous process of the image thinning, by removing all small branches connected with vessels. Such branches will be removed if their lengths are less than or equal to 7 pixels. The maximum length of 7 has been deduced through many experiments. This process is exemplified in the subsequent figure.

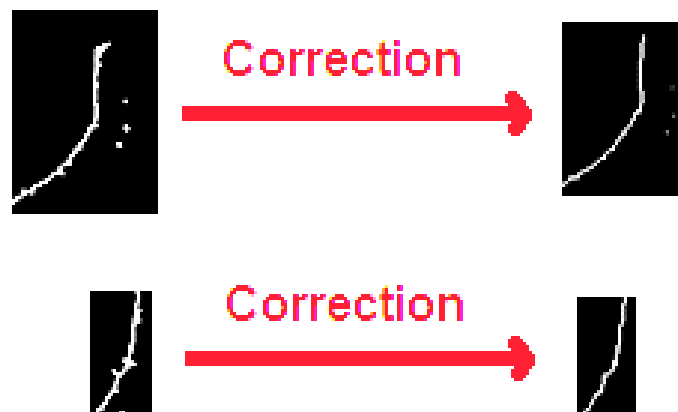


FIGURE 6.2.5.6 - 1: THE REMOVAL OF SMALL BRANCHES FROM VESSELS

This process has been repeated twice to remove even a branch that contains another branch, as shown in the two next figures. Taking into account that this process does not affect the extracted vessels (vessels skeleton) in the absence of any small branches.

The idea of such process is to remove any line which its length is less than given length (a length with 7 pixels) and any of its white pixels (pixel value=255) has only one surrounding white pixel. The tricky process is how to remove the root of such line, which is the first white pixel in this line that connected with the main line. Such trick is achieved by the following algorithm:

Firstly, assume the following pattern:

A00	A01	A02
A10	P	A12
A20	A21	A22

Where P is a tested white pixel (pixel value=255) and A00 to A22 are surrounding pixels.

The developed algorithm:

Case 1:

If A00 , A01, A02, A10, and A12 are all background pixel (black point) and the sum of the remaining surrounding points is greater than or equal 255, the tested white pixel (P) will be removed.

Case 2:

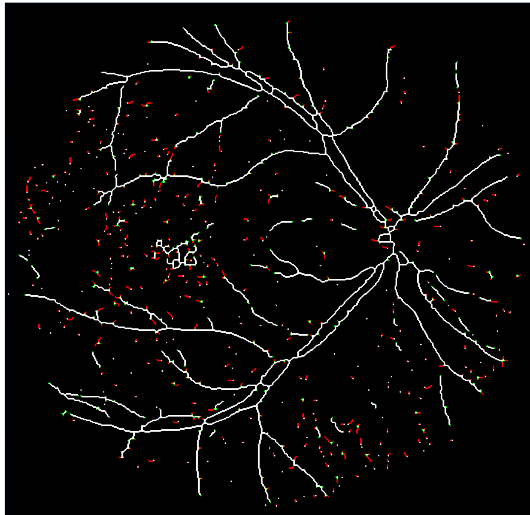
If A20 , A21, A22, A10, and A12 are all background pixel (black point) and the sum of the remaining surrounding points is greater than or equal 255, the tested white pixel (P) will be removed.

Case 3:

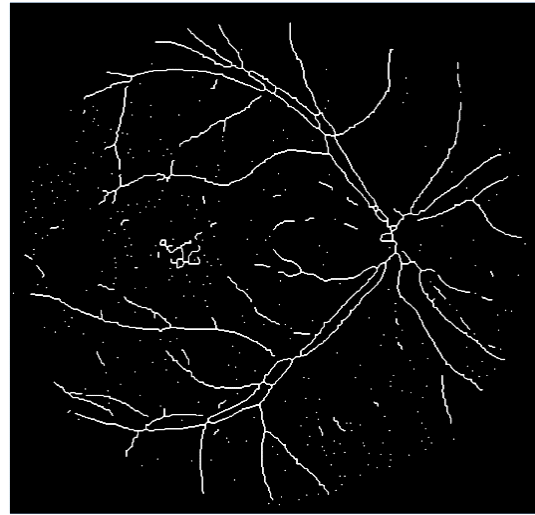
If A02 , A12, A22, A01, and A21 are all background pixel (black point) and the sum of the remaining surrounding points is greater than or equal 255, the tested white pixel (P) will be removed.

Case 4:

If A00 , A10, A20, A01, and A21 are all background pixel (black point) and the sum of the remaining surrounding points is greater than or equal 255, the tested white pixel (P) will be removed.

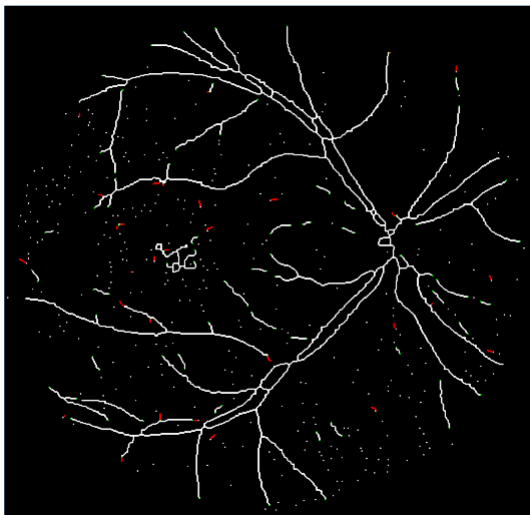


a) The removed pixels (red points)

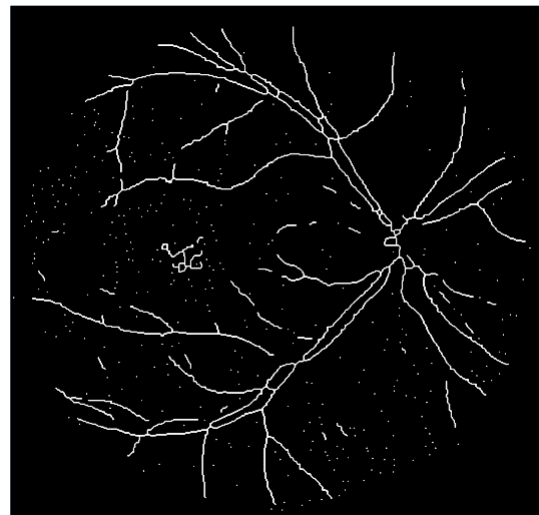


b) The result after removing of Small Branches

*FIGURE 6.2.5.6 - 2: THE RESULT OF FIRST EXECUTION OF SMALL BRANCHES CUTTING*



a) The removed pixels (red points)



b) The result after removing of small branches

*FIGURE 8.2.6 - 3: THE RESULT OF SECOND EXECUTION OF SMALL BRANCHES CUTTING*

### 6.2.5.7 Removing the patterns with small dimensions

This is removing any pattern that its height or its width is less than or equal specific value. This value is 70 pixels deduced through many experiments. The following three figures represent an example of such operation. The next figure shows the detected patterns in vessels skeleton, each pattern is shown with a specific colour.



FIGURE 6.2.5.7 - 1: PATTERN DETECTION OF BIFURCATIONS SKELETON AFTER ENHANCEMENT [5  
DETECTED PATTERNS]

The following figure is an example of the small patterns that have been removed.

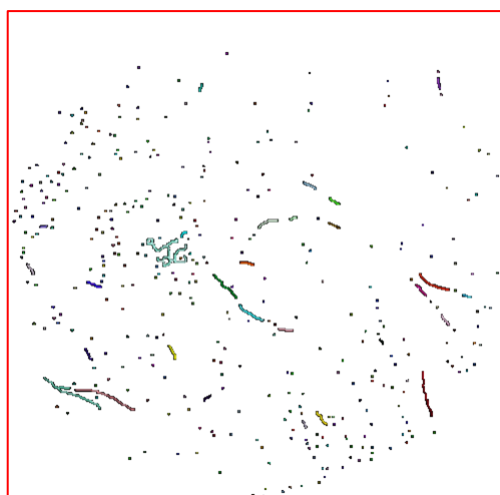


FIGURE 6.2.5.7 - 2: THE REMOVED PATTERNS FROM VESSELS SKELETON AFTER ENHANCEMENT [38]  
REMOVED PATTERNS]

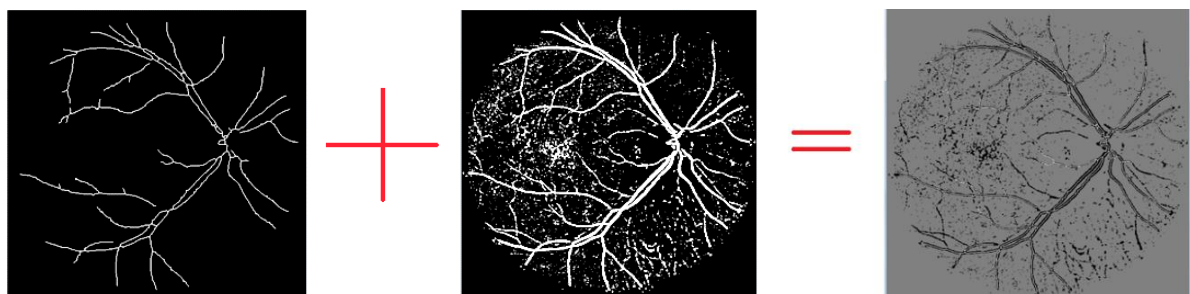
The next figure shows the vessels skeleton, in green colour, within a retinal image, after removing of all the patterns with small dimensions.



*FIGURE 6.2.5.7 - 3: THE BIFURCATION SKELETON, IN GREEN COLOUR, WITHIN A RETINAL IMAGE, AFTER REMOVING OF ALL THE PATTERNS WITH SMALL DIMENSIONS.*

### 6.2.5.8 Creating of Watershed marker for vessel segmentation

It is required to create a specific marker for applying Watershed algorithm for vessel segmentation. The next figure shows the developed process for creating such marker. It is created by incorporation of the resulting images from the two processes of Skeletonization and its Thinning, in the specific form, where the Black pixels in both these images will become Gray pixels in the Marker, the White pixels in Thinning image will become White pixels in the Marker, and the White pixels in Skeletonization image will become Black pixels in the Marker.



a) Thin Vessels Skeletonization.

b) Skeletonization result.

c) A Watershed marker as a result of incorporation process.

*FIGURE 6.2.5.8 - 1: THE INCORPORATION PROCESS OF CREATING A WATERSHED MARKER FOR BIFURCATION DETECTION*



### 6.2.5.9 Segmentation by Watershed

It is performed by applying Watershed algorithm (Beucher, 2010) (MathWorks, 1994-2015) on a retinal image with using the designed marker. The next figure is an example of the results of such vessel segmentation.

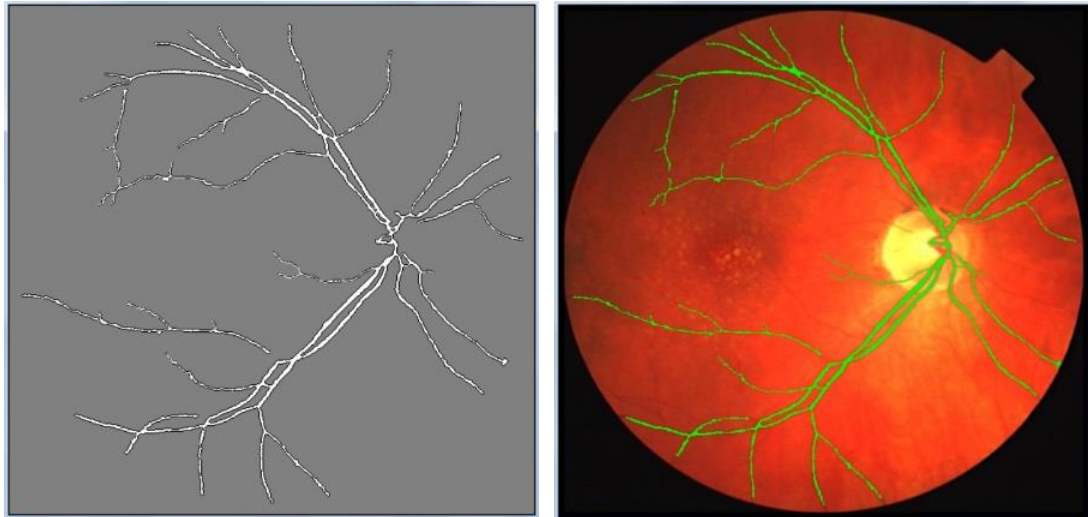


FIGURE 6.2.5.9 - 1: THE RESULT OF SEGMENTATION

### 6.2.5.10 The overall algorithm of the developed method for retinal Bifurcation Detection

The previous nine processes are the main operations in the developed algorithm for retinal vessels segmentation. These processes can be explained in detail in the following twenty-two steps within two stages:

#### **Stage 1: Image Loading and Pre-processing**

- 1) Loading of the retinal image *Img*.
- 2) Image Resizing to reduce the size of retinal image to speed up the following operations. The size of an image is reduced to 500x500 pixels instead of the actual size: 2912 x 2912 pixels.
- 3) Retina Cropping
- 4) Background extension
- 5) Green Channel Separation
- 6) Background Extension
- 7) Deriving the potential retina area [ Retina Mask 1 ]
- 8) Weber Space Transformation (Saffarzadeh, et al., 2014)
- 9) Reducing Bright Lesions By K-means Clustering
- 10) Border Extending

11) Deriving the potential retina area, RetinaMask2, from extended image

**Note:** the result image after implementing pre-processing is stored in EnhancedImage.

## **Stage 2: The vessels segmentation**

12) Create VesselByWatershedOutput as new black image in Gray colour space with the same size of the tested image Img, to store one of the outputs of this algorithm. This output is the retinal vessels detected by Watershed algorithm.

13) Create ThinnedVesselsOutput as new black image in Gray colour space with the same size of the tested image Img, to store the second output of this algorithm. This output is the detected retinal vessels in thin form.

14) Skeletonization: This process is the detection of vessels skeleton which is a structure of retinal vessels. It depends on a specific parameter, kernelSize. This parameter is used for erosion and dilation algorithms. The optimal value for this parameter is 7 for vessel segmentation. Its value has been deduced through many experiments. This process involves five operations as the following:

- a. Eroding, apply erosion algorithm on EnhancedImage. ErodedImg is the output of this operation.
- b. Dilating, apply dilation algorithm on ErodedImg. DilatedImg is the output of this operation.
- c. Subtracting of EnhancedImage from DilatedImg. Skel is the output of this operation.
- d. Calculating of the optimal threshold, this is achieved by calculating the optimal threshold value, OptimalThreshold, by using Otsu algorithm on Skel image.
- e. Deriving of VesselsMask. This operation is to convert the subtraction result, Skel, to binary image, black and white image, by changing all the colour values that are between OptimalThreshold-2 and 255 to white colour value, 255. With taking into the consideration that if OptimalThreshold-2 is less than zero, then the range of colour values become between 1 and 255. In other words, the colour values that are between 1 and 255 will be changed to white colour value, 255.

- 15) Image thinning for Skeletonization. This process is to convert VesselsMask to thin form by applying eight common thinning filters. ThinVessels is the output of this operation.
- 16) Small patterns removal. This operation is a correction of thinning process by removing the small patterns in the thin form of vessels, ThinVessels. This operation is achieved by applying dilating and eroding on each detected pattern in ThinVessels, not on whole image of ThinVessels. The output of correction is ThinVessels2.
- 17) The verification of the Skeletonization Thinning. It is another correction of thinning process. It checks each pixel in ThinVessels2. It is correct pixel If it is white and the corresponding pixel in VesselsMask is white. Otherwise, it becomes black. The output of this correction is in ThinVessels3.
- 18) Image thinning for ThinVessels3. This process to ensure ThinVessels3 is still thin, in particular after the process of small patterns removal.
- 19) Cutting Small Branches. This process is another correction by removing all small branches connected with vessels and store the output in ThinVessels4.
- 20) Removing the patterns with small dimensions. This process is additional correction by removing any pattern, in ThinVessels4, that its height or its width is less than or equal specific value which is 70 pixels according to the experiments results. The output of this process is in ThinVessels5.
- 21) Creating of Watershed marker for vessel segmentation. The invented Watershed marker is created by incorporation of the resulting images from the two processes of Skeletonization and its Thinning, VesselsMask and ThinVessels4, in the specific form, where the Black pixels in both these images will become Gray pixels in the Marker, the White pixels in Thinning image will become White pixels in the Marker, and the White pixels in Skeletonization image will become Black pixels in the Marker.
- 22) Vessel segmentation by Watershed. It is a process of applying image segmentation using Watershed algorithm with the innovative marker.

### **6.3 Future Works**

The proposed bifurcation algorithm, in this study, detects any branch in a retina. It could use this algorithm to detect only vessels accurately by some modification in the method.

### **6.4 Conclusion**

Control points are a vital part in retinal image registration system. Such points can be identified from the vascular structure of a retina or through bifurcations in a retina. These points are used to compute the possible displacements for the registration process.

Through the previous studies, some pre-processes should be implemented before applying of the vessel detection, for instance, using a green channel, Weber's law space, a border extension technique, and bright lesions reduction algorithm such as the method that uses K-means segmentation algorithm.

Overall, the research topic regarding control points detection is defined and the required algorithm is identified and achieved as a result of the current investigation and practical outcomes.

## **Chapter 7 – Registration and Changes Detection**

### **Overview**

This chapter starts by covering the state of the art about the techniques of image registration. Next, this chapter describes the theory of registration and its problems. It explains the reasons why the registration is difficult and why it is required to use control points and comparison techniques. Then, the chapter mentions the process of image rotation that could be required for registration. Subsequently, it presents the algorithm developed in this research for registration, “Bifurcation-based Registration Algorithm”.

Furthermore, this chapter includes the evaluation and the results of the developed algorithm. Then, the processes required for the detection of changes are illustrated. Such changes are the differences between two registered images. In the end of the chapter, the future works and the overall conclusion are presented.

### **7.1 Previous Approaches in Image Registration**

Regarding the related works, there are a various number of existing or common algorithms. They essentially depend on the field of required application. For instance, there are several approaches for medical image registration due to many reasons such as displacement, image quality, or the features or the structure of the part of human body in such images.

#### **7.1.1 Image registration classifications**

There are several classification for image registration methods. In general, there are four major categories: 1) View-Point Registration, for the images taken from various view-points or angles in a 3D stereo view; 2) Multimodal Registration, for images taken from varied sensors or cameras, from the same viewpoint; 3) Temporal Registration, for images taken over a time-separated period; and 4) Template Registration, a template matching to detect the common pattern or points.

Furthermore, as mentioned in (Andreou & Achim, 2010), there are four categories concerning an image registration: 1) Fourier-domain based; 2) point matching; 3) elastic model-based; and 4) correlation-based approaches.

However, the most comprehensive algorithm classification regarding image registration is as clarified in the paper of Sindhu Madhuri G. (G., 2014), which are:

1. Intensity-based versus feature-based: Intensity-based methods compare intensity patterns in images via correlation metrics, while feature-based methods find correspondence between image features such as points, lines, and contours.
2. Transformation models: They depend on used transformation models. There are two common categories: linear transformations and elastic or non-rigid transformations. The linear transformations include rotation, scaling, translation, and other affine transforms, whereas non-rigid transformations involve radial basis functions, physical continuum models (viscous fluids), and large deformation models.
3. Spatial versus frequency domain methods: Spatial methods are a matching of intensity patterns or features in images, whereas frequency domain methods works in the transform domain such as the phase correlation that uses the Fourier transform.
4. Single- versus multi-modality methods: The single-modality methods register the images that are acquired by the same scanner/sensor type, whilst multi-modality approaches register the images which are acquired by different scanner/sensor types.
5. Automatic versus interactive methods: They are based on the level of automation, to be manual, interactive or semi-automatic, or automatic.
6. Similarity modals : They are image similarity measures for image registration, to quantify the degree of similarity between intensity patterns in two images. They depend on the modality of the images to be registered. cross-correlation, mutual information are common examples of such methods.
7. Uncertainty models: They quantify a level of uncertainty associated with registering images that have any spatio-temporal differences; Such measure of uncertainty is critical for many change detection applications such as medical diagnostics; And in remote sensing applications where a digital image pixel may represent several kilometers of spatial distance.
8. Optimization models: They aim to minimize the deformation, the difference, between the two registered images. There are a variety of optimization methods of image registration, in particular in the metric used to determine the difference. There are a number of algorithms assume some restrictions on the deformation, some approaches concentrate on special aspects of the image, and others regularize the deformation to be smooth.

9. Parametric and non-parametric models: Such methods depend on sets of parameters and/or image features. The fundamental concept of these approaches is by marking some signs, landmarks, to align the registered images by specific transformation according to these markers. It is a process of matching the markers.
10. Rigid and non-rigid models: The rigid methods deal with an image as an object that can be translated or rotated, whereas non-rigid ones apply processes making changes in shape in addition to translation and rotation.

Furthermore, (Maintz & Viergever, 1996) presents classification for medical registration methods to nine criteria, as in the following figure.

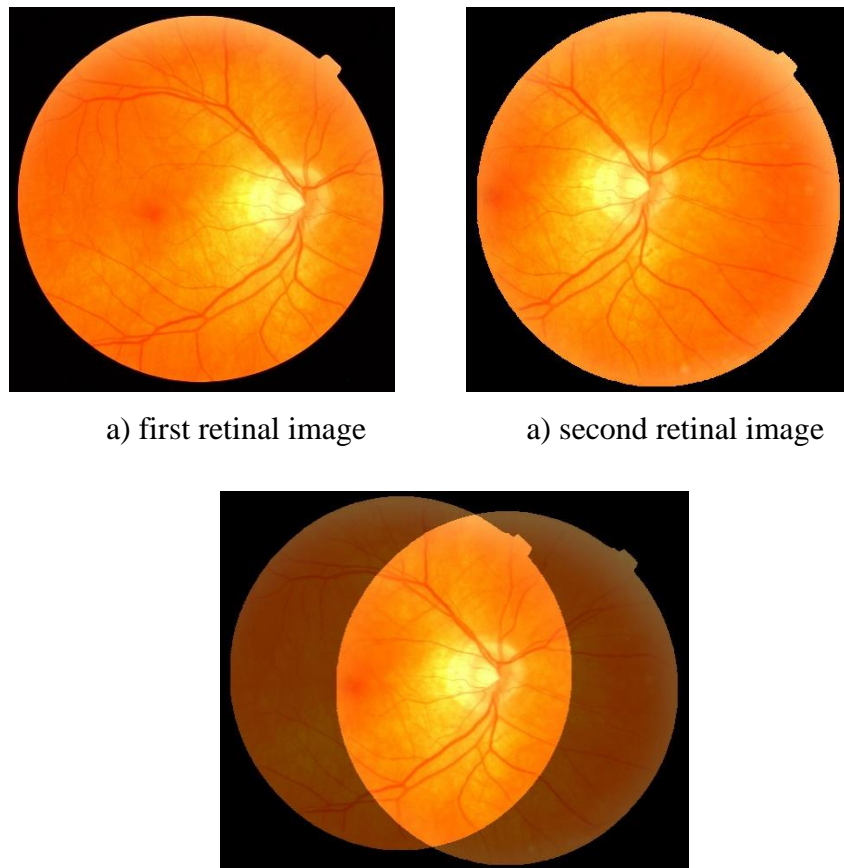
- I. Dimensionality:**
  - a. Spatial dimensions only: 1. 2D/2D 2. 2D/3D 3. 3D/3D
  - b. Time series (more than two images), with spatial dimensions:
    - 1. 2D/2D 2. 2D/3D 3. 3D/3D
- II. Nature of registration basis:**
  - a. Extrinsic:
    - 1. Invasive: A. Stereotactic frame B. Fiducials (screw markers)
    - 2. Non-invasive:
      - A. Mould, frame, dental adapter, *etc.* B. Fiducials (skin markers)
  - b. Intrinsic:
    - 1. Landmark based:
      - A. Anatomical B. Geometrical
    - 2. Segmentation based:
      - A. Rigid models (points, curves, surfaces)
      - B. Deformable models (snakes, nets)
    - 3. Voxel property based:
      - A. Reduction to scalars/vectors (moments, principal axes)
      - B. Using full image content
  - c. Non-image based (calibrated coordinate systems)
- III. Nature of transformation:**
  - a. Rigid b. Affine c. Projective d. Curved
- IV. Domain of transformation:** a. Local b. Global
- V. Interaction:**
  - a. Interactive: 1. Initialization supplied 2. No initialization supplied
  - b. Semi-automatic:
    - 1. User initializing 2. User steering/correcting 3. Both
  - c. Automatic
- VI. Optimization procedure:**
  - a. Parameters computed b. Parameters searched for
- VII. Modalities involved:**
  - a. Mono-modal:
    - 1. Autoradiographic 2. CT or CTA 3. MR
    - 4. PET 5. Portal 6. SPECT
    - 7. US 8. Video 9. X-ray or DSA
  - b. Multi-modal:
    - 1. CT—MR 2. CT—PET 3. CT—SPECT
    - 4. DSA—MR 5. PET—MR 6. PET—US
    - 7. SPECT—MR 8. SPECT—US 9. TMS—MR
    - 10. US—CT 11. US—MR 12. X-ray—CT
    - 13. X-ray—MR 14. X-ray—portal 15. X-ray—US
    - 16. Video—CT 17. Video—MR
  - c. Modality to model: 1. CT 2. MR 3. SPECT 4. X-ray
  - d. Patient to modality: 1. CT 2. MR 3. PET 4. Portal 5. X-ray
- VIII. Subject:** a. Intrasubject (1) b. Intersubject c. Atlas
- IX. Object:**
  - a. Head: 1. Brain or skull 2. Eye 3. Dental
  - b. Thorax: 1. Entire 2. Cardiac 3. Breast
  - c. Abdomen: 1. General 2. Kidney 3. Liver
  - d. Pelvis and perineum
  - e. Limbs (orthopedic): 1. General 2. Femur 3. Humerus 4. Hand
  - f. Spine and vertebrae

FIGURE 7.1.1 - 1: MEDICAL REGISTRATION CLASSIFICATION (MAINTZ & VIERGEVER, 1996).



### 7.1.2 Retinal image registration and its classifications

The most approaches of retinal registration are arranged in two classes: the former is vessel-based whilst the latter is automation-based. However, the majority of common algorithms are a temporal registration, and either they are feature-based, or point matching methods as clarified by Andreou and Achim (2010) due to the type of distortions occurring in retinal images. These methods depend on the detection of particular components of the whole retinal image. Such components are as points, warps, and features. They are required to determine the appropriate transformation for the registration. The following figure is an example of the registration of retinal images by the developed algorithm in this study.



The registration between the two images

*FIGURE 7.1.2 - 1: AN EXAMPLE OF THE REGISTRATION OF TWO RETINAL IMAGES BY THE DEVELOPED ALGORITHM.*

In addition, there are several methods of elastic transformation models such as the two supposed methods of (Can, et al., 2000) for a retina mosaicking. A review on mosaicking techniques in image processing is illustrated in the paper of (Abraham & Simon, 2013).

Furthermore, the majority of retinal image registration algorithms involve optic disc and vessel segmentation.

#### **7.1.2.1 Vessel-based Classifications**

This category includes two sorts: **vessel-based** and **non-vessel-based** methods. This is due to the nature of the retina structure involving the vessel network as the permanent existing landmark (Ferreira, 2012).

##### **7.1.2.1.1 Vessel-based Methods**

According to (Ferreira, 2012) and as stated by (Deng, et al., 2010), the geometry of retinal vascular bifurcations are unique and can be used in feature matching for registration.

The majority of methods in such category uses a feature matching technique and a describer for vascular structure. For instance, the algorithms of (Deng, et al., 2010), (Bhuiyan, et al., 2011), and (Chen, et al., 2011) as stated in (Ferreira, 2012) .

There are various representations of the describer of a vascular structure. It depends on a used algorithm. For example, (Bhuiyan, et al., 2011) describes each bifurcation, branch and crossover points, whereas (Chen, et al., 2011)'s describer involves a master bifurcation point and its three direct connected neighbours, in addition to the description of branching angle and branch length at each point.

The methodology of (Deng, et al., 2010) is by applying two algorithms together, ICP with quadratic transformation model, for registration of vascular models. Whilst, (Bhuiyan, et al., 2011) has concentrated on features extraction of vessels by segmenting of them and forming their feature vector representing the structure of vascular network. In contrast, the registration algorithm of (Ritchings, et al., 2006) is based on the matching being between the two optic disc centres detected by optic disc segmentation. Followed by image rotation of which the angle is calculated by fuzzy classifier depending on vessels structure of the retina. Firstly, the image segmentation of optic disc is achieved by histogram-based operations and the gradient circular Hough transform. Followed by the translation which is a matching of the two centres of each optic disc in both of retinal images. Next, the rotation is applied around the common centre of optic disc. The angle of rotation is calculated by the algorithm of the fuzzy classifier, depending on vessels structure of the retina. Finally, the differences between a pair of images

are detected by using the Euclidean distance between the corresponding pixels colours in the images.

#### **7.1.2.1.2 Non-vessel-based methods**

Most of recent algorithms are automatic image registration. In such methods, there are not any process or calculation depending on vessels structure. It is common in most of these algorithms to derive some parameters or features, for example, as in (Senol, et al., 2011), (Yang, et al., 2011), and (Ferreira, 2012). It is common that these features are points such as in (Andreou & Achim, 2010) and (Ferreira, 2012).

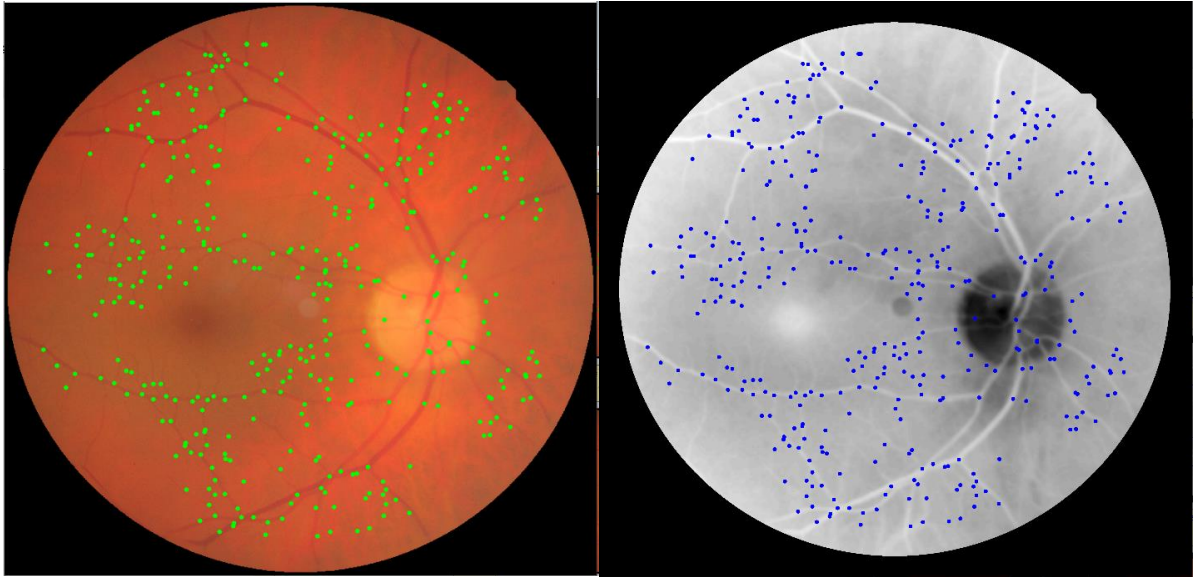
Furthermore, it is common that there is a correction of the mismatched correspondences, elimination of unwanted matches, in the methods that are based on features extraction, such as in (Ferreira, 2012) and (Yang, et al., 2011).

There are several methodologies of such approaches, for instance, as shown in (Ferreira, 2012), an automatic image registration algorithm is suggested by (Gonçalves, et al., 2011) using histogram-based image segmentation merged with objects extraction and matching in addition to some filters such as blurring. By comparison, in the paper of (Bardera, et al., 2010), the image registration is achieved by a method depending on compression between a pair of images. Another solution for the automatic registration is proposed by (Senol, et al., 2011); They based on deriving the parameters of geometrical transformation by using a radial basis function neural network algorithm. Such neural network is proven to be better than a feed forward neural network in the automatic image registration. Furthermore, the Robust Hybrid Image Matching algorithm is described by (Yang, et al., 2011). It aims to improve feature extraction and matching by applying a dynamic outlier rejection and a refinement technique to correct the mismatched correspondences. An additional methodology is developed by (Gonçalves, et al., 2011). It is a combination of three algorithms: an image segmentation, Scale Invariant Feature Transform, and robust outlier removal.

The (Andreou & Achim, 2010)'s registration technique is introduced by using the detected centroid of optic disc as an anchor point with some calculated points to perform the matching of registration. This matching depends on Mean Squared Error calculation, MSE. Such registration is not based on vessels to identify vascular crossing points and use them as anchor points. Also, its major processes such as rotation, scaling, and matching are not based on vessels. This is due to the low-quality of the used image, images of the murine eye. In such

images, there can be a noticeable vascular dissimilarities, noise, blurring, and distortions. (Andreou & Achim, 2010) proposed to use a combination of K-Means Clustering and A Trous , Stationery Wavelet Transform, for Vessels Segmentation required for change detection. For Optic disc detection, it depended on Thresholding, Dilation-Erosion and Centroid Calculation. Thresholding is applied twice, the former is applied to the high magnitude image pixels, i.e. the largest value ,bin, of the equalized histogram. In contrast, the later is achieved by discarding all the regions being smaller than the optic disc region where it is the largest region of connected high luminance pixels.

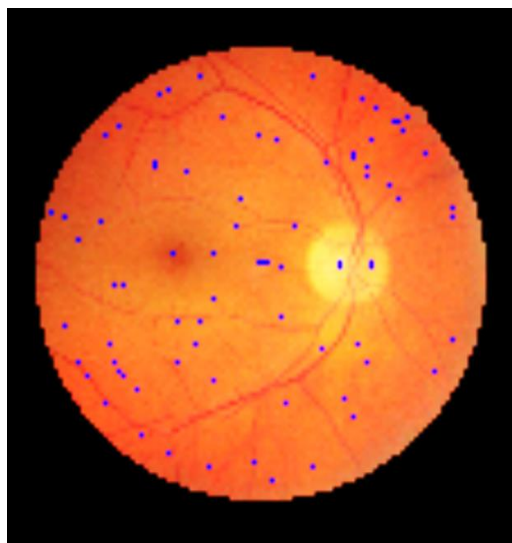
The other significant example of such methods is that in the suggestion of (Ferreira, 2012) using Scale Invariant Feature Transform, SIFT, as proposed by (Lowe, 2004). In such approach, each invariant key point is described by its position and direction, in addition to a computed descriptor in the form of a matrix. A key-point, sometimes is referred as a control point or an anchor point, is invariant when is not affected by rotation or image scaling. Subsequently, such points are matched by using a nearest neighbour approach through the Euclidian distance. Then, the elimination of unwanted matches is achieved by using a false positive algorithm. The proposed methodology of Lowe (2004) involves scale-space extrema detection, orientation and magnitude assignment, key-point descriptor. The scale-space extrema detection is to seek and locate steady features, key-points, through all potential scales. Then, the orientation and gradient magnitude of each key-point is calculated according to local image properties. The descriptor of each key-point is an array derived by using histogram analysis for surrounding pixels with depending on a key-point's orientation and gradient magnitude. This array will be used subsequently in the matching. In such algorithm, there are not any process or calculation depending on vessels structure, although the majority of key-points are on vessels network as shown in the example in the next figure.



*FIGURE 7.1.2.1.2 - 1: AN EXAMPLE OF 390 DETECTED CONTROL POINTS FROM FIRE DATASET IMAGE CODE: S03\_2 (BY THE CURRENT DEVELOPED ALGORITHM).*

### **7.1.2.2 Automation-based classifications**

In contrast, in this category, retinal registration systems can be classified to be **manual**, **semi-automated**, or **fully automated**. A manual system is based completely on the interaction of a user, by placement of a number of control marks, commonly points, within two images whereas there is no necessity to any user action during a fully automated registration which such those control marks are detected by the system itself. In contrast, a semi-automated system requires a limited user input, entering some marks, in addition to the computerized processes of a system. The following figure is an example of such marking.



*FIGURE 7.1.2.2 - 1: THE CONTROL MARKS*

## 7.2 Image Registration

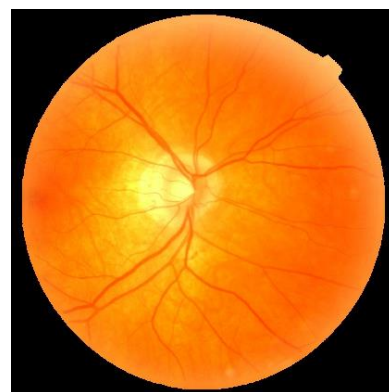
To develop a new algorithm, the theory of registration should be understood and therefore the problems or the issues regarding this process can be addressed.

### 7.2.1 Registration Theory

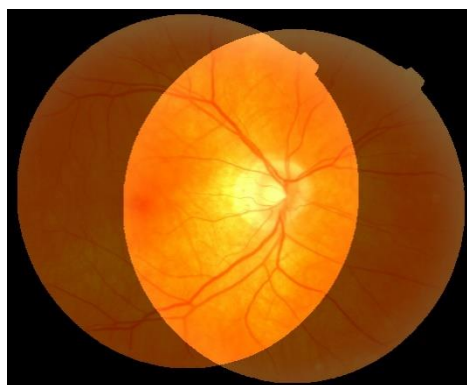
The concept of image registration can be considered as a process of a mapping transformation, from one image to another. The next figure presents a result of such operation by the developed algorithm in this study. This transformation depends on specific parameters. The identification of such parameters is considered as the major problem in the registration process. The correct choice of these parameters ensures the best transformation that can be applied for successful image registration.



a) First retinal image



b) Second retinal image



c) The registration between the two images

*FIGURE 7.2.1 - 1: IMAGE REGISTRATION.*

### **7.2.2 The Registration Problem**

To develop an efficient algorithm for registration of retinal images, the problems of such operation, must be addressed. The most significant processes for achieving of the registration are: Feature Extraction and Similarity measurement. These complex operations can be listed as in the following two questions:

*What are the most suitable features that can be used as control points to apply the registration?*

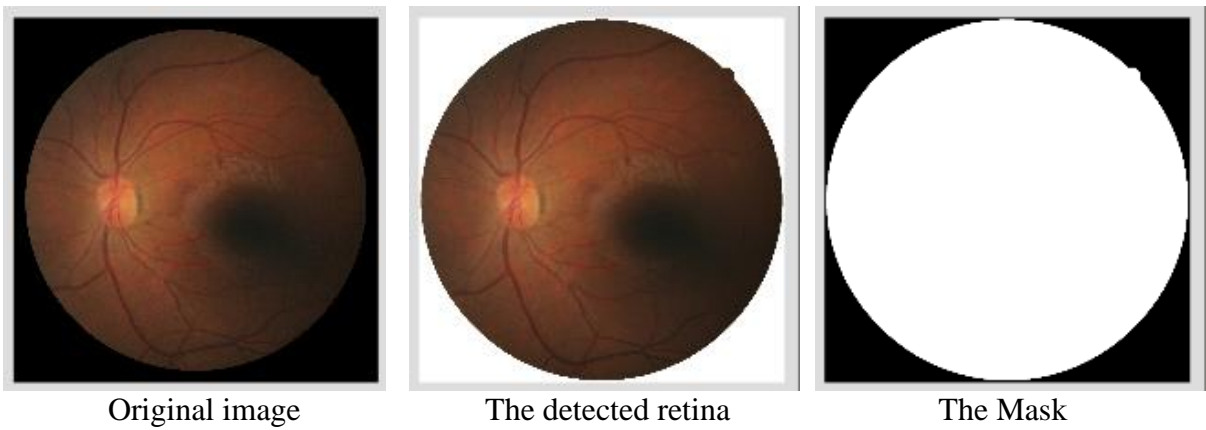
*How to measure the similarity of each possible match to find the best match between two parts of the two tested images.*

### **7.3 The Developed Algorithm**

The aim of the registration process is to match two retinal images by finding the common or overlapped area between them. On the other hand, it aims to find a corresponding point in an image to a point in the other image within overlap area. The processes of the developed algorithm were chosen following extensive experimentation, involving many attempts to develop a variety of processes evaluated by a large number of tests. The algorithm processes can be divided into three stages: control points detection, inliers extraction, and the calculation of the coordinates of the corresponding point.

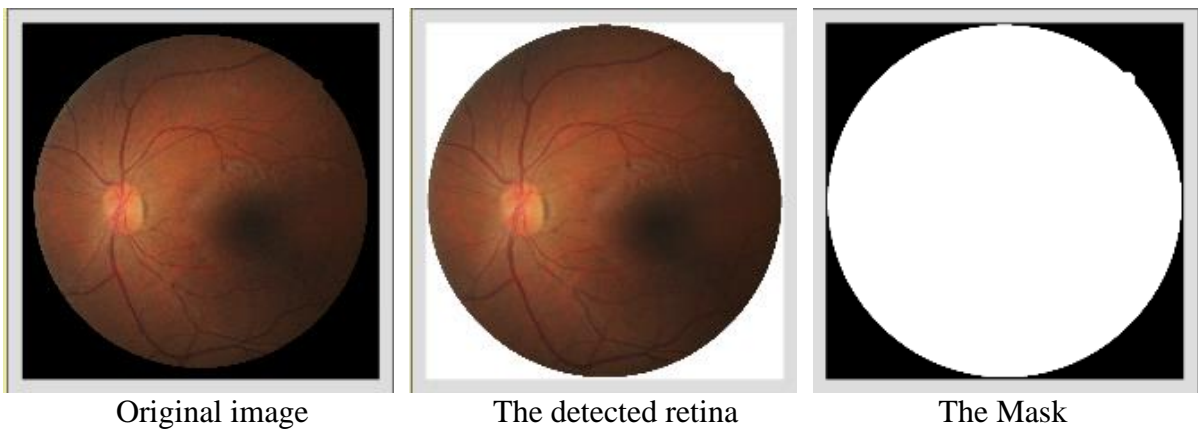
The first stage is to detect the positions of control points. This stage involves some pre-processes which are identify the retina area, resizing (to 500x500 pixels), background enlarging, colour matching, and finding masks that locates the retina area including dark spots in a retina. A retina size is resized to reduce the time required to detect control points. In the current developed algorithm, the image size is reduced to 500x500 pixels instead of the actual size: 2912 x 2912 pixels).

The developed method uses the cross points among bifurcations, in a retina, as control points. The next two figures are examples of the retina area detection in dark retinal images.



Original image                      The detected retina                      The Mask

*FIGURE 7.3 - 1: THE EXAMPLE-1 OF THE RETINA AREA DETECTION FOR A DARK RETINAL IMAGE  
(IMAGE FIRE DATASET CODE: S37\_1)*

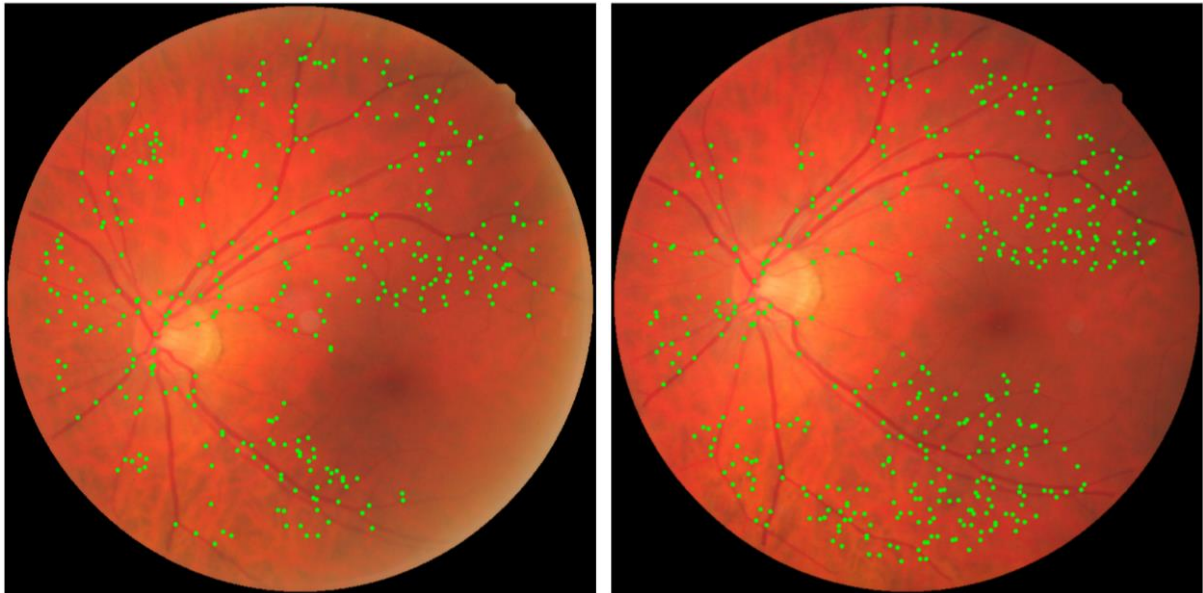


Original image                      The detected retina                      The Mask

*FIGURE 7.3 - 2: THE EXAMPLE-2 OF THE RETINA AREA DETECTION FOR A DARK RETINAL IMAGE  
(IMAGE FIRE DATASET CODE: S42\_2)*

The subsequent stage is to identify the right matches between the detected control points. For example, as shown in the next figure, through the image pair S71 in FIRE dataset, 342 control points are detected in a reference image, and 440 points in a tested image. So, there are 136,800 (342 x 440) possible matches. If it is considered some points in the first image have not any match in the second image, therefore it is required at most 342 matches of 136,800 possible matches.





342 control points are detected  
in a reference image

440 control points are detected  
in a tested image

*FIGURE 7.3 - 3: AN EXAMPLE OF CONTROL POINTS DETECTION FOR FIRE DATASET IMAGE PAIR: S71*

This stage depends on RANSAC algorithm (Martin A. & Robert C., June 1981) and similarity measurement. The RANSAC algorithm is used to estimate the correct correspondences. RANSAC is a robust estimation approach which aims to conclude the best point pairs (inliers) among many matches including some wrong ones (outliers). However, RANSAC algorithm cannot give good estimation when there are a huge number of outliers (noise points). For instance, though FIRE image pair: S71, RANSAC fails to derive the correct inliers among 136,800 correspondences. Therefore, it is required to minimize the number of outliers (wrong correspondences).

At the beginning, the two retinal images are converted to Gray scale following by Bitwise-Not operation. After that, the colours of the two images are normalized so that their colour values become between 0 and 255. The result of such operations can be exemplified in the next figure. It presents the pre-processed image from the retinal image of FIRE dataset (FIRE image code: S03\_1). Such pre-processed images are used for similarity measurement.



*FIGURE 7.3 - 4: THE PRE-PROCESSED IMAGE, FIRE CODE: S03\_1, USED FOR SIMILARITY MEASUREMENT.*

Subsequently, the similarity value is computed between each control point in a reference image and each control point in a tested image. For instance, regarding FIRE set: S71, 136,800 similarity values are calculated. The similarity is measured by Normalized Cross Correlation, a Template Matching method (Brunelli, March 2009), within the overlap between two tested areas (which their sizes: 157 x 157 each). The overlap area must be detected so that it does not include any background points. The presence of a black dot or a background point very negatively affects the outcome. Before measuring the similarity, within the overlap region, colours of the tested area in the second image is normalized to the colours of the tested area in the first image (reference image). Another consideration is that the number of pixels in the overlapped area must be greater than a quarter of the number of points in the tested area of the reference image, otherwise the Similarity Value equals -1 (not matched). In another meaning, in the case of there is small overlap, the similarity measurement will be ignored. The computed Similarity Value is percentage value, ranged between 0 and 1. The number 1 means: the two areas are 100% matched.

The following processes designed for this stage, depends on three parameters. They are identified through some processes in the developed method. These parameters are: the maximum Allowed Displacement (AD), the best RANSAC Threshold (RT), and the best Equal Similarity limit (ES) that can be considered two matches have same similarity value. To determine the values of these parameters, firstly a study achieved on the 710 ground truth points in S-Category image pairs in FIRE dataset. Three numbers are computed trough this investigation. They are the maximum displacement in x-axis and y-axis coordinates (GT\_max\_Dx, GT\_max\_Dy) and maximum distance (GT\_max\_Distance) between two

corresponding points. Their values are 103, 291, and 291 respectively. These are used as the initial values to find the best values of the three parameters: AD, RT, and ES. Taking into consideration, these values (GT\_max\_Dx, GT\_max\_Dy and GT\_max\_Distance) can be ignored, however, this leads to more execution time.

All corresponding points are tested through several different values for AD, RT and SS. In each test, the number of inliers (N) is calculated and through that, the best values for AD, RT and ES are at the largest value of N.

Subsequently, the possible matches are identified by using the computed values of the maximum allowed displacement (AD) and the best similarity difference (ES). For example, through this operation on FIRE set: S71, the number of correspondences becomes 4979 instead of 136,800, decreased by 96.36%.

Next, the value of the best RANSAC Threshold (RT) are chosen among the RANSAC Threshold values: 28 to 31. For each value of them, the number of inliers is calculated, by RANSAC method, through the last identified correspondences. As a result, the best RANSAC Threshold is the threshold value that gives the largest number of inliers.

The final step for detecting the correct matches (inliers) is by applying RANSAC approach with using the last best value calculated for ANSAC Threshold. As an example, within FIRE set: S71, the number of inliers obtained by this process is 197 matches with RANSAC Threshold equals 31.

The last stage is to compute the corresponding coordinate for any given coordinate (x1,y1). The main target of this stage is to find the Transformation formula (Transformation Matrix). The first process in this stage is to find the two centroids of inliers in reference image and tested image. They are centroid1 (AvgX1,AvgY1) and centroid2 (AvgX2,AvgY2) respectively. Then the displacement of each inlier, in the reference image and the tested image, is calculated from the image centroid. The subsequent operation is to derive perspective transformation matrix between the calculated displacements in the first image and those are in the second image, using RANSAC as a Homography Method with RANSAC Threshold equals 31. This computed transformation could be considered as a rotation formula (matrix). Next, the transition value (TrX,TrY) is computed by applying warpPerspective using perspective transformation (Transformation Matrix) to find the corresponding point (x2,y2) in the tested image to the reference image point (x1=0,y1=0) according to the following formula:

$$x2 = (\text{TransMatrix}[0, 0] * x1 + \text{TransMatrix}[0, 1] * y1 + \text{TransMatrix}[0, 2]) / (\text{TransMatrix}[2, 0] * x1 + \text{TransMatrix}[2, 1] * y1 + \text{TransMatrix}[2, 2])$$

$$y2 = (\text{TransMatrix}[1, 0] * x1 + \text{TransMatrix}[1, 1] * y1 + \text{TransMatrix}[1, 2]) / (\text{TransMatrix}[2, 0] * x1 + \text{TransMatrix}[2, 1] * y1 + \text{TransMatrix}[2, 2])$$

$$x2 = \text{TransMatrix}[0, 2] / \text{TransMatrix}[2, 2]$$

$$y2 = \text{TransMatrix}[1, 2] / \text{TransMatrix}[2, 2]$$

Then,  $\text{TrX} = \text{AvgX2} + x2$ ,  $\text{TrY} = \text{AvgY2} + y2$

Accordingly, the corresponding point (X2,Y2) in a tested image for a given coordinate (X1,Y1) in a reference image is detected by applying warpPerspective using perspective transformation (Transformation Matrix) as follows:

$$x1 = X1 - \text{AvgX1} \quad , \quad y1 = Y1 - \text{AvgY1}$$

$$x2 = (\text{TransMatrix}[0, 0] * x1 + \text{TransMatrix}[0, 1] * y1 + \text{TransMatrix}[0, 2]) / (\text{TransMatrix}[2, 0] * x1 + \text{TransMatrix}[2, 1] * y1 + \text{TransMatrix}[2, 2])$$

$$y2 = (\text{TransMatrix}[1, 0] * x1 + \text{TransMatrix}[1, 1] * y1 + \text{TransMatrix}[1, 2]) / (\text{TransMatrix}[2, 0] * x1 + \text{TransMatrix}[2, 1] * y1 + \text{TransMatrix}[2, 2]);$$

$$\text{Then } X2 = x2 + \text{TrX} \quad , \quad Y2 = y2 + \text{TrY}$$

The following step is to find the best match location of the corresponding point (X2,Y2). This step is a correction for the previous process. It searches for the best similarity between the point (X1,Y1) and the points (X2+j,Y2+i) where i and j range from -C to C. The value of C is identified through testing 710 points of FIRE ground truth points, it is found that the maximum correction in either x-axis or y-axis does not exceed 49 pixels. Therefore, C equals 49. The value of C could be more than 49, however, this makes the process takes longer. The largest similarity value refers to the best match. This process is repeated twice, one uses Feature Dimension equals 97 and the second repetition uses Feature Dimension equals 177. The Feature Dimension is a dimension of the surrounding area of a point. In other words, if Feature Dimension is 97, the tested area will be 97 x 97 pixels. The two values, 97 and 177, are identified through many experiments to get more accurate similarity measurement than using only one testing size.

Before similarity is measured, the overlap area is detected between the two tested areas. Then the height and width of the overlap are computed. If one of its dimensions is less than Small Dimension Limit, Feature Dimension will be increase as follows:

$$\text{FeatureDimension} = 2 * \text{FeatureDimension} - \min(h,w), \text{ where } h \text{ and } w \text{ are height and width of the overlap respectively.}$$

Through experiments, the best value of Small Dimension Limit is 95. That means the height and width of the overlap must be at least 95 pixels. The next figure shows an example of small overlap. The size of the overlap area is 44 x 145 (Width=145 , Height=44).

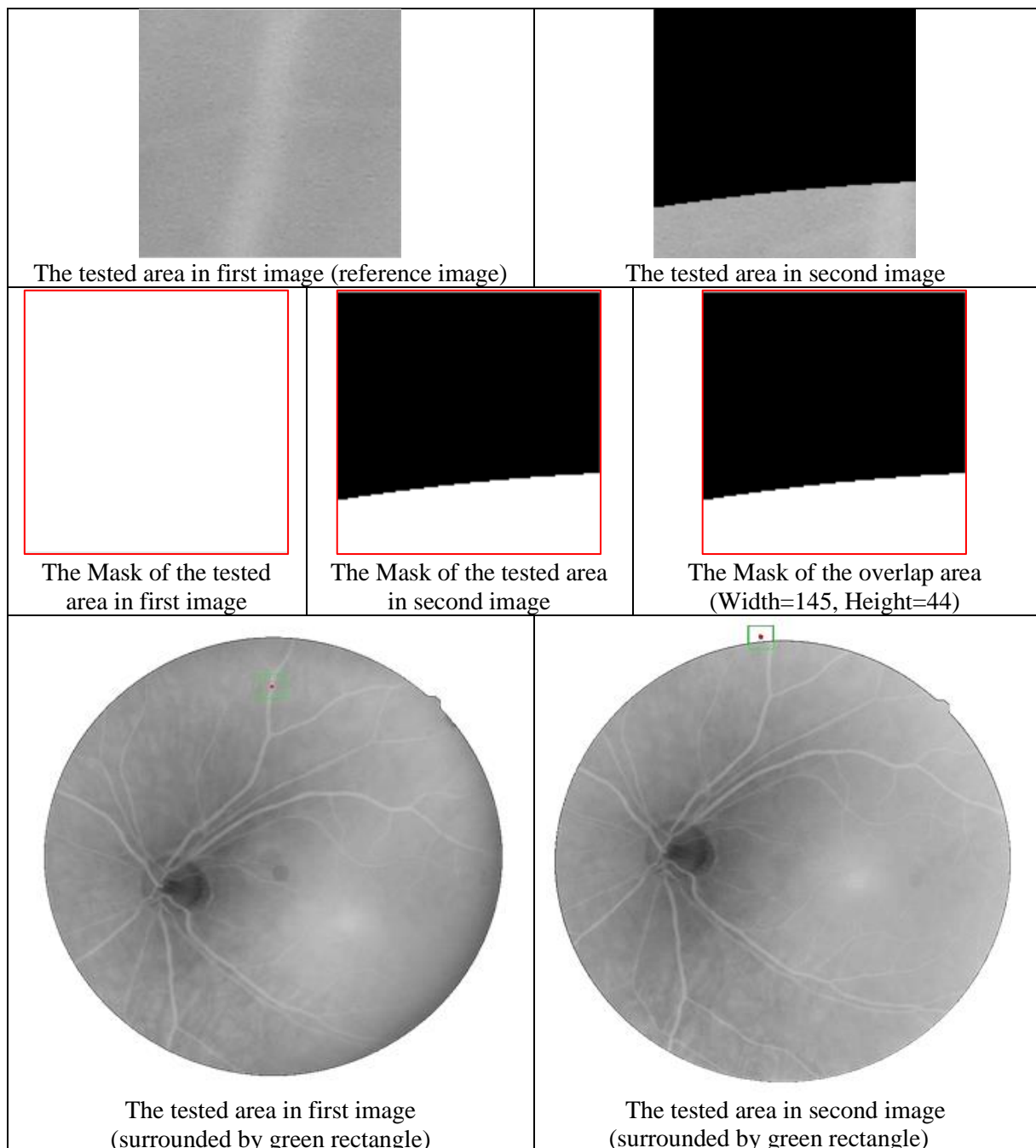


FIGURE 7.3 - 5: AN EXAMPLE OF SMALL OVERLAP DURING COMPARING THE FIRE IMAGE PAIR: S71 IN THE FIRST GROUND TRUTH POINT.

Previously, the small overlap case is ignored. In other words, the similarity is not measured when there is small overlap. However, currently, the developed algorithm solves this issue by increasing the size of the test area. This conception is obvious in the following figure (same example of the previous figure). As presented, the overlap size is larger than the original overlap size that is shown in the small overlap example in the previous figure.

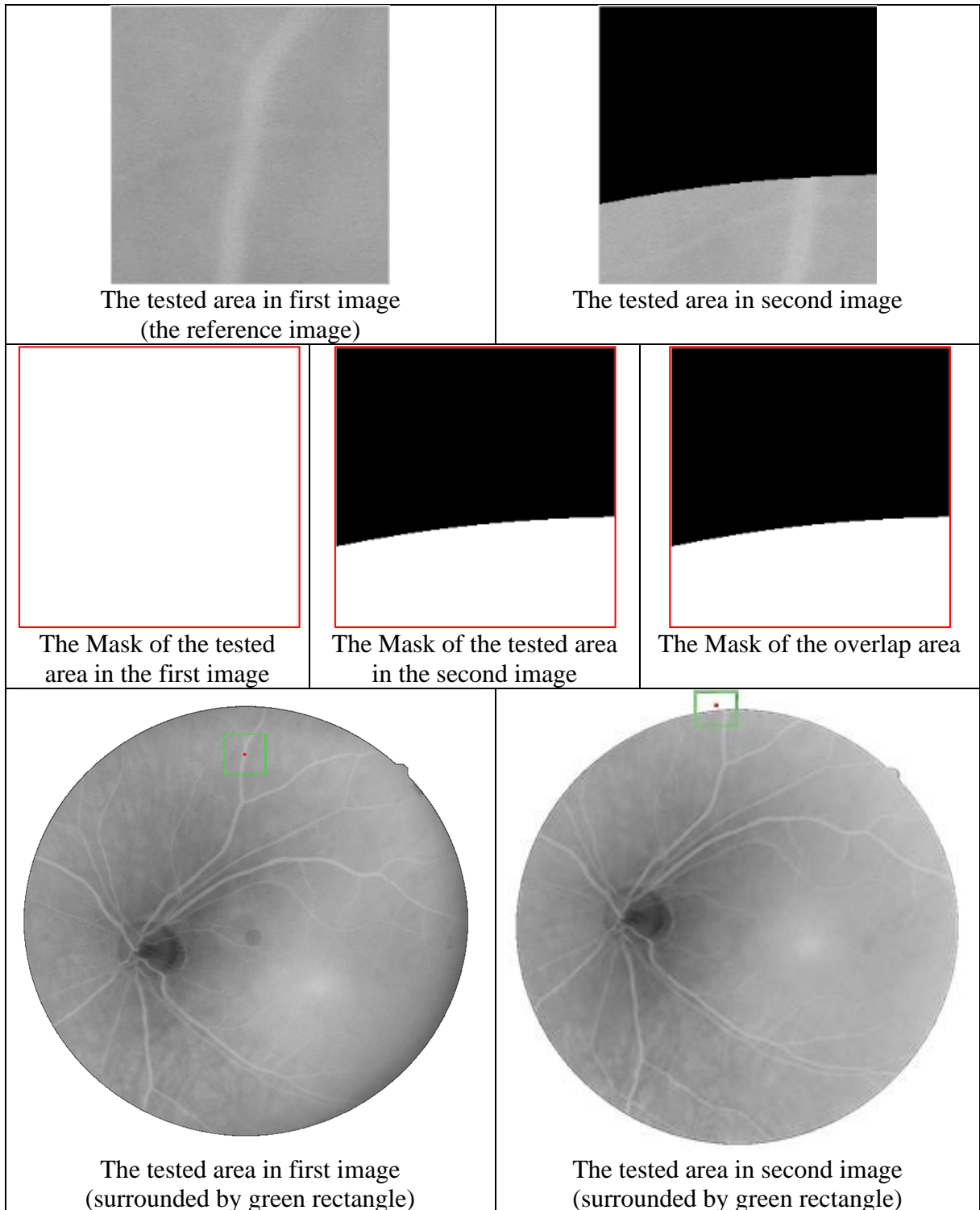
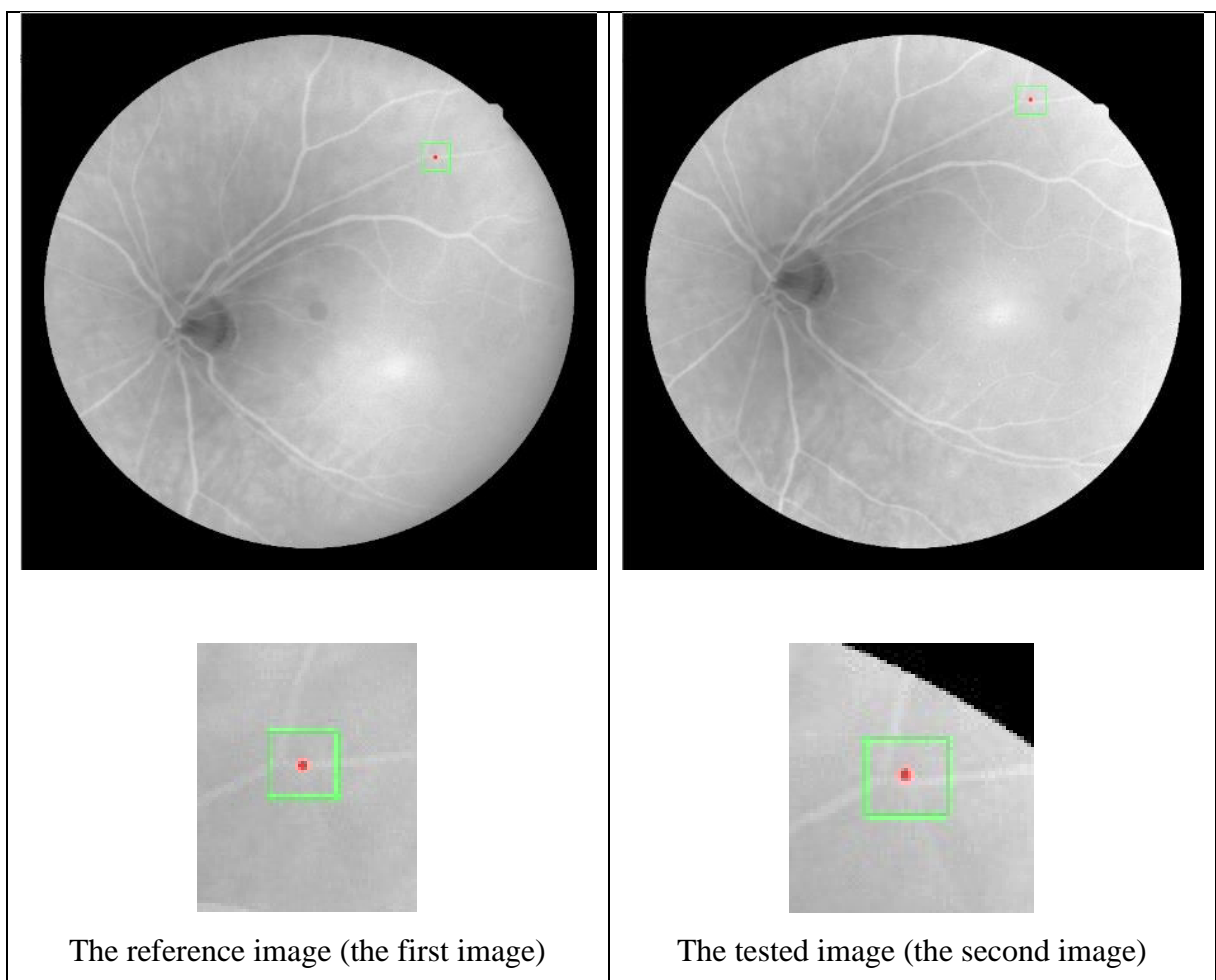


FIGURE 7.3 - 6: AN EXAMPLE OF SMALL OVERLAP DURING COMPARING THE FIRE IMAGE PAIR: S71 IN THE FIRST GROUND TRUTH POINT.

Subsequently, in the overlap area, the specific area in a tested image is normalized to have the same range of colour values for the pixels in the specific area in reference image. Finally, the similarity is measured by using CcorrNormed method which is one of common Template Matching methods. The similarity value ranges from 0 to 100%. The largest value refers to the best similarity, therefore to the best match.

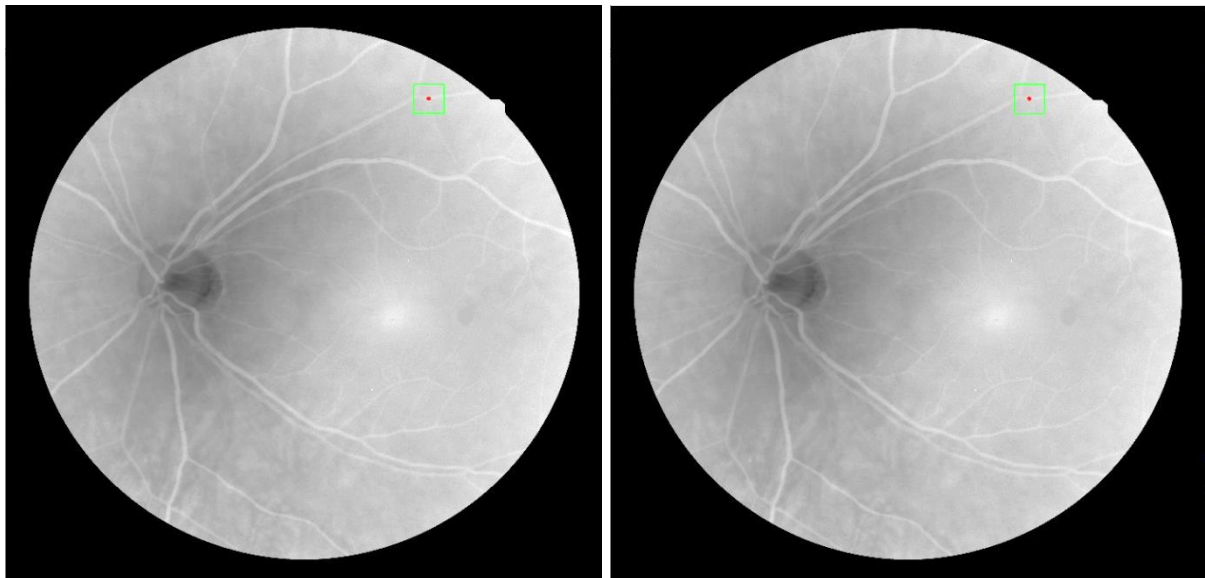
To clarify the importance of the correction process, the next figure shows the last result of the matched point of the second ground truth point, in FIRE image pair: S71, before the correction. Obviously, the matched point should be more down and a little to the right.



*FIGURE 7.3 - 7: AN EXAMPLE OF A DETECTED MATCHED POINT BEFORE THE PROCESS OF THE BEST MATCH DETECTION (OR CORRECTION PROCESS), THROUGH FIRE IMAGE PAIR: S71 IN THE SECOND GROUND TRUTH POINT, THE CALCULATED SIMILARITY VALUE IS 0.999 (OR 99.9%).*

The following figure presents the result of the correction comparing with the right result from the FIRE dataset. According to the similarity measurement results, the match obtained by the

developed algorithm (99.9677%) is better than the one that is identified by the ground truth of the FIRE dataset (99.9458%).

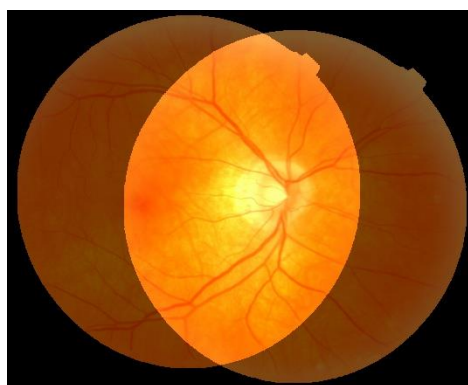


a) The best match in the second image

b) The FIRE dataset's ground truth

*FIGURE 7.3 - 8: THE DETECTION OF THE BEST MATCH, THROUGH FIRE IMAGE PAIR: S71 IN THE SECOND GROUND TRUTH POINT, SIMILARITY VALUE (OF THE RESULT OF THE DEVELOPED ALGORITHM) IS 0.999677, WHEREAS SIMILARITY VALUE (OF THE GROUND TRUTH) 0.999458.*

The final result of this developed registration algorithm is obtained after a number of matches. This result is exemplified in the next figure.



*FIGURE 7.3 - 9: THE REGISTRATION RESULT BY THE DEVELOPED BIFURCATIONS-BASED ALGORITHM.*



## **7.4 The Evaluation and Results**

In order to evaluate the developed registration algorithm, several tests are achieved by using different retinal images from specific dataset; In addition to the evaluation of the cross points detection.

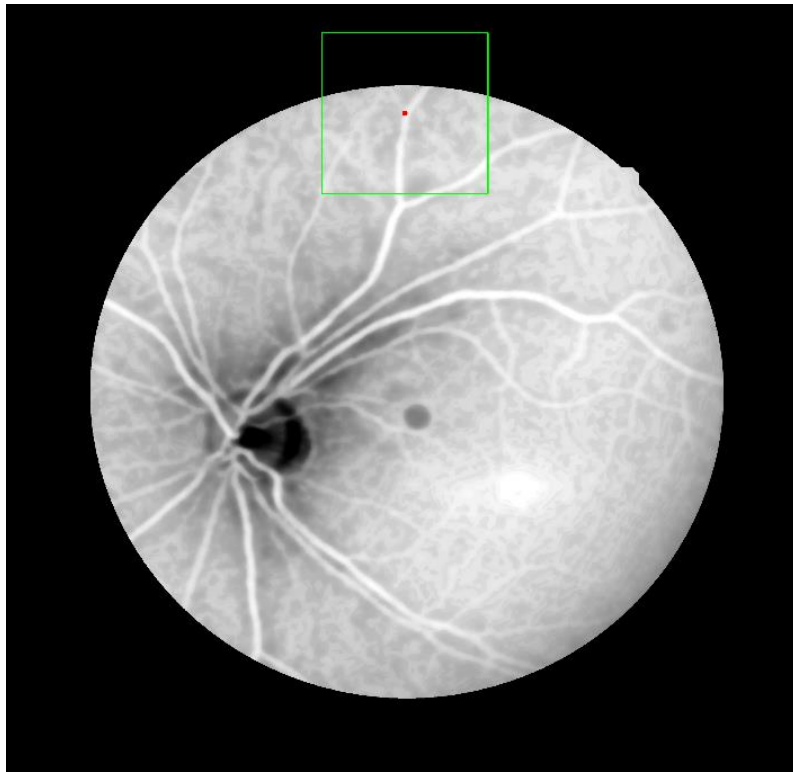
### **7.4.1 FIRE: Fundus Image Registration Dataset**

“The FIRE dataset consists of 129 retinal images forming 134 image pairs. These image pairs are split into 3 different categories depending on their characteristics. The images were acquired with a Nidek AFC-210 fundus camera, which acquires images with a resolution of 2912x2912 pixels and a FOV of 45° both in the x and y dimensions. Images were acquired at the Papageorgiou Hospital, Aristotle University of Thessaloniki, Thessaloniki from 39 patients.” (Hernandez-Matas, et al., Jul. 2017)

The three categories are: S, P, and A. Only the S-category image pairs are used in this study. S stands for Similar. S-category has significant overlap, no anatomic change, and a lot of potential information to use in registration.

### **7.4.2 Evaluation**

This evaluation shows Registration-Error Results comparison, between the developed method and other four existed Methods. Firstly, to understand the value of a Registration-Error Result, the following three images show a red dot in a retina image (the next first picture) with size equals 21 x 21 pixels. As shown in the next second picture, the x-coordinate of the most-left pixel in the dot is 21, whereas the most-right one is 41 (as in the next third picture). Therefore, the width of the dot is  $41-21+1=21$  pixels. This example can show how big there is 21 pixels, or how big there is to be a mismatch by 21 pixels. This gives a perception that if there is a mismatch error (Registration-Error) of less than 7 pixels, such error could be difficult to be distinguished by the human eye. Actually, that was the goal of the current developed system for Registration-Error to be less than 7 pixels.



*FIGURE 7.4.2 - 1: REFERENCE IMAGE (FIRE IMAGE PAIR: S71) (A KEYPOINT IS COLORED BY RED, AND SURROUNDED BY GREEN RECTANGLE WHICH IS REPRESENTED THE TESTING AREA IN MATCHING PROCESS)*

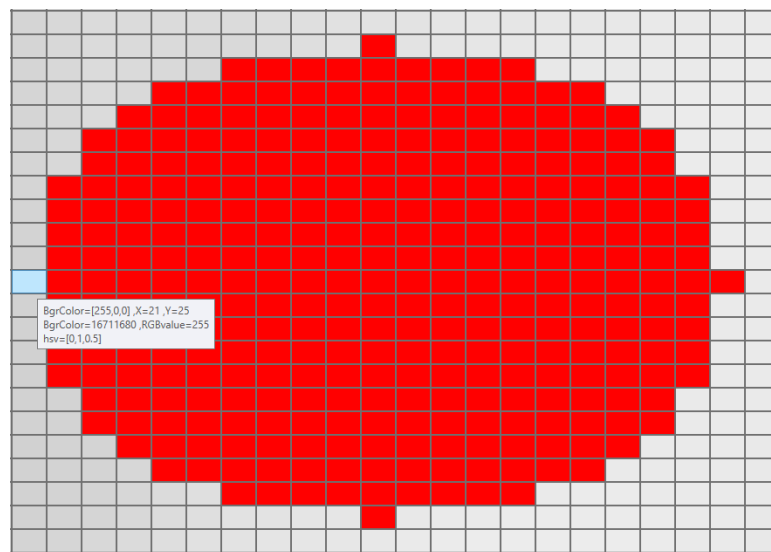


Figure 7.4.2 - 2: The x-coordinate of the most-left pixel in the red dot (x=21)

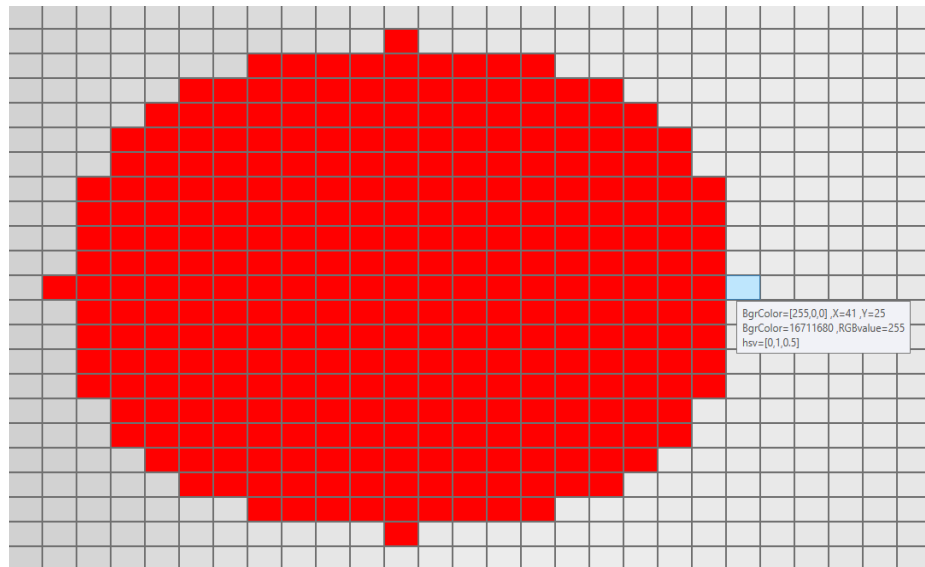


FIGURE 7.4.2 - 3: THE X-COORDINATE OF THE MOST-RIGHT PIXEL IN THE RED DOT (X=41)

Registration Error is calculated by computing the distance between two points: a ground truth point in a tested image and the registered point detected by the developed algorithm. The Distance between two points P(x1,y1) and Q(x2,y2) is given by:

$$d(P, Q) = \text{sqrt}((x2 - x1)^2 + (y2 - y1)^2)$$

#### 7.4.2.1 Using SURF features as Control Points

In the early stages of developing the algorithm, SURF algorithm is used to extract features (points) to be used as Control Points instead of intersection points between bifurcations.

To find out what are the best points can be used as Control Points, intersection points or SURF-points, an initial evaluation is implemented. It uses the first ten images in FIRE dataset in S-category. These images are shown in the next figure.

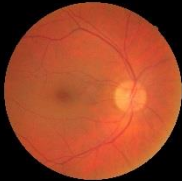
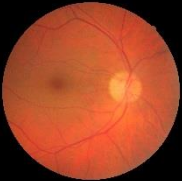

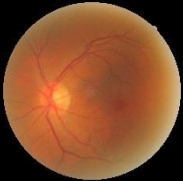

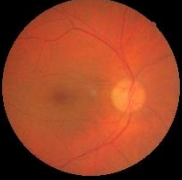
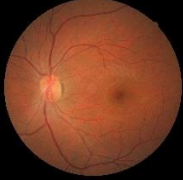

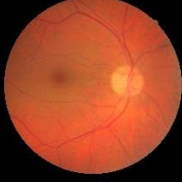
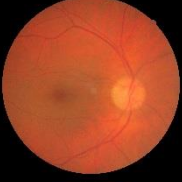

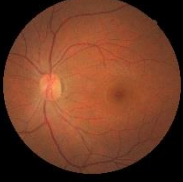
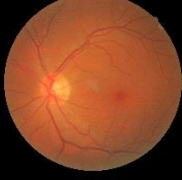


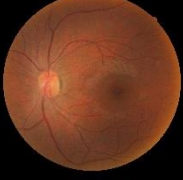




Set Number	Reference Image	Tested Image	Set Number	Reference Image	Tested Image
S1			S6		
S2			S7		
S3			S8		
S4			S9		
S5			S10		

FIGURE 7.4.2-1: FIRST TEN IMAGES IN FIRE DATASET IN S-CATEGORY  
(THE IMAGES WHICH ARE USED IN THE INITIAL EVALUATION)

In each FIRE image pair, there are 10 ground truths (points). Therefore, this initial evaluation involves 100 tests (10 pairs x 10 points). The following table present the results of the initial evaluation. It shows the average of 10 Registration Errors for both use of cross bifurcations and SURF of using Bifurcation-Cross-Points and SURF points. Where each pair contains 10 ground truth points.

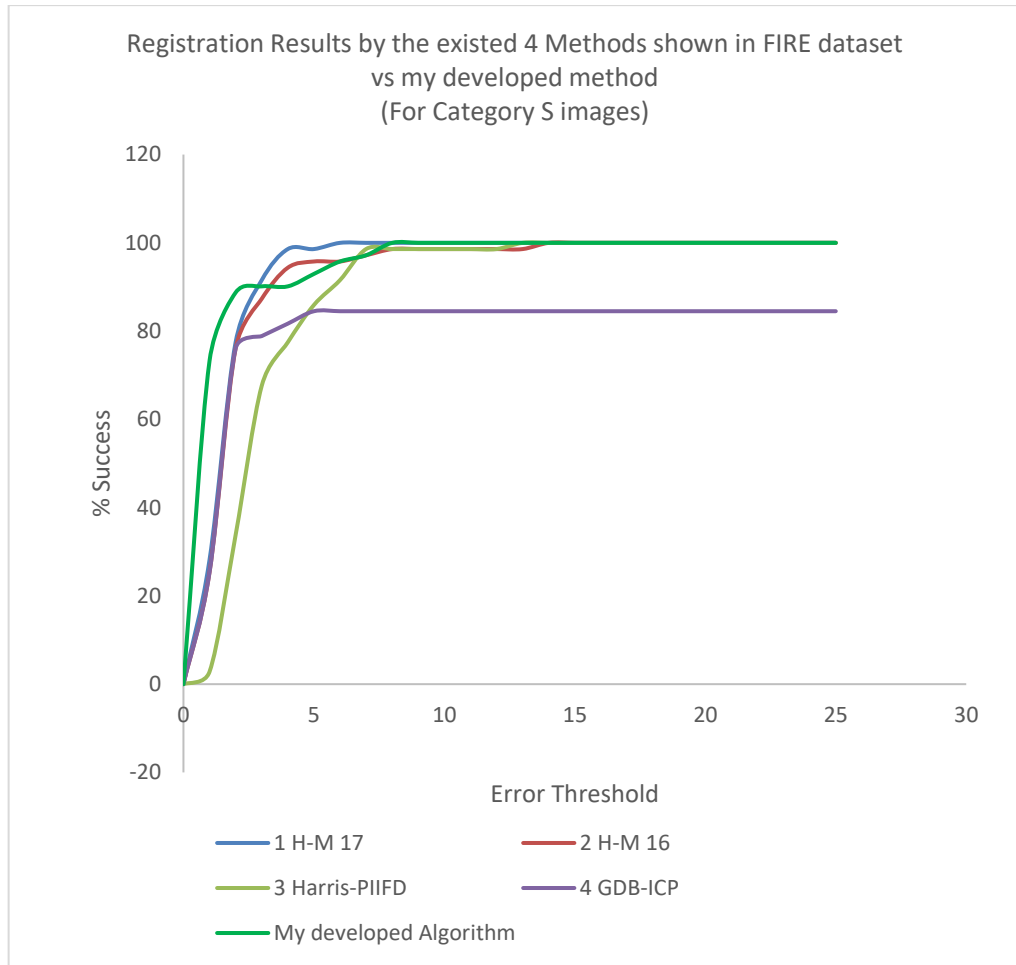
Number of a set	The Average of Registration Errors (using SURF-points) (pixels)	The Average of Registration Errors (using Bifurcation-Cross-Points) (pixels)
1	0.986	0.899
2	3.159	1.271
3	5.621	1.687
4	1.157	0.511
5	3.488	0.383
6	1.502	0.989
7	1.432	0.783
8	1.042	0.709
9	3.594	3.572
10	2.700	3.518
Average	<b>2.468</b> pixels	<b>1.432</b> pixels

*Table 7.4.2-1: The initial evaluation.*

Through the previous evaluation results, it can be concluded that by using of cross-points, the registration will be more accurate. Accordingly, cross-points are better than SURF-points to be used as control points for the registration process. This is because the SURF-based method is very sensitive to changing in image's features. While most of the intersection points are presented in the two images. There is a common number of intersection points between the two images even if there are some differences in one of the two images.

#### **7.4.2.2 The evaluation of the developed Bifurcations-based Registration Algorithm**

By the end of the algorithm development, the evaluation is achieved to test the developed system. This evaluation involves comparison between the developed system and four existed methods shown in FIRE dataset using all S-Category images in FIRE dataset (71 image pairs, 10 ground truth points each). In other words, 710 tests are achieved to evaluate the developed algorithm. The next chart presents the Registration Results “The x axis of the plot corresponds to the value of an error threshold. If the registration error of an image pair is below this threshold, the registration is considered as successful. The y axis of the plot corresponds to the percentage of successfully registered image pairs for a given threshold.” (FIRE, 2017)



*FIGURE 7.4.2.2 - 1: THE EVALUATION RESULTS BETWEEN THE CURRENT DEVELOPED SYSTEM AND FOUR EXISTED METHODS SHOWN IN FIRE DATASET*

The following table includes the values of the Area Under Curve (AUC) (Higher is better), averages, and the maximum and minimum values, from the previous chart. Such values can provide a perception of which method is better.

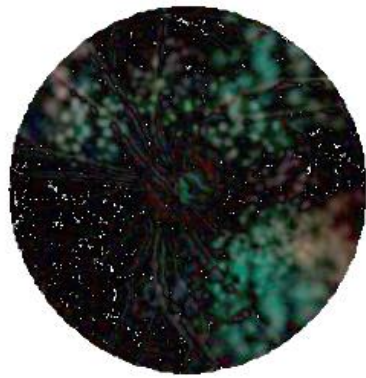
Method	Registration-Error Results for FIRE's Category S images			
	AUC	Average	Minimum Value	Maximum Value
1 REMPE (H-M 17)	0.958	1.609	0.489	5.696
2 H-M 16	0.945	1.94917	0.554	13.903
3 Harris-PIIFD	0.900	2.981	0.785	12.85
4 GDB-ICP	0.814	1.426183	0.486	4.575
<b>5 My developed method</b>	<b>0.971</b>	<b>1.217</b>	<b>0.1</b>	<b>7.945</b>

Table: Registration-Error Results comparison, between the existed 4 Methods shown in FIRE dataset and the current developed method, for FIRE's Category S images, using Area Under Curve (AUC) values (Higher is better), averages, and minimum and maximum value.

According to previous results, all methods have averages less than 3 pixels. However, AUC values show that the first, second, and fifth (the developed system) method are the best ones. Their AUC values are larger than 0.94. The developed system has given the minimum Registration-Error value, and approximately the median value within the obtained maximum values. Overall, the developed system has presented competitive results.

### 7.5 The Developed Algorithm for Change Detection

An algorithm is developed in this research to detect the changes between the two images which are registered through registration processes. This algorithm compares the corresponding pixels in both images in the overlap area between these images. This comparison is achieved by implementing a subtraction or an absolute difference operation with using thresholding process to remove no-change pixels. The process of removing unchanged pixels is a correction process. It removes any wrong difference between two corresponding pixels. This difference cannot be distinguished by the human eye. However, it exists. This is due to the small value of this difference, it approaches zero. Such difference can be assumed to be equal. The subsequent figure shows an example of change detection before and after the correction process.



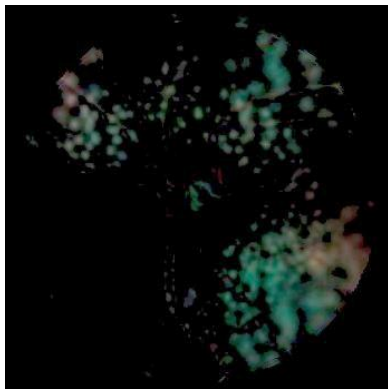
a) Before



b) After

*FIGURE 7.5- 1: CHANGE DETECTION CORRECTION BY REMOVING THE NO-CHANGE PIXELS*

Furthermore, this developed algorithm involves several visualization approaches for displaying the changes. These approaches are described in the following five figures. The next figure clarifies the detected differences in black background and white background.



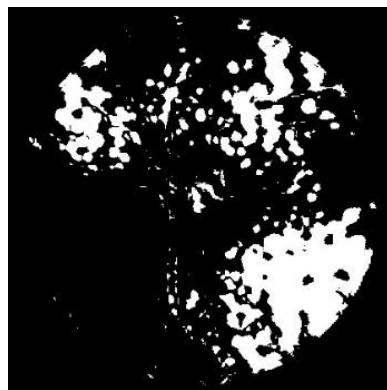
a) The detected changes



b) The detected changes in white background

*FIGURE 7.5- 2: THE DETECTED CHANGES*

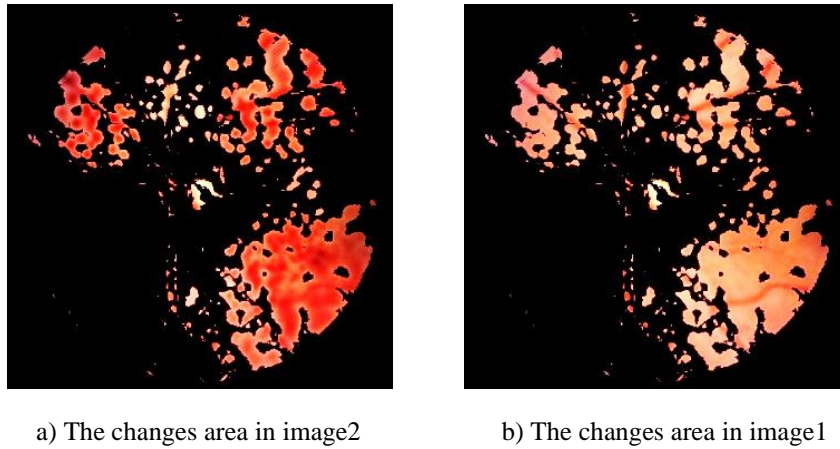
The binary representation, whites (ones) and blacks (zeros), of the detected changes is shown in the subsequent figure.



*FIGURE 7.5- 3: THE MASK OF THE DETECTED CHANGES (THE BINARY IMAGE)*

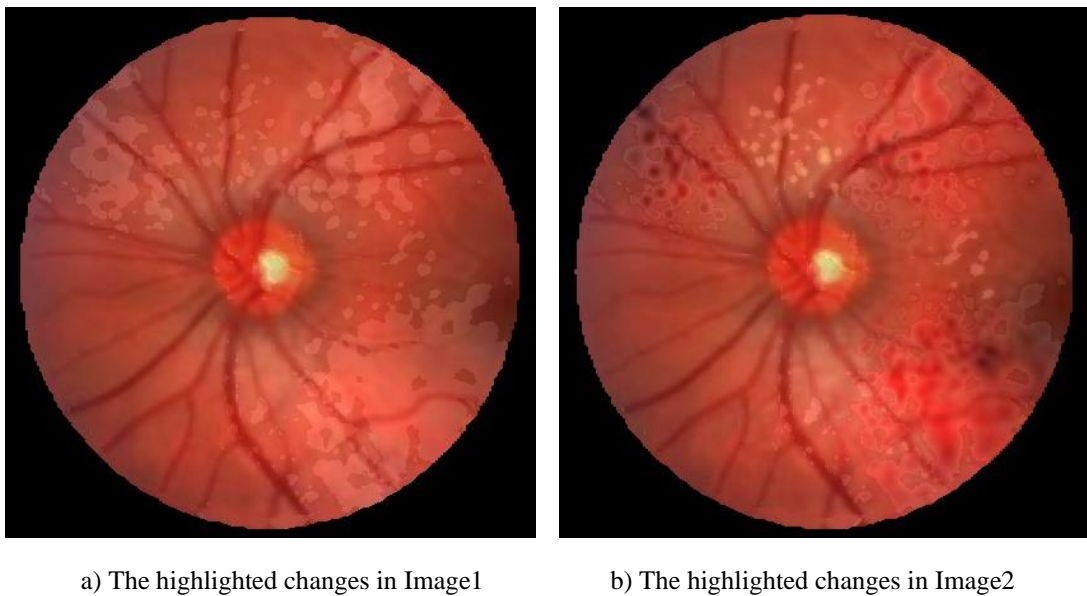


The following figure clarifies the changes in the overlap area between both images.



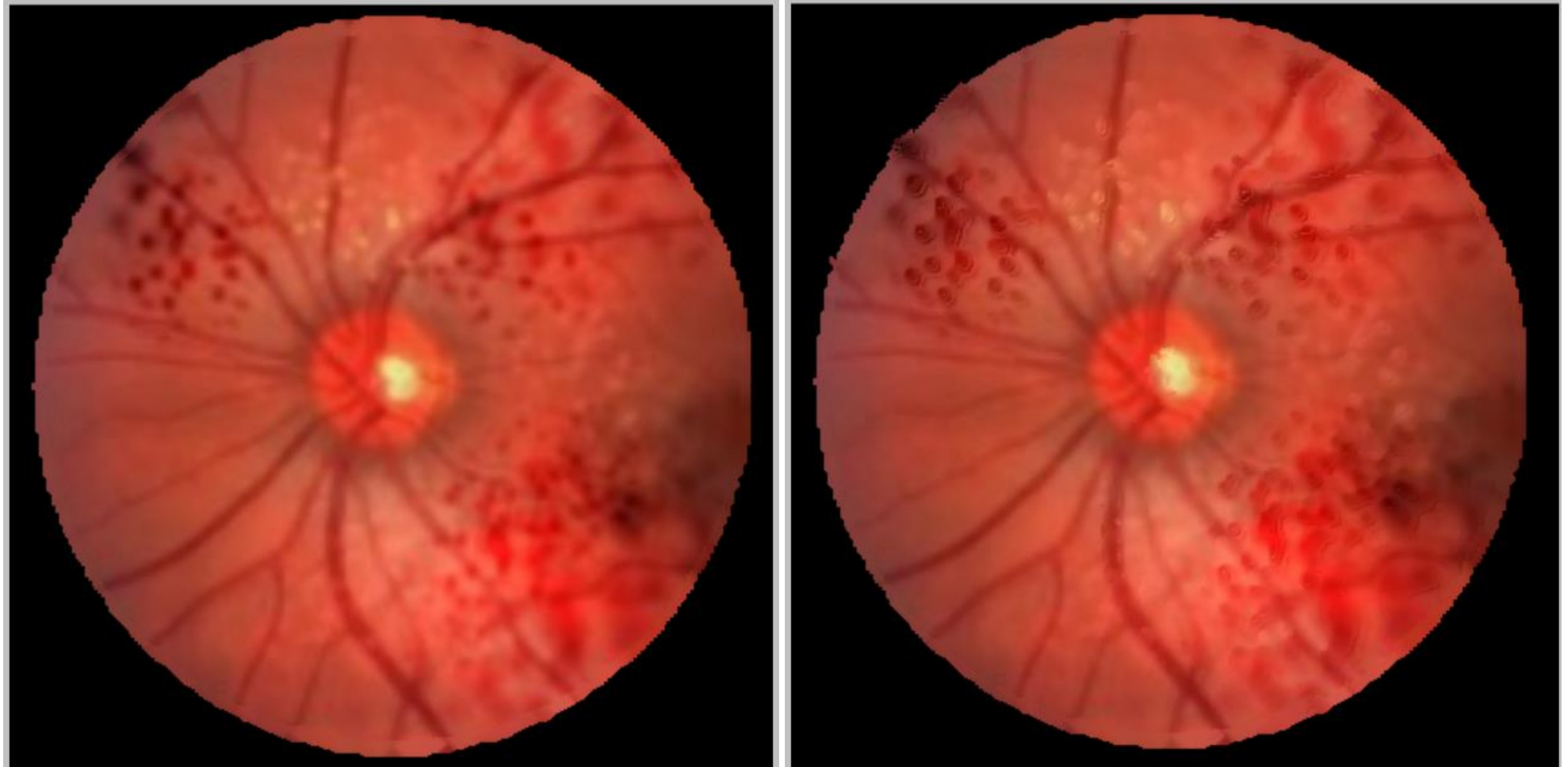
*FIGURE 7.5-4: THE CHANGES IN OVERLAP AREA IN BOTH IMAGES*

Another developed visualization feature is described in the next figure, where the changes are highlighted, in both images.



*FIGURE 7.5-5: THE HIGHLIGHTING OF CHANGES IN BOTH IMAGES*

The last developed visualization feature is shown in the following figure, where the changes are highlighted in 3D, the changes appear prominent.



a) The original Image2

b) The 3D-highlighting of the changes in Image2

*FIGURE 7.5-6: AN EXAMPLE OF THE 3D-HIGHLIGHTING OF CHANGES IN THE SECOND IMAGE OF A TEST PAIR*

## 7.6 The Future Works

The future works could include visualization enhancement for results display such as using 3D for showing the vessels, the optic disc, and the changes between two images. In addition, the subsequent required process is changes classification. After identification of the difference map between the two registered images, it is required to analyze the data of this map to identify the changes and to calculate their volume. These detected changes are classified depending on their characteristics.

## 7.7 Conclusion

There are limitations or drawbacks in several of known methods for image registration, such as a high computational complexity, a time-consuming. However, the significant advantage of such techniques is their novel methodologies which present new ideas for more future researches.

Despite all existed methods, this technique is still under developing as result of a variety of retinal images due to several reasons, for example ages and conditions of patients, cameras, distortions, and levels of illumination.

Overall, for retinal image registration, the most beneficial techniques or facts that can be extracted from the existed methods involve:

- ✓ Most existed methods are based on a feature extraction.
- ✓ A displacement is calculated according to specific features or points.
- ✓ Using a green channel could be a good representation for an image.
- ✓ The necessity of image enhancement.
- ✓ A border extension technique is required for accurate results of vessel segmentation.
- ✓ The requirement to reduce bright lesions such as by using K-means algorithm.

Consequently, it can propose a method for automatic retinal image registration by using specific control points or features. The proposed registration algorithm is based on the matching between the control points detected from bifurcations in a retina.

Furthermore, it should develop a method to overcome non-uniform illumination and poor contrast in colour retinal images. It can be by achieving several operations for image enhancements such as converting to a green space (channel) and using border extension

technique to separate between the border and vessels of retina. Another approach, to solve the problem of non-uniform illumination and poor contrast, is by using K-means segmentation to reduce bright lesions.

Concerning cross point between optic disc and vessels, such points cannot be used for the matching between two images because it is difficult to identify the optic disc boundary to be the same in both tested images. This due to the changes resulting from: age progression, external influences such as changing in lighting, or disease signs.

Furthermore, it can be concluded that the developed algorithm has presented competitive results (Registration error is less than 8 pixels), because of the following reasons:

- ✓ The Registration process depends on multi displacements.
- ✓ The Weber Space conversion process is not used.
- ✓ The whole retina is used in registration process.
- ✓ Using more accurate method (an existed method) to measure the similarity between two images.
- ✓ Most Registration processes (All except control points detection) are implemented in original image size (2912 x 2912).
- ✓ The size of tested area will be increased in the case of Small Overlap.
- ✓ Large number of control points are detected
- ✓ Large number of Ground Truth points are tested for validation of the developed algorithm

## **Chapter 8: Thesis Conclusion**

### **Overview**

This chapter presents the overall findings from this research. It includes the summary of the thesis, the technical problems of the research, the contributions, the summary of the results, the developed algorithms, the future work, and the overall conclusion.

### **8.1 Summary of the Thesis**

The sight is an extremely important human sense. Any tools which can improve the probability of detecting eye-disease could be considered beneficial. The early ophthalmic anomaly detection can prevent the impairment or loss of vision. It is required to analyse retinal images automatically instead of the current manual system of retinal screening which could make an error in diagnosis, in particular in the case of slow disease progression. This study investigates computer vision and image processing techniques to analyse retinal images automatically. This analysis aimed to present the main image-processing-based algorithms that can be used for image enhancement, feature extraction, image segmentation, image registration, and change detection of retinal images, or for any future research studies regarding retinal images analysis.

This Thesis was divided into eight chapters. The first chapter provided introductory details regarding this research and the next chapter outlined some medical background concepts related to this study. The next chapter focused on the measurement of the colour difference between images. This measurement is required to compute the similarity which is used in the registration process or could be used in change classification. Then, Chapter 4 presented the colour mapping process as a solution of the problem of comparing images with different colour tints. This process ensures the two images have equal or near colours. Consequently, the results of the subsequent processes related to segmentation or registration will be more efficient. There are some processes sensitive to the variety of the colours. For example, the two processes of the detection of edges and circles need specific parameters. The values of these parameters vary according to the colours of the image. Chapter 5 described the processes required before the registration. The following chapter was dedicated to the control points detection. These points are required to identify the possible registration and to detect

the matching. Chapter 7 presented the registration and the change detection process. This final chapter presents the overall research findings.

## **8.2 Research Progress History**

This research investigates development of a registration algorithm for retinal images. The processes of the developed algorithm were chosen following extensive experimentation, involving many attempts to develop a variety of processes evaluated by a large number of tests.

In the early development stages, the goal of the research was to find the best displacement and rotation for the second image to match with the first image in a pair. Such matching (registration) was based on finding the optic disc and use it as a center of rotation. Subsequently, vessels are detected. Then, deducing the points of intersection between these vessels and use them to determine potential matches. Next, the process of comparing the details of the two images is done. These details include only vessels and optic disc. Any other details are ignored in the comparison between the two images. Such comparison is achieved by measuring of colour difference.

That methodology is completely wrong. Firstly, regarding one displacement for retinal image registration, through FIRE dataset, there could be various differences among corresponding points between two images. The FIRE dataset includes Ground Truth points. They are coordinates values of ten points (reference points) in the first image in a pair of retinal images, and the ten corresponding points in the second image (The image to be moved or displaced to match the first image). By calculating the difference between each of reference point and its corresponding point, it is found that there could be a difference in the values of the offset between these points. In other words, there is more than one offset. Consequently, the principle of registration process that is based on only one displacement is wrong. The methodology is improved by dividing an image to many partitions. Then, the best offset is found for each part instead of just one displacement for the entire image. According to the developed system, an image is divided twice, one to 16 (4x4) partitions (in reduced image size) and another time to 144 (12x12) partitions (in original image size). However, this approach is not very accurate because it does not depend on the actual image size. Therefore, the approach is improved. There is not any partitioning in the current method. All processes are applying on the whole size of an original image except those related to control points detection.

Relating to rotation, through evaluating the developed method, it was found that when performing any rotation on a part of an image with a displacement, the result obtained without rotation is better than that is with rotation. Therefore, there is not any rotation in the developed methodology.

Furthermore, the new methodology does not include optic disc segmentation. Optic disc is not used in the registration. Because there is no rotation, and it is not used in the comparison process.

Concerning vessel segmentation and control points detection, the old developed method cannot detect all vessels in a retina. In addition, the whole retina was not used in registration process and the dark colours in a retina were ignored. Therefore, it had to be improved. With the presence of several vessels will be more points of intersection between the vessels. On other hands, it will be more control points that will be used in registration. The old method was improved to detect any bifurcation, not just vessels, in a retinal image. In addition, after applying the new developed image enhancement method, more vessels are appeared. Such vessels cannot be seen by the eye before. Furthermore, more improvements are made. They include not to use Weber Space conversion and use the whole retina in registration process including the dark colours area. Consequently, the number of control points detected by the current developed algorithm is more than that by the previous one.

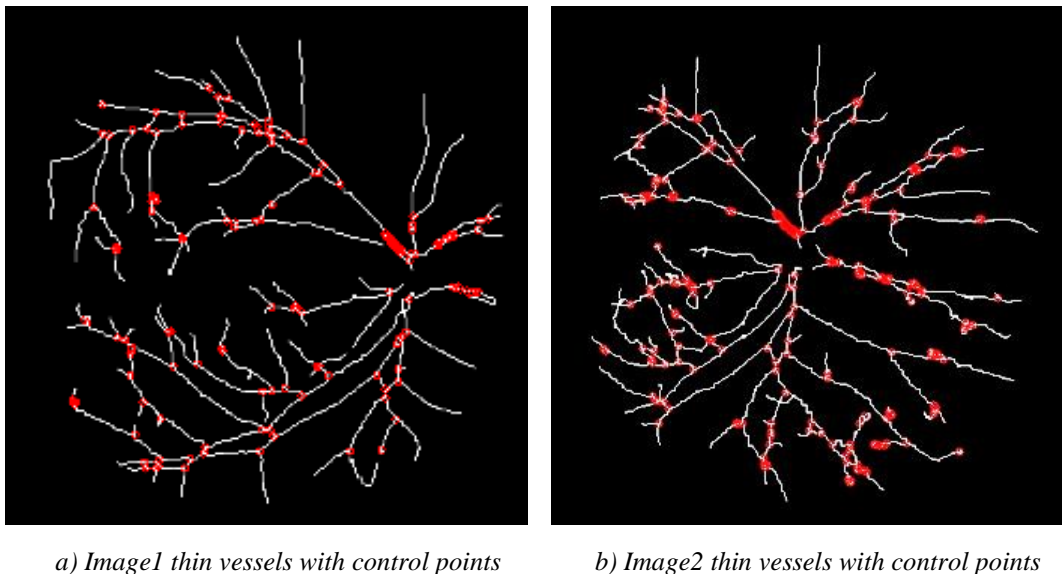
Regarding colour difference measurement, many attempts have been made to develop an accurate measurement method. This method must be effective to show true difference value that fits with image details rather than image colours. Recently, a successful algorithm is developed and used for comparison among image partitions to detect the best registration. Previously, in the case of small overlap between the two tested images, similarity is not measured. In the current methodology, in the case of Small Overlap, the size of tested area will be increased. In addition, an existed method is used to compute the similarity value. It is called Normalized Cross Correlation. It is one of Template Matching methods (Brunelli, March 2009). Furthermore, some different image pre-processes are used. Accordingly, the results are more accurate than the previous ones in the early development stages.

Actually, there are two developed methods for registration. The former one depends on the cross points among bifurcations in a retina. In contrast, the latter method is based on SURF points. Through evaluation results of the two method. The cross-points-based method is better than the second one. This is because the SURF-based method is very sensitive to changing in

image's features. While most of the intersection points are present in the two images. There is a common number of intersection points between the two images even if there are some differences in one of the two images. Consequently, only cross points are used as control points in the current developed algorithm.

### 8.3 Technical Problems of the Research

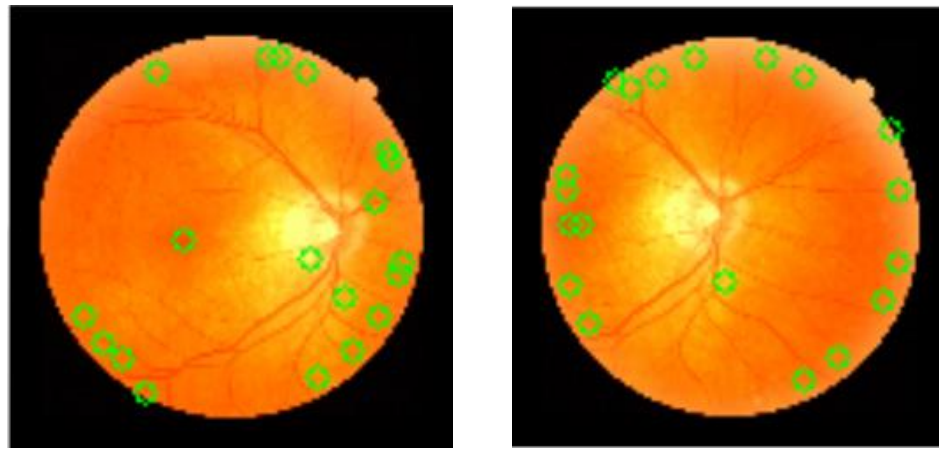
The key research problem focuses on **how to apply an image registration algorithm followed by change detection between retinal images automatically, efficiently, accurately and robustly.** Based on the experimental findings of this study and the considerable experience gained, the key issue required to be solved to successfully implement the image registration is **the detection of control points.** This process involves feature extraction operations. Two methods are used in this research for such operations. The first method is a new one developed in this study. It depends on detection of bifurcations and their cross points in a retina. In this developed algorithm, control points are the cross points between the detected bifurcations. For instance, the next figure is an example of the result of this developed method.



**FIGURE 8.3 - 1: THE DETECTED CONTROL POINTS, HIGHLIGHTED BY RED CIRCLES, DETECTED BY THE DEVELOPED BIFURCATIONS-BASED ALGORITHM.**



In contrast, the second method is an existing algorithm, SURF, which is considered as the fastest common method for feature extraction. The features detected by the SURF algorithm are used as control points. For example, the result of this method is as shown in the following figure.

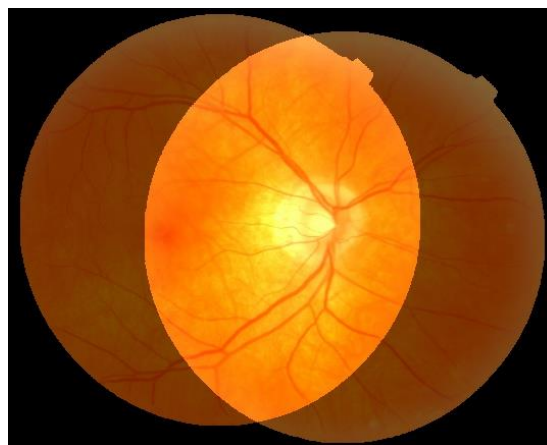


a) Image1 with detected features

b) Image2 with detected features

*FIGURE 8.3 - 2: AN EXAMPLE OF A PAIR OF RETINAL IMAGES WITH THE CONTROL POINTS, HIGHLIGHTED BY GREEN CIRCLES, WHICH ARE THE FEATURES DETECTED BY SURF ALGORITHM.*

The image registration output resulting from using the both methods, the developed bifurcations-based algorithm and the SURF algorithm, on the same retinal image pair, is equal as clarified in the next figure as a result of using the control points shown in the previous two figures.



*FIGURE 8.3 - 3: IMAGE REGISTRATION*

Another issue is the need to make the colours of both images equal or very similar in order to ensure that all the applied processes have the same accuracy and efficiency, in particular those processes depending on specific parameters such as the detection of edges. This required process is known as **colour mapping**.

Regarding **image segmentation**, it is required to derive a reliable marker for the Watershed algorithm. Typically, in this research, a marker is required for bifurcations detection. Actually, this process is a part of **control points detection**.

Another requirement for image registration is the **calculation of the similarity** between two colour retinal image partitions.

Furthermore, the fundamental operations include **finding the correct matches (inliers)** among the detected control points and **calculating of matched point** (finding a point in a second image corresponding to a point in a first image).

In conclusion, the most technically challenging problems regarding the development of a new system for retinal image registration and changes detection are **colour mapping, the detection of control points, similarity measurement, inliers deriving, and identification of a matched point**.

## **8.4 Contributions**

The contributions that are obtained from this study can be listed in the following:

- ✓ A study of the existing algorithms regarding colour distance measurement, colour mapping, vessel segmentation, retinal image registration. This study is a literature review for the most suitable algorithms from the existing ones that can be used for computer analysis of retinal images, especially for each process required for retinal image registration.
- ✓ A new approach for pre-processing of retinal images before registration. This approach includes a combination of some pre-processes such as image resizing, retina cropping, background extension, green channel separation, deriving retina mask, bright lesions reduction, and borders extending.
- ✓ A new approach for difference measurement between images.

- ✓ A new approach for colour mapping. This approach is a normalization operation to equalize the colours of the two images
- ✓ A new approach for detection of bifurcations and their cross points in a retina.
- ✓ A new approach for the registration of retinal images. It is “bifurcations-based Registration Algorithm”.
- ✓ An approach for detection of changes between two registered retinal images.

All processes, developed in this research, are either new or selected from existing algorithms with specific setting and arranged in specific sequence according to the experimental results and the conclusions and results of existing research publications.

### 8.5 Summary of the results

The overall results or outputs of the developed algorithms, achieved in this study, can be listed as shown in the following four figures, as examples of such results:

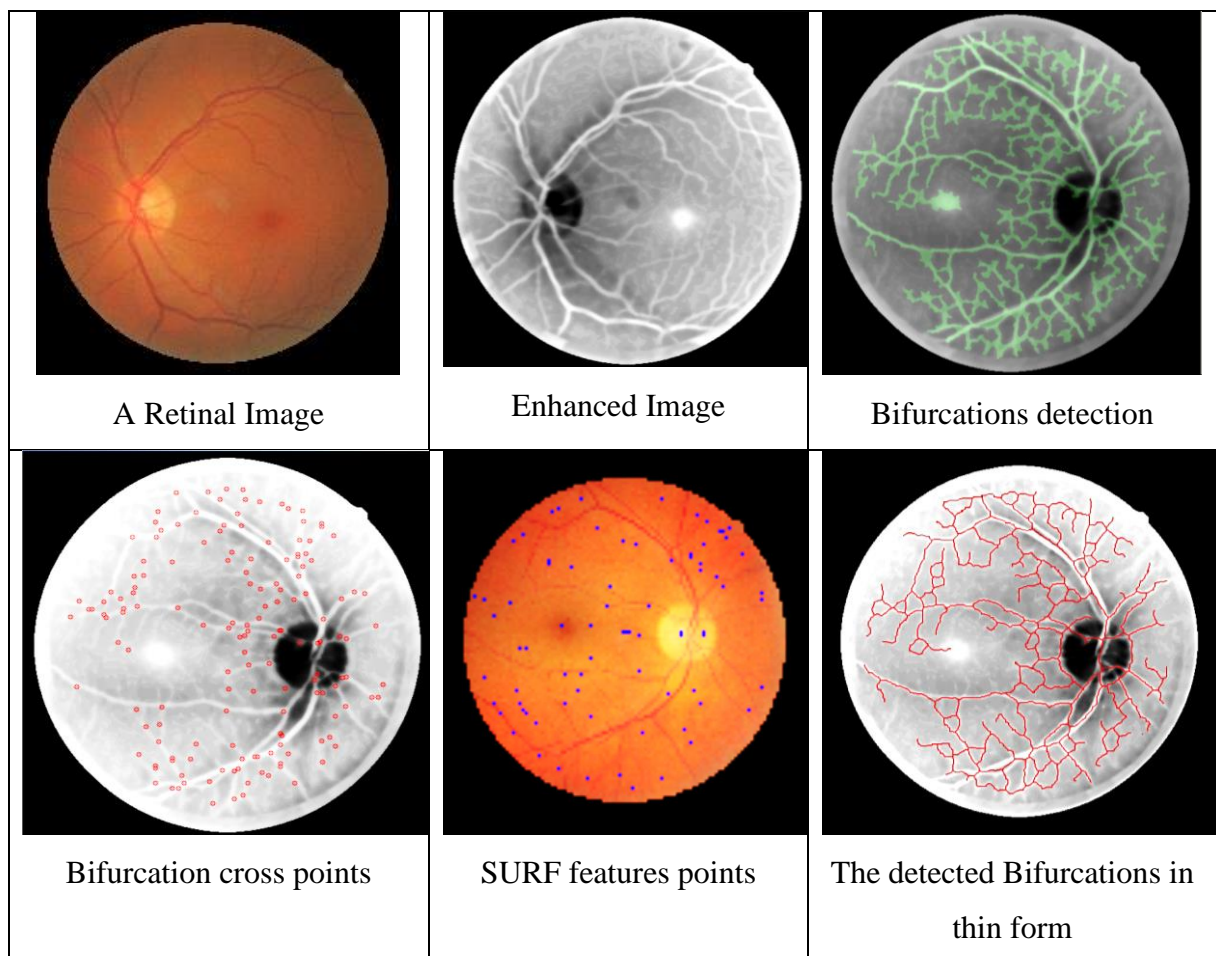
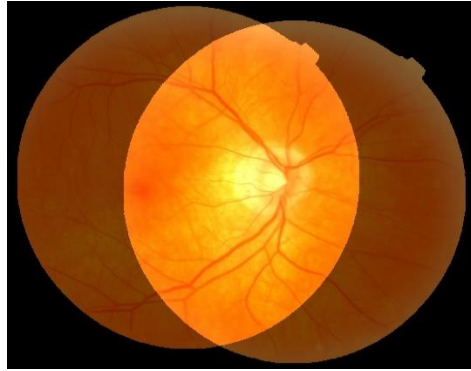
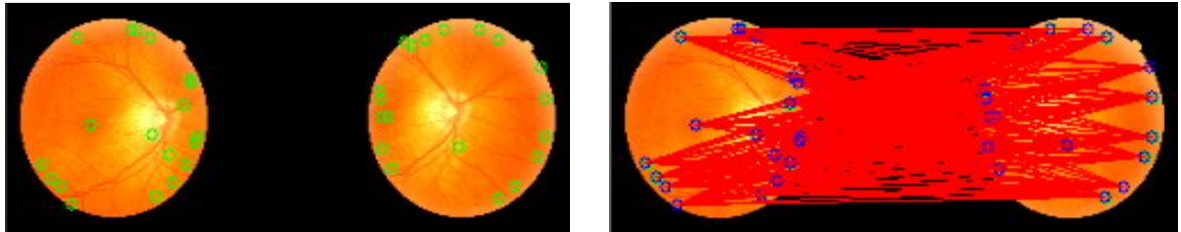


FIGURE 8.5 - 1: THE OUTPUTS OF THE DEVELOPED SYSTEM.



*FIGURE 8.5 -2: THE REGISTRATION RESULT ALGORITHM.*



a) Retinal images pair with detected SURF features

b) The possible matches among the detected SURF features.

*FIGURE 8.5 -3: THE POSSIBLE MATCHES AMONG THE CONTROL POINTS.*






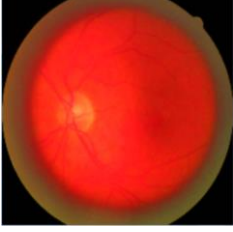




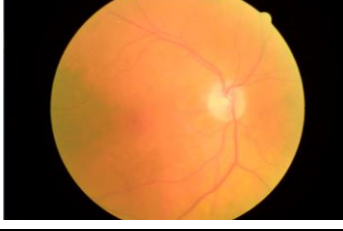

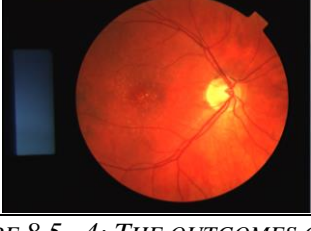


Original Image	Reference Image	The outcome of the developed algorithm
		
		
		
		
		

FIGURE 8.5 - 4: THE OUTCOMES OF THE PROPOSED ALGORITHM FOR IMAGE COLOUR MAPPING.

Regarding colour mapping, the developed method is tested and compared with Histogram specification. Its evaluation results show its validity for colour mapping process between two retinal images, in particular in different colours.

## 8.6 Additional Developing Features

In addition to the developed algorithms, there are two useful features in the developed software. Firstly, parallel programming is used to speed up the implementation of some developed algorithms. The second feature is the visualization facilities of the developed software. They are developed in this research to help to implement and test the proposed algorithms. They are as a result of using the powerful abilities of Visual C# with its WPF framework. Several visualization operations have been achieved, such as showing pixel values of a selected area in an image, an image resizing, displaying unlimited number of images with a navigation facility using scroll bar, and choosing two image and displaying them in one window in maximized size as a comparative tool between two images. The following three figures show such facilities; The next figure shows the feature of displaying of unlimited number of images with a navigation facility using scroll bar.

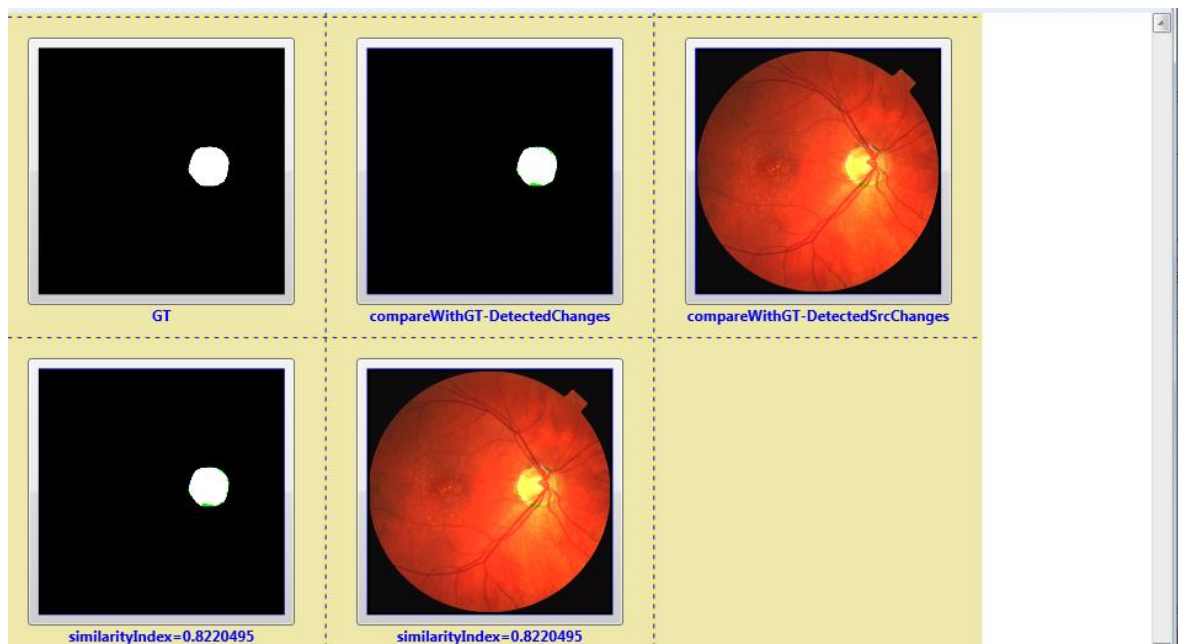


FIGURE 8.6 - 1: THE SOFTWARE FEATURE OF DISPLAYING OF UNLIMITED NUMBER OF IMAGES WITH A NAVIGATION FACILITY USING SCROLL BAR.

Whereas the following figure presents the advantage that shows pixel values of the selected area of the displayed image.



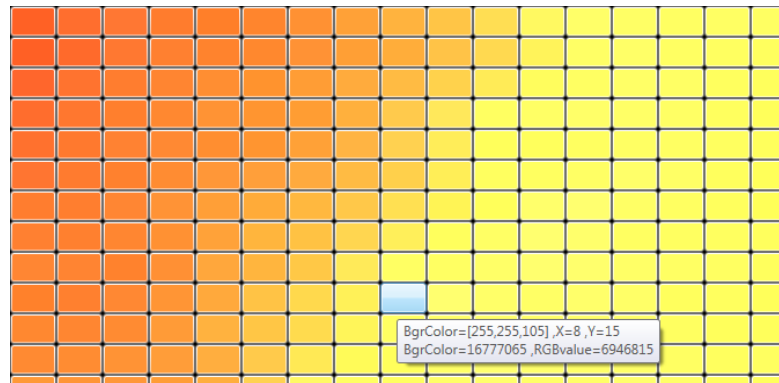


FIGURE 8.6 - 2: THE SOFTWARE FEATURE OF SHOWING PIXEL VALUES OF A SELECTED AREA IN AN IMAGE

Whilst the next figure shows the characteristic of choosing two images and displaying them in one window in maximized size.

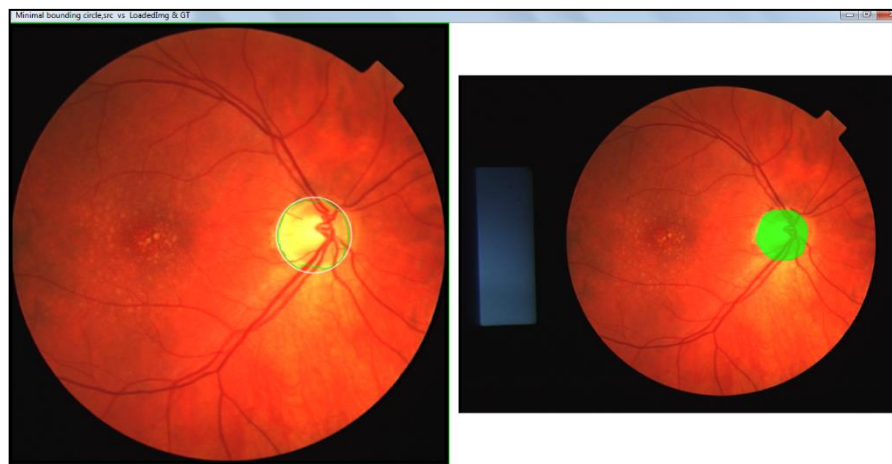


FIGURE 8.6 - 3: THE SOFTWARE FEATURE OF CHOOSING TWO IMAGE AND DISPLAYING THEM IN ONE WINDOW IN MAXIMIZED SIZE.

## 8.7 Future Work

For further work, it is required for developing an algorithm for **change classification**. The location of any change should be investigated with the aim of assessing whether it is significant or not. After locating of a significant change, the classification algorithm will examine the characteristics in the change's area to identify the importance and type of change. In other words, the classifier, based on a suitable rule set, decides if the changes are significant or not and what the changes are. The characteristics that can be used for changes classification could be the shape, the size, or the colours density. Such classification requires

some operations to distinguish an abnormal feature among a variety of artefacts and pathological changes. According to the findings of this research, the change classification method is expected to be developed depending on the colour distance calculation such as that used for the measurement of the similarity in registration process. In addition, this classification may involve segmentation process such as optic disc or vessels segmentation.

Concerning the proposed **bifurcation detection** algorithm, in this study, needs to be developed further to detect just vessels.

The future works could include **visualization** enhancement for results display such as using 3D for showing the vessels, the optic disc, and the changes between two images.

## **8.8 Overall Conclusion**

The processes, developed in this research, can be classified into four stages: initial processes, landmarks detection, registration, and change detection. The first stage involves several processes for image enhancement such as noise and bright lesions reduction and border extension, in addition to retina cropping. Then, the second step aims to detect the main landmarks, and it includes specific features extraction. The next operation, the registration, involves the alignment process between two images, which is according to the extracted information from the previous stage. Finally, the last stage is to extract changes between a pair of images.

As a result of all approaches developed in this research, all the objectives of this research have been achieved. This is evident in the development of the automate, efficient, accurate and robust algorithm for comparison of retinal images and change location detection in them. In addition to the development of the methods regarding pre-processing, and vessel segmentation, which are part of the registration and change detection algorithm.

The importance of the developed approaches in this research is clarified in the automatic, efficient, accurate, and robust implementation of these methods. This importance is more obvious in the results obtained from the implementation of these methods. In terms of this research, the automation means that all developed processes operate by themselves without any human intervention or control. Whilst the efficiency represents the optimal use of the available resources such as computer memory in as minimum time as possible. The accuracy and the robustness are that the output of registration process is a complete match between the



overlap area between the two images without affecting on their features, in particular the signs of illness.

Consequently, the research topic regarding retinal image registration and change detection is defined and the required algorithm is identified and achieved as a result of the current investigation and practical outcomes.

## References

Abraham, R. & Simon, P., 2013. Review on Mosaicing Techniques in Image Processing. *International Journal of Software Engineering Research & Practices Vol.3, Issue 1*, April.

Abràmoff, M. D. & Niemeijer, M., 2006. *The automatic detection of the optic disc location in retinal images using optic disc location regression*. New York, IEEE.

ADCIS-SA, 2017. *Messidor*. [Online]

Available at: <http://www.adcis.net/en/Download-Third-Party/Messidor.html>

Aforge.net, 2006-2013. *Aforge.net*. [Online]

Available at: <http://www.aforgenet.com>

[Accessed 2016].

Anbeek, P. et al., 2005. Probabilistic segmentation of brain tissue in MR imaging. *NeuroImage*, Volume 27, p. 795 – 804.

Andreou, L. & Achim, A., 2010. *Temporal registration for low-quality retinal images of the murine eye*. Buenos Aires/Argentina, 32nd Annual International Conference of the IEEE EMBS.

Ang, B., 2010-2015. *Diabetic retinopathy*. [Online]

Available at: <http://www.vision-and-eye-health.com/diabetic-retinopathy.html>

[Accessed 2015].

Anon., n.d. *Explain difference between opencv's template matching methods*. [Online]  
Available at: <https://stackoverflow.com/questions/48799711/explain-difference-between-opencvs-template-matching-methods-in-non-mathematica>

ArcSoft, 2016 . *What is Color Space*. [Online]  
Available at: <http://www.arcsoft.com/topics/photostudio-darkroom/what-is-color-space.html>

Athitsos, V., Swain, M. J. & Frankel, C., 1997. Distinguishing Photographs and Graphics on the World Wide Web. *IEEE Workshop on Content-Based Access of Image and Video*, pp. 10-17.

Attar, A., Rad, R. M. & Atani, R. E., 2011. A survey of image spamming and filtering techniques. *Springer Science+Business Media B.V. Published online: 2011*, p. *Artif Intell Rev* (2013) 40:71–105.

Bankhead, P., Scholfield, C. N., McGeown, J. G. & Curtis, T. M., 2012. Fast Retinal Vessel Detection and Measurement Using Wavelets and Edge Location Refinement. *PLoS One.v7(3)*, 12 Mar., p. .

Bardera, A., Feixas, M., Boada, I. & Sbert, M., 2010. Image registration by compression. *Information Sciences, vol. 180*, pp. 1121-1133.

Bardera, A., Feixas, M., Boada, I. & Sbert, M., 2010. Image registration by compression. *Information Sciences, vol. 180*, pp. 1121-1133.

Bay, H., Tuytelaars, T. & Gool, L. V., 2006. *SURF: Speeded Up Robust Features*. Graz, Austria, Springer Berlin Heidelberg, pp. 404-417.

Becker, B. C. & Riviere, C. N., 2013. *Real-Time Retinal Vessel Mapping and Localization for Intraocular*. Karlsruhe, Germany, IEEE International Conference on Robotics and Automation (ICRA).

Beucher, S., 2010. *MAGE SEGMENTATION AND MATHEMATICAL MORPHOLOGY*. [Online]

Available at: <http://cmm.ensmp.fr/~beucher/wtshed.html>

[Accessed 2015].

- Bhuiyan, A. et al., 2011. Retinal Image Matching Using Hierarchical Vascular Features. *Computacional Intelligence and Neuroscience*, pp. 1-7.
- Brown, L. G., 1992. A survey of image registration techniques (abstract). *ACM Computing Surveys (CSUR) archive, volume 24, issue 4*, December, pp. 325 - 376.
- Brunelli, R., March 2009. *Template Matching Techniques in Computer Vision: Theory and Practice*. s.l.:Wiley.
- Bubak, M., Albada, G. D. v., Sloot, P. M. & Dongarra, J., 2004. *Computational Science — ICCS 2004: 4th International Conference ..., Part 4*. Kraków, Poland, Springer, pp. 37-40.
- Can, A., Stewart, C. V., Roysam, B. & Tanenbaum, H. L., 2000. *A Feature-Based Technique for Joint, Linear Estimation of High-Order Image-to-Mosaic Transformations: Application to Mosaicing the Curved Human Retina*. Hilton Head Island, South Carolina, IEEE Conference on Computer Vision and Pattern Recognition, vol. 2,.
- Canny, J., 1986. A Computational Approach To Edge Detection. *IEEE Trans. Pattern Analysis and Machine Intelligence*, 8(6), , p. 679–698.
- Chen, L., Xiang, Y., Chen, Y. & Zhang, X., 2011. Retinal Image Registration Using Bifurcation Structures. *IEEE International Conference on Image Processing, vol. 18*, pp. 2169-2172.
- Chen, Y., Li, Z., Li, M. & Ma, W.-Y., 2006. *AUTOMATIC CLASSIFICATION OF PHOTOGRAPHS AND GRAPHICS*. Toronto, Ont., Canada, IEEE, pp. 973-976.
- CHUA, S. H. et al., 2015. ColorBless: Augmenting Visual Information for Colorblind People. *ACM Transactions on Computer-Human Interaction, Vol. 21, No. 6, Article 32, Publication date: January 2015*, pp. 32:1--32:20.
- CIE Central Bureau, 1995. *CIE Publication 116: Industrial Colour-Difference Evaluation*, Vienna: CIE .
- colormine, 2017. *colormine.org*. [Online]  
Available at: <http://colormine.org/delta-e-calculator>
- Dashtbozorg, B., Mendonça, A. M. & Campilho, A., 2013. Optic disc segmentation using the sliding band filter. *Computerized Medical Imaging and Graphics*, 37 (5), pp. 409-417.

Datacolor, 2017. *Color Differences & Tolerances: Commercial Color Acceptability*. [Online] Available at: <http://industrial.datacolor.com/support/wp-content/uploads/2013/01/Color-Differences-Tolerances.pdf>

Deng, K. et al., 2010. Retinal Fundus Image Registration via Vascular Structure Graph Matching. *International Journal of Biomedical Imaging*, , pp. 1-13.

Dice, L., 1945. Measures of the amount of ecologic association between. *Ecology*, Volume 26, p. 297– 302.

Doxygen, 2017. *Histogram comparison methods*. [Online] Available at: [http://docs.opencv.org/trunk/d6/dc7/group\\_imgproc\\_hist.html#ga994f53817d621e2e4228fc646342d386](http://docs.opencv.org/trunk/d6/dc7/group_imgproc_hist.html#ga994f53817d621e2e4228fc646342d386)

Dr.Neuhoff, L. S., 2015. *OCULAR CONDITIONS*. [Online] Available at: <http://www.drneuhoff.com/education.html> [Accessed 2015].

El-gayar, M., Soliman, H. & Meko, N., 2013. A comparative study of image low level feature extraction algorithms. *Egyptian Informatics Journal, Volume 14, Issue 2*, pp. 175-181.

EMGU Corporation, 2016. *SURF Constructor*. [Online] Available at: <http://www.emgu.com/wiki/files/3.2.0/document/html/fa2375c0-5333-8897-5ab2-c823e25e9a5c.htm>

EmguCV, 2008-2016. *Emgu CV*. [Online] Available at: <http://www.emgu.com> [Accessed 2016].

EmguCV, 2016. *Emgu CV*. [Online] Available at: <http://www.emgu.com> [Accessed 2016].

Eswaran, A. W., Reza, S. & Hati, S., 2008. *Extraction of the contours of optic disc and exudates based on marker-controlled watershed segmentation*. Singapore, IEEE in Computer Science and Information Technology, ICCSIT 2008, pp. 719-723.

Feijoo, J. G. et al., 2008. *DRIONS-DB: Digital Retinal Images for Optic Nerve Segmentation Database*. [Online]

Available at: <http://www.ia.uned.es/~ejcarmona/DRIONS-DB.html>

[Accessed 2015].

Félix, 2011. *OpenCV - Morphological Skeleton*. [Online]

Available at: <http://felix.abecassis.me/2011/09/opencv-morphological-skeleton/>

[Accessed 2015].

Ferreira, T. L. L. d. B., 2012. *MSc. Dissertation: Algorithms for Ophthalmology Image*.

[Online]

Available at:

[https://estudogeral.sib.uc.pt/bitstream/10316/25196/1/Thesis\\_TiagoBessaFerreira\\_2012.pdf](https://estudogeral.sib.uc.pt/bitstream/10316/25196/1/Thesis_TiagoBessaFerreira_2012.pdf)

[Accessed 11 11 2014].

Fisher, R., Perkins, S., Walker, A. & Wolfart, E., 2003 . *Hough Transform*. [Online]

Available at: <http://homepages.inf.ed.ac.uk/rbf/HIPR2/hough.htm>

[Accessed 2015].

G., S. M., 2014. Classification of Image Registration Techniques and Algorithms in Digital Image Processing – A Research Survey. *International Journal of Computer Trends and Technology (IJCTT)*, Sep , p. volume 15 number 2.

Garfield, J. & Neil-Dwyer, G., 1975. Delay in diagnosis of optic nerve and chiasmal compression presenting with unilateral failing vision. *The British Medical Journal*, Volume Vol. 1, No. 5948 (Jan. 4, 1975) , Published by: BMJ, pp. 22-25.

Gonçalves, H., Corte-Real, L. & Gonçalves, J. A., 2011. Automatic Image Registration Through Image Segmentation and SIFT. *IEEE Transactions on Geoscience and Remote Sensing*, vol. 49, no. 7, , pp. 2589-2600.

Gonçalves, H., Gonçalves, J. A. & Corte-Real, L., 2011. HAIRIS: A Method for Automatic Image Registration Through Histogram-Based Image Segmentation. *IEEE Transactions on Image Processing*, vol. 20, no. 3, pp. 776-789.

Gonzalez, R. C. & Woods, R. E., 2002. *Digital Image Processing*. 2nd ed. s.l.:Pearson.

Guthrie, I., 2007. *PhD thesis: The Intelligent Registration of Retinal Images*, Manchester/UK: University of Salford.

H. Gonçalves, J. A. G. a. L. C.-R., 2011. HAIRIS: A Method for Automatic Image Registration Through Histogram-Based Image Segmentation. *IEEE Transactions on Image Processing*, vol. 20, no. 3, , pp. 776-789.

Hafner, J. et al., 1995. Efficient color histogram indexing for quadratic form distance functions. *PAMI*.

Hernandez-Matas, C. et al., Jul. 2017. FIRE: Fundus Image Registration Dataset. *Journal for Modeling in Ophthalmology*, vol. 1, no. 4,, pp. 16-28,.

Hong, G. & Luo, M., 2006. New algorithm for calculating perceived colour difference of images. *Imaging Science Journal*, 54(2), pp. Science Journal, 54, 86-91..

Howitt, D. & Cramer, D., 2008. *Introduction to Statistics in Psychology (Fourth ed.)*. s.l.:Prentice Hall.

Image Sciences Institute, 2001-2016. *DRIVE: Digital Retinal Images for Vessel Extraction*. [Online]

Available at: <http://www.isi.uu.nl/Research/Databases/DRIVE/>

[Accessed 2016].

Itseez, 2015. OpenCV Tutorials. In: O. D. Team, ed. *The OpenCV Tutorials Release 2.4.9.0 April15, 2014*. -: OpenCV, pp. 250 [Remapping], 256 [Affine Transformation], 286 [Template Matching], 262 [Histogram Equalization], 186 [image smoothing], 191-203 [Morphology Transformations].

Itseez, 2015. OpenCV Tutorials. In: O. D. Team, ed. *The OpenCV Tutorials Release 2.4.9.0 April15, 2014*. -: OpenCV, pp. 250 [Remapping] , 256 [Affine Transformation].

Itseez, 2015. OpenCV Tutorials. In: O. D. Team, ed. *The OpenCV Tutorials Release 2.4.9.0 April15, 2014*. -: OpenCV, pp. 250 [Remapping], 256 [Affine Transformation], 286 [Template Matching].

Johnson, G. M., Song, X., Montag, E. D. & Fairchild, M. D., 2010. Measurement, Derivation of a Color Space for Image Color Difference. *Wiley*, Volume 35, Number 6.

Kim, J. H., 2014. *OpenCV EMD*. [Online]

Available at: <http://study.marearts.com/2014/11/opencv-emdearth-mover-distance-example.html>

Kumara, A., Gaurb, A. & Srivastava, M., 2012. *A Segment based Technique for detecting Exudate from*. Rourkela, Odisha, India, Elsevier.

Kumar, V., Nagpal, A. & Bajaj, A., Sep 2011. Image Resizing using Bilinear Interpolation. *International Journal of ElectroComputational World & Knowledge Interface*, 1(1), pp. 49-53.

Lantuéjoul, C., 1977. "Sur le modèle de Johnson-Mehl généralisé", *Internal report of the Centre de Morph. Math.*, Fontainebleau, France: s.n.

Liu, Q. et al., 2010. *Feature selection for image spam classification*. Chengdu, China, IEEE, pp. 294-297.

Lowe, D. G., 2004. Distinctive Image Features from Scale-Invariant Keypoints. *International Journal of Computer Vision*, , pp. 1-28.

MacQueen, J. B., 1967. *Some Methods for classification and Analysis of Multivariate Observations*. , Proceedings of 5-th Berkeley Symposium on Mathematical Statistics and Probability, Berkeley, University of California Press, 1:281-297.

Macula Center, 2015. *Macula Center – Eye Anatomy*. [Online]

Available at: <http://maculacenter.com/eye-anatomy/>

[Accessed 17 2 2015].

Maintz, J. B. A. & Viergever, M. A., 1996. *An overview of medical image registration methods*. [Online]

Available at:

<http://citeseerx.ist.psu.edu/viewdoc/download?doi=10.1.1.39.4417&rep=rep1&type=pdf>

[Accessed 2015].

Mangawhai Optometrists, 2015. *Mangawhai Optometrists - Eye Anatomy*. [Online]

Available at: <http://www.eyesonheads.co.nz/eye-anatomy.html>

[Accessed 17 2 2015].

Marin, D., Aquino, A., Gegundez-Arias, M. & Bravo, J., 2011. A New Supervised Method for Blood Vessel Segmentation in Retinal Images by Using Gray-Level and Moment Invariants-Based Features. *IEEE TRANSACTIONS ON MEDICAL IMAGING (Volume:30 , Issue: 1 )*, Jan, pp. 146 - 158.

Martin A., F. & Robert C., B., June 1981. *Random Sample Consensus: A Paradigm for Model Fitting with Applications to Image Analysis and Automated Cartography*, s.l.: Comm. ACM. 24 (6): 381–395.

Mathiak, B. et al., 2006. *Using image classification for biomedical literature retrieval*. Hong Kong, China , IEEE, pp. 185-189.

MathWorks, 1994-2015 . *Segmentation methods in image processing and analysis*. [Online] Available at: <https://uk.mathworks.com/discovery/image-segmentation.html> [Accessed 2015].

MathWorks, 1994-2015. *Marker-Controlled Watershed Segmentation*. [Online] Available at: [http://uk.mathworks.com/help/images/examples/marker-controlled-watershed-segmentation.html?s\\_cid=srchtitle](http://uk.mathworks.com/help/images/examples/marker-controlled-watershed-segmentation.html?s_cid=srchtitle) [Accessed 2015].

Matković, K., 1997. *Phd Dissertation: Tone Mapping Techniques and Color Image Difference in Global Illumination*. Vienna : Institute for Computer Graphics, the Vienna University of Technology.

mgid, 2015. *exudates retina*. [Online] Available at: <http://galleryhip.com/exudates-retina.html> [Accessed 2015].

Mokrzycki, W. & Tatol, M., 2012. Colour difference dE - A survey. *Machine Graphic & Vision*.

Morales, S. et al., 2012. *AUTOMATIC DETECTION OF OPTIC DISC BASED ON PCA AND STOCHASTIC*. Bucharest, Romania, 20th European Signal Processing Conference (EUSIPCO 2012).



Morales, S. et al., 2012. *Automatic detection of optic disc based on PCA and stochastic watershed*. Bucharest, Romania, 20th European Signal Processing Conference (EUSIPCO 2012)\ Medical Imaging, IEEE Transactions on (2013, Volume:32, Issue:4, pp 786-796).

Mudassar, A. A. & Butt, S., 2013. Application of Principal Component Analysis in Automatic Localization of Optic Disc and Fovea in Retinal Images. *Journal of Medical Engineering*, 2013(989712), p. 12.

Mudassar, A. A. & Butt, S., 2013. Application of Principal Component Analysis in Automatic Localization of Optic Disc and Fovea in Retinal Images. *Journal of Medical Engineering*, 2013(989712), p. 12.

Neuhoff, D. L. S., 2015. *OCULAR CONDITIONS*. [Online]

Available at: <http://www.drneuhoff.com/education.html>

[Accessed 2015].

OLIVEIRA, C. J. S., ARAÚJO, A. D. A., JR., C. A. S. & GOMES, D. R., 2002. *Classifying Images Collected on the World Wide Web*. Fortaleza-CE, Brazil, Brazil, IEEE, pp. 327-334.

OMIC, b. D. C. B. M., 1995. *OMIC*. [Online]

Available at: <http://www.omic.com/medication-errors-result-in-costly-claims-for-ophthalmologists/>

[Accessed 2016].

OpenCV dev.team, 2015. *OpenCV 2.4.9.0 documentation*. [Online]

Available at: <http://docs.opencv.org/index.html>

[Accessed 2014-2015].

OpenCV, 2015. *OpenCV 2.4.11.0 documentation*. [Online]

Available at: For Color Spaces:

[http://docs.opencv.org/modules/imgproc/doc/miscellaneous\\_transformations.html?highlight=cvtColor#cv.CvtColor](http://docs.opencv.org/modules/imgproc/doc/miscellaneous_transformations.html?highlight=cvtColor#cv.CvtColor)

[Accessed 2014-2015].

OpenCV, 2015. OpenCV Tutorials. In: O. D. Team, ed. *The OpenCV Tutorials Release 2.4.9.0 April 15, 2014*. -: OpenCV, p. 256 [Remapping].

OpenCV, 2020. *Template Matching*. [Online]

Available at: [https://docs.opencv.org/3.4/de/da9/tutorial\\_template\\_matching.html](https://docs.opencv.org/3.4/de/da9/tutorial_template_matching.html)

OpenCVDev.Team, 2017. *compareHist*. [Online]

Available at:

<http://docs.opencv.org/2.4/modules/imgproc/doc/histograms.html?highlight=comparehist#comparehist>

OpenCVDev.Team, 2017. *EMD*. [Online]

Available at: <http://docs.opencv.org/2.4/modules/imgproc/doc/histograms.html#emd>

OpenCVDev.Team, 2017. *EMD*. [Online]

Available at: <http://docs.opencv.org/2.4/modules/imgproc/doc/histograms.html#emd>

OpenCVDev.Team, 2017. *Histogram Comparison*. [Online]

Available at:

[http://docs.opencv.org/2.4/doc/tutorials/imgproc/histograms/histogram\\_comparison/histogram\\_comparison.html](http://docs.opencv.org/2.4/doc/tutorials/imgproc/histograms/histogram_comparison/histogram_comparison.html)

Pearson, K., 1895. "Contributions to the Mathematical Theory of Evolution. II. Skew Variation in Homogeneous Material". *Philosophical Transactions of the Royal Society A: Mathematical, Physical and Engineering Sciences*, Volume 186, p. 343–414.

Qureshi, R. et al., 2012. Combining algorithms for automatic detection of optic disc and macula in fundus images. *Elsevier-Computer Vision And Image Understanding*, 116(1)(1), pp. 138-145.

Ramponi, G., Strobel, N., Mitra, S. K. & Yu, T., 1996. Nonlinear Unsharp masking for contrast enhancement. *Journal of Electronic Imaging* 5(3), pp. 353-366.

RetinaCAD, 2014-2016. *RetinaCAD*. [Online]

Available at: <https://sites.google.com/site/retinacad/files>

[Accessed 2016].

Ritchings, T., Guthrie, I. & Wood, I., 2006. *Robust Registration and Change Detection in Time-separated Retinopathy Images*. Cambridge, UK, ARVO.

Ritchings, T., Guthrie, I. & Wood, I., 2012. *Robust Registration and Change Detection in Time-separated Retinopathy Images*, Manchester/UK: University of Salford.

RNIB, 2016. *Diabetes information*. [Online]

Available at: <http://www.rnib.org.uk/eye-health-eye-conditions/diabetes-information>

[Accessed 2016].

RNIB, 2016. *Key information and statistics*. [Online]

Available at: <http://www.rnib.org.uk/knowledge-and-research-hub/key-information-and-statistics>

[Accessed 2016].

Rother, C., Kolmogorov, V. & Blake, A., 2004. interactive foreground extraction using iterated graph cuts. *ACM Transactions on Graphics (TOG) - Proceedings of ACM SIGGRAPH*, New York, NY, USA, , pp. Volume 23 Issue 3 Pages 309-314.

Rotterdam-Ophthalmic-Institute, 2017. *Rotterdam Ophthalmic Data Repository*. [Online]

Available at: <http://rod-rep.com>

Rueckert, D., 2013. *Image Registration: Techniques and Applications*. [Online]

Available at: [cvn.ecp.fr/teaching/biomed/2013/rueckert.pdf](http://cvn.ecp.fr/teaching/biomed/2013/rueckert.pdf)

[Accessed 2015].

Russell, S. R., Niemeijer, M. & Abramoff, M. D., 2010. *Automated detection of diabetic retinopathy: barriers to translation into clinical practice*, COPYRIGHT 2010 Expert Reviews Ltd (Expert Review of Medical Devices), [website:Health and Wellness Resource Center].

[Online]

Available at: <http://www.salford.ac.uk/library>

[Accessed 9 Mar 2015].

Saffarzadeh, V. M., Osareh, A. & Shadgar, B., 2014. Vessel Segmentation in Retinal Images Using Multi-scale Line Operator and K-Means Clustering. *Journal of Medical Signals and Sensors*, Apr-Jun, p. 4(2): 122–129.

Saffarzadeh, V. M., Osareh, A. & Shadgar, B., 2014. Vessel Segmentation in Retinal Images Using Multi-scale Line Operator and K-Means Clustering. *Journal of Medical Signals and Sensors*, Apr-Jun, p. 4(2): 122–129.

Sathya, S. & Manavalan, R., Dec 2011. Analysis of background detetion and contrast enhancement of MRI images. *IEEE computer applications*, pp. 16-20.

Schuessler, Z., 2017. *Delta E 101*. [Online]

Available at: <http://zschuessler.github.io/DeltaE/learn/>

SC, L., ET, L., RM, K. & al., e., 2001. Comparison of Diagnosis of Early Retinal Lesions of Diabetic Retinopathy Between a Computer System and Human Experts. *Arch Ophthalmol*, Volume 119(4), pp. 509-515.

Sebbe, R., 2006. *PhD dissertation: Computer-aided Diagnosis of Pulmonary Embolism in Opacified CT Images*, s.l.: Universite d'Orleans.

Senol, Sarnel, H. & Y., 2011. Accurate and Robust image registration based on radial basis neural networks. *Neural Comput & Applic*, vol. 20, pp. 1255-1262.

Serra, J., 1982. *Image Analysis and Mathematical Morphology*. ISBN 0-12-637240-3 ed. s.l.:s.n.

Shapiro, L. G. & Stockman, G. C., 2001. In: *Computer Vision*. New Jersey: Prentice-Hall, ISBN 0-13-030796-3, pp. 279-325.

Smirnov, B. M., 1996. Comparison of histograms of data banks. *Physica Scripta*, Volume 54, Number 1, pp. 125-128.

Soares, J. et al., 2006 . Retinal Vessel Segmentation Using the 2-D Gabor Wavelet and Supervised Classification. *IEEE TRANSACTIONS ON MEDICAL IMAGING*, VOL. 25, NO. 9, Sept., pp. 1214 - 1222.

Specialists, R. E., 2015. *NON-PROLIFERATIVE DIABETIC RETINOPATHY*. [Online]

Available at: <http://www.retinaeye.com/nonprodiabeticretinopathy.html>

[Accessed April 2015].

SRINIVASAN, G. & G., D. S., 2007. Segmentation Techniques for Target Recognition.

*INTERNATIONAL JOURNAL OF COMPUTERS AND COMMUNICATIONS Issue 3, Volume 1*.

Stack-Exchange, 2017. *what is the function to find otsu threshold in emgu cv?*. [Online]

Available at: <https://stackoverflow.com/questions/25989754/what-is-the-function-to-find->

otsu-threshold-in-emgu-cv

[Accessed 2017].

STARE Project by Goldbaum MH, 1975 . *STRUCTURED ANALYSIS OF THE RETINA*. [Online]

Available at: <http://www.ces.clemson.edu/~ahoover/stare/>

STUMPF, A., 2013. *OPTICAL IMAGE MATCHING TECHNIQUES*. [Online]

Available at: [omiv2.u-strasbg.fr/imagemining/documents/IMAGEMINING-Stumpf.pdf](http://omiv2.u-strasbg.fr/imagemining/documents/IMAGEMINING-Stumpf.pdf)

[Accessed 2015].

Suzuki, S. a. A. K., 1985. *Topological Structural Analysis of Digitized Binary Images by Border Following*. , CVGIP 30 1, pp. 32-46.

Thyagarajan, K. & Minu, R., 2013. Prevalent Color Extraction and Indexing. *International Journal of Engineering and Technology (IJET)*, pp. 4841-4849, Vol 5 No 6 Dec 2013-Jan 2014.

Thyagarajan, K. & Minu, R., 2014. Semantic Rule Based Image Visual Feature Ontology Creation. *International Journal of Automation and Computing*, pp. 11(5), October 2014, 489-499.

Tian, D. p., 2013. A Review on Image Feature Extraction and Representation Techniques. *International Journal of Multimedia and Ubiquitous Engineering*, July, pp. Vol. 8, No. 4.

vision and eye health, 2010-2015. *Diabetic retinopathy*. [Online]

Available at: <http://www.vision-and-eye-health.com/diabetic-retinopathy.html>

[Accessed 2015].

Wang, R., 2013. *Histogram Specification*. [Online]

Available at: [http://fourier.eng.hmc.edu/e161/lectures/contrast\\_transform/node3.html](http://fourier.eng.hmc.edu/e161/lectures/contrast_transform/node3.html)

[Accessed 2015].

WebMD, 2015. *WebMD - Eye Health Center*. [Online]

Available at: <http://www.webmd.com/eye-health/picture-of-the-eyes>

[Accessed 18 2 2015].

WHO Press, 2007. *VISION 2020 report, global initiative for the elimination of avoidable blindness: action plan 2006 - 2011*, Switzerland: World Health Organization.

Wisaeng, K., Hiransakolwong, N. & Pothiruk, E., 2014. Automatic Detection of Optic Disc in Digital Retinal Images. *International Journal of Computer Applications (0975 – 8887)*, 90 – No 5(0975 – 8887).

Yang, J. et al., 2011. A Robust hybrid method for nonrigid image registration. *Pattern Recognition, vol. 44*, , pp. 764-776.

Yuen, H. K., Princen, J. & Illingworth, J. a. K. J., 1990. Comparative study of Hough transform methods for circle finding. *Image Vision Comput. 8 1*, , p. 71–77.

Zhan, D., Zuo, W. & Li, N., 2016. *Medical Biometrics: Computerized TCM Data Analysis*. 2016 ed. China: Higher Education Press limited Company , World Scientific Publishing Co. Pte. Ltd..

Zijdenbos, A., Dawant, B., Margolin, R. & Palmer, A., 1994. Morphometric analysis of white matter lesions in MR images: method an validation.. *IEEE Trans. Med. Imaging*, Volume 13, p. 716–724.